Investigation of Channel Adaptation and Interference for Multiantenna OFDM

Figueiredo, Daniel Vaz Pato

Publication date:
2008

Document Version
Publisher's PDF, also known as Version of record

Investigation of Channel Adaptation and Interference for Multiantenna OFDM

by

Daniel Vaz Pato Figueiredo, MSc

Dissertation

Presented to the Faculty of Engineering and Science of

Aalborg University

in Partial Fulfillment of the Requirements for the Degree of

Doctor of Philosophy

Aalborg University

Department of Electronic Systems

February 2008

Supervisors

Prof. Ramjee Prasad, Aalborg University, Denmark

Assoc. Prof. Troels Bundgaard Sørensen, Aalborg University, Denmark

Assessment Committee

Prof. Preben Elgaard Mogensen, Aalborg University, Denmark (Chairman)

Prof. Mary Ann Ingram, Georgia Institute of Technology, USA

Assoc. Prof. António José Castelo Branco Rodrigues, Technical University of Lisbon, Portugal

Moderator

Assoc. Prof. Flemming Bjerge Frederiksen, Aalborg University, Denmark

ISBN: 978-87-92328-01-4

Abstract

The new use of internet through social networks, combined with popular bandwidth consuming applications, and the need to deliver high data rate connections to highly mobile users, is the driving force behind the requirements for future wireless networks. In this context, spectral efficient techniques constitute vital improvements in high data rate services. The design of robust systems is an essential factor in coping with the random and dynamic nature of the multipath in the wireless environment.

This thesis focuses on multiantenna Orthogonal Frequency Division Multiplexing (OFDM) processing applied with the purpose of increasing the signal strength, of boosting the data rate, and of increasing the reliability of the wireless link. The author investigates the interaction between different multiantenna processing algorithms and downlink adaptive transmission, based on link quality information in time-varying channels.

A tradeoff between spatial diversity and multiplexing is offered by the linear dispersion framework for space-frequency processing. This thesis evaluates the performance of the unitary trace orthogonal design, along with linear receivers and channel coding, and its interaction with link adaptation. Although this coding scheme achieves a superior performance for low rate modes, the inter-stream interference effect on the probability of error imposes a poor performance for high order modulations.

In high mobility scenarios, the performance of channel-aware transmission adaptation is highly dependent on the feedback delay. This thesis develops an analytical framework designed to investigate the performance of rate adaptation in a time-varying channel for selected Multiple Input Multiple Output (MIMO) schemes: spatial diversity, multiplex-

ing, and antenna selection. The probability of bit error is evaluated in a Rayleigh scenario for a rate adaptive system operating on outdated channel information, and closed-form expressions for the average probability of error are derived for each MIMO scheme. As a result, we propose analytical thresholds for rate adaptation, based on outdated channel information. In continuation, this thesis, supported by the study of the robustness of the feedback channel, proposes a mechanism to select the modulation and MIMO scheme in a multimode transmission system.

The effect of cochannel signals in a cellular scenario is studied in analytical and simulation contexts to assess the performance of spatial diversity and OFDM transmissions. On the basis of an analytical framework, we detect a relation between the number of interfering sources on the probability of error of a high-order spatial diversity link. In cellular systems, a suboptimal interference cancelation, for the downlink inter-cell interference, is shown to attain significant performance for a single transmit antenna, but a limited effect for spatial transmit diversity, due to its sensitivity to channel estimation error.

Besides the concrete solution proposals, the thesis leads to a better understanding of practical aspects from integration of MIMO in wireless scenarios.

Dansk Resumé

Den nye brug af Internettet baseret på sociale netværk i kombination med populære bredbåndsbaserede applikationer, og behovet for at levere høje dataoverførselshastigheder til mobile brugere, er de drivende kræfter bag kravene til fremtidens trådløse netværk. Set i denne sammenhæng udgør spektraleffektive teknologier en væsentlig del af de forventede forbedringer til dataintensive services. Designet af robuste systemer er en essentiel faktor i håndteringen af den tilfældige og dynamiske karakter af flervejsudbredelse i trådløse scenarier.

Denne afhandling fokuserer på multiantenne processering i Orthogonal Frequency Division Multiplexing (OFDM) anvendt med henblik på at øge signalstyrken, forøge dataoverførselshastigheden og øge pålideligheden i den trådløse forbindelse. Forfatteren undersøger interaktionen mellem forskellige multiantenne processeringsalgoritmer og adaptive transmission i downlink baseret på link kvalitetsinformation i tidsvarierende kanaler.

En afvejning mellem diversity og multipleksing er mulig ved hjælp af en model for lineær spredning i rum og frekvens. Afhandlingen evaluerer ydeevnen af unitary trace orthogonal design med lineære modtagere og kanalkodning, samt interaktionen med linkadaptering. Selvom den lineære spredningskodning opnår overlegen ydeevne ved lav modulationsorden, betyder indvirkningen på fejlsandsynligheden fra interferens mellem de transmitterede datastrømme en dårligere ydelse ved høj modulationsorden.

I scenarier med høj mobilitet, er ydeevnen af den kanaladaptive transmission særdeles afhængig af forsinkelsen på kanalinformationen. Denne afhandling udvikler en analytisk model for ydeevnen af kanaladaptiv transmission i en tidsvariende kanal for udvalgte

Multiple Input Multiple Output (MIMO) systemer baseret på diversity, multipleksing og antenneselektion. Sandsynligheden for bitfejl er evalueret for et scenarie med Rayleigh-kanal og kanaltilpasning baseret på uddateret kanalinformation. I denne sammenhæng er der udledt lukkede udtryk for middel fejlsandsynligheden for hvert MIMO system. Som resultat heraf anbefales analytisk udledte tærskelværdier for kanaltilpasningen under hensyntagen til den uddaterede kanalinformation. I forlængelse heraf, og baseret på studiet af feedback, anbefales en mekanisme til at vælge modulation og MIMO system i et mulitmodalt transmissionssystem.

Effekten af co-channel signaler i et cellulært scenarie er undersøgt analytisk og ved simulering for at måle ydeevnen af diversity i OFDM transmission. På basis af den analytiske udledning er der bestemt en sammenhæng mellem antallet af interfererende signaler og fejlsandsynligheden i et MIMO diversity system. I et cellulært system med downlink inter-celle interferens er det vist at en suboptimal interferensudligner opnår en betydelig ydeevne i tilfældet med en enkelt senderantenne, mens flere senderantenner har en begrænset effekt på grund af følsomheden overfor kanalestimeringsfejl i dette sidste tilfælde.

Ud over de konkrete løsningsforslag bidrager afhandlingen til en øget forståelse af de praktisk relaterede aspekter vedrørende integrationen af MIMO i trådløse scenarier.

Dedicated to my beloved family and friends.

Preface and Acknowledgments

The work in this dissertation is the result of research carried out at the Department of Electronic Systems at Aalborg University, Denmark. The research has been co-financed by Samsung Electronics, the Department of Electronic Systems, and the European Union. The contributions of the thesis are presented in Chapters 2–5. The reader unfamiliar with the technical concepts addressed in the contributions may profit from the introductory background in Appendices A–E for a better understanding of the technical details of the description of contributions.

In the first place, I am grateful to Ramjee Prasad for his support and for having believed in my success until the end. Special thanks to Troels Sørensen that supervised me during the second part of the Ph.D. for the significant contribution in making this thesis a reality. I would like to thank to the guidance given during earlier stages of my Ph.D. studies from Frank Fitzek, Elisabeth de Carvalho, and Zihuai Lin.

I would like to leave a word of gratitude to my colleagues and friends of the Wireless Networking Group (WING) and fellow Ph.D. students in the JADE project. Muhmmad Imadur Rahman has been an amazing colleague that always supported me, and with whom I have learned a lot. Together with Nicola Marchetti and Suvra Das we have had many fruitful discussions. I would also like to express my gratitude to my colleagues at the Radio Access Technology (RATE) section that made a very friendly and productive working environment, without forgetting the very competitive table tennis matches after lunch.

I am thankful to the friends I have made during my stay at Aalborg, they are the support and kindness I needed for living far away from home. I will keep in my heart the new family we have imagined in the early days at Aalborg. The biggest thanks to my

girlfriend Dalia Tiesyte for the support, the patience, the travels, and the proof-reading of this thesis. In my mind are and will always be my home friends back in Lisbon.

Finally, I would like to thank my family in Portugal, and, especially, my parents, brother, and sister for their full support, patience, entertaining phone calls, and writing advice.

Daniel Vaz Pato Figueiredo

Aalborg University

February 2008

Contents

List of Figures

List of Tables

List of Symbols

f_c	Carrier frequency
B	Bandwidth
λ	Wavelength
B_c	Coherence bandwidth
T_c	Coherence time
f_d	Doppler frequency
$\mathbf{d}$	Data vector
$\mathbf{s}$	Transmitted signal vector
$\mathbf{h}$	Channel coefficients vector
$\mathbf{H}$	Channel coefficients matrix
$\mathbf{y}$	Received signal vector
$\mathbf{w}$	Noise vector
E_s	Transmitted signal power
N_0	Noise power
γ	Signal to noise ratio at the receiver
γ_b	Signal to noise ratio per bit at the receiver
ρ^a	Signal to noise ratio per receiver antenna
N_t	Number of transmit antennas
N_r	Number of receive antennas
q	Transmit antenna index
p	Receive antenna index
N_a	Number of receive/transmit antennas for SM
T	Number of channel uses in the ST code
N_s	Number of symbols in the ST code
$\mathbf{Y}$	Received signal block matrix
$\mathbf{S}$	Transmitted signal block matrix
$\mathbf{W}$	Noise block matrix

$\mathbb{F}$	Discrete Fourier Transform
N	Number of OFDM subcarriers
k	Subcarrier index
N_d	Number of data subcarriers
T_s	Total OFDM symbol duration
T_f	Frame duration
M	Modulation order
R	Number of constellations
b	Bit per modulation symbol
P_b or BER	Bit error probability
P_s	Symbol error probability
η	Throughput
ρ	Time correlation
τ	Time delay
ψ	Delay/prediction thresholds for MIMO selection
n	Time domain index
$\hat{\gamma}$	Predicted SNR at the receiver
$\upsilon_{\mathbf{h}\epsilon_\mathbf{h}}$	Relative variance of the prediction error
$\hat{\mathbf{h}}$	Predicted channel coefficient
$\epsilon_\mathbf{h}$	Channel prediction error
p	Channel power
$\hat{p}$	Predicted channel power
ϵ_p	Predicted channel power error
L	Number of interferers
E_i	Interference signal power
$\mathbf{g}$	Interference channel vector response
ρ^I	Interference to noise ratio at the receiver

List of Acronyms

2G	Second Generation
3G	Third Generation
3GPP	The Third Generation Partnership Project
4G	Fourth Generation
AMC	Adaptive Modulation and Coding
AS	Antenna Selection
AWGN	Additive White Gaussian Noise
BER	Bit Error Rate
BLER	Block Error Rate
BPSK	Binary Phase Shift Keying
BS	Base Station
CCI	Cochannel Interference
CDF	Cumulative Distribution Function
CIR	Channel Impulse Response
CP	Cyclic Prefix
CRC	Cyclic Redundancy Check
CSI	Channel State Information
DAB	Digital Audio Broadcasting
DIV	Diversity

DFT	Discrete Fourier Transform
DoA	Direction of Arrival
DoD	Direction of Departure
DSL	Digital Subscriber Line
DVB	Digital Video Broadcasting
EESM	Exponential Effective SNR Mapping
E-UTRA	Evolved UMTS Terrestrial Radio Access
FDD	Frequency Division Duplex
FDM	Frequency Division Multiplexing
FFT	Fast Fourier Transform
HARQ	Hybrid Automatic Repeat Request
HSPA	High-Speed Packet Access
ICI	Inter-Carrier Interference
IDFT	Inverse Discrete Fourier Transform
IEEE	Institute of Electrical and Electronics Engineers
IFFT	Inverse Fast Fourier Transform
INR	Interference to Noise Ratio
ISD	Inter-Site Distance
ISI	Inter-Symbol Interference
ISR	Interference to Signal Ratio
LDC	Linear Dispersion Codes
LOC	Localized
LOS	Line of Sight
LS	Least-Square
LTE	Long Term Evolution
MCS	Modulation Code Schemes

MIMO	Multiple Input Multiple Output
MISO	Multiple Input Single Output
MMSE	Minimum Mean Square Error
MRC	Maximal Ratio Combining
MS	Mobile Station
MSE	Mean Square Error
MUD	Multiuser Diversity
NLOS	Non Line of Sight
OFDM	Orthogonal Frequency Division Multiplexing
OFDMA	Orthogonal Frequency Division Multiple Access
PAPR	Peak to Average Power Ratio
PARC	Per Antenna Rate Control
PDF	Probability Density Function
PDP	Power Delay Profile
PSK	Phase Shift Keying
QAM	Quadrature Amplitude Modulation
QoS	Quality of Service
QPSK	Quadrature Phase Shift Keying
RMS	Root Mean Square
SFBC	Space-Frequency Block Code
SFC	Space-Frequency Coding
SIMO	Single Input Multiple Output
SINR	Signal to Interference and Noise Ratio
SIR	Signal to Interference Ratio
SISO	Single Input Single Output
SM	Spatial Multiplexing

SNR	Signal to Noise Ratio
SVD	Singular Value Decomposition
STBC	Space-Time Block Code
STC	Space-Time Coding
TDD	Time Division Duplex
TDMA	Time Division Multiple Access
UTRA	UMTS Terrestrial Radio Access
UTOD	Unitary Trace Orthogonal Design
WCDMA	Wideband Code Division Multiple Access
WAN	Wide Area Network
WiMAX	Worldwide Interoperability for Microwave Access
WLAN	Wireless Local Area Network
ZF	Zero Forcing

Chapter 1

Introduction

Over the last two decades, wireless communications have been enthusiastically accepted by the world's population a large, to become an essential tool in our day-to-day lives. This is largely due to the Second Generation (2G) wireless systems. Although 2G networks focused on delivering speech services, the explosion of internet connections in the home, along with increasing availability of broadband connections has created a considerable demand for wireless data services. Moreover, bandwidth intensive or high-speed applications, such as media streaming offered by YouTube and other media sharing sites, are expected to drive huge demands on wireless networks' resources, as they become available in mobile devices. Once the growth in social networks, such as Facebook and MySpace, is extended to wireless networks, the multimedia sharing experience enters the next level of anytime and anywhere access to one's community.

1.1 Motivation

Designed to enable the access to broadband connection through a cellular phone, the Third Generation (3G) was introduced by The Third Generation Partnership Project (3GPP). This project promised peak data rates to the order of 10 Mbit/s along with Wideband Code Division Multiple Access (WCDMA) and High-Speed Packet Access (HSPA) [HT04, HT06]. In parallel, other development groups within the 802 family of

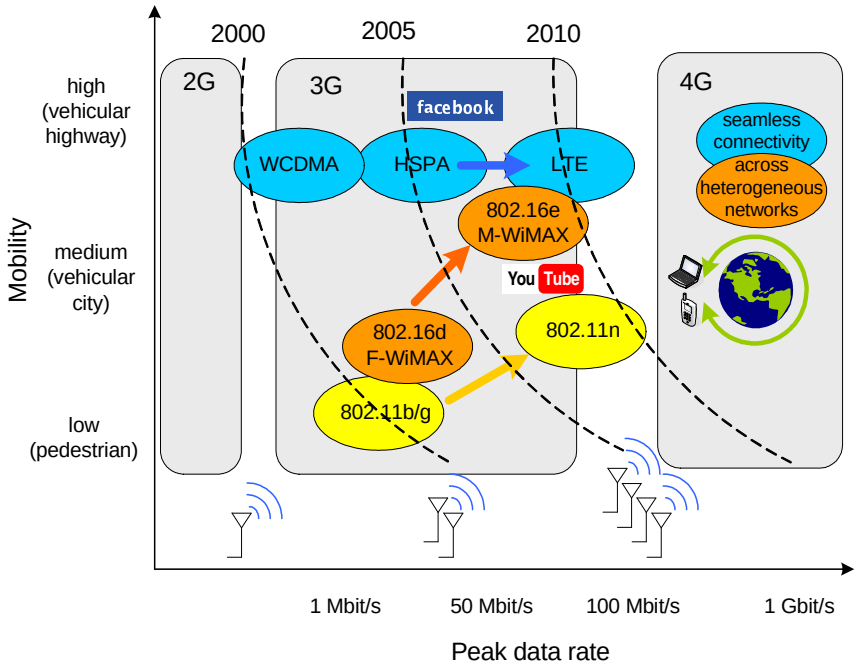

Figure 1.1: Evolution of global standards

the Institute of Electrical and Electronics Engineers (IEEE) standards promote nomadic broadband wireless data access that have led to the the popular Wireless Local Area Networks (WLANs), 802.11b/g, and the fixed Worldwide Interoperability for Microwave Access (WiMAX), known as 802.16d-2004 [IEE04].

Along the path to Fourth Generation (4G) systems, even higher spectral efficiency is sought to achieve a data rate within the order of 100 Mbit/s in mobile outdoor scenarios, and 1 Gbit/s in nomadic scenarios. The definition of the 4G systems has not yet been agreed upon and still awaits standardization and the release of spectrum, whereas evolutions of 3G systems are expected to be competitive for several years to come. The mobile WiMAX 802.16e-2005 [IEE06] and the Long Term Evolution (LTE) [3GP06b] of 3GPP are competing as leaders in radio access technology in the direction of 4G systems. One important requirement for the 4G is the seamless connectivity and smooth handoff across heterogeneous networks. Figure 1.1 represents the evolution of standards in terms of data rate and user mobility.

The new requirements for high-speed data are the driving force behind research into

wireless networks. Thus, several techniques that enhance the spectral efficiency of systems and allow for an increased throughput with the same spectrum have received considerable attention from the research community. A fundamental feature of wireless fading channels is the dynamic random variation of the channel's strengths. In fact, multipath and mobile environments introduce fading and uncertainty in the channel, which complicates any efforts to deliver high-speed data connections. The effect of simply increasing the transmit power or of using an additional bandwidth may not be the solution to achieve a robust broadband system [Kim02]. Therefore, advanced physical layer techniques are required to reduce the effect of fading in both the transmitter and receiver, without excessively increasing the system's complexity and cost.

In recent years, several spectral efficient techniques have received considerable interest and support from both the research community and industry. This thesis focuses on three groups of physical layer techniques: multicarrier transmission, multiantenna processing, and channel-aware schemes. The aim of this thesis is to provide a better understanding of multiantenna processing integration in the next generation wireless systems. In fact, multiantenna processing is of particular interest, and several flavors of the technique are already being supported by the new wireless systems. However, several practical problems must be addressed regarding the up-coming generations of wireless networks.

1.2 State-of-the-Art

1.2.1 OFDM

OFDM is an effective multicarrier technique that has the ability to cope with the severe channel characteristics without requiring high complexity equalization receivers [NP00]. OFDM, custom-designed for broadband channels, converts the wideband frequency selective channel into multiple narrowband flat channels. One of the main advantages of multicarrier systems is that it permits transmission over frequency-selective channels at a low receiver implementation cost. OFDM is therefore commonly accepted as being the most effective transmission technology for the downlink of future high data rate broad-

band systems [HP03]. However, some drawbacks affect the performance of OFDM in cellular scenarios. A widely known problem of multicarrier transmission is its vulnerability to synchronization errors. The Doppler shift, caused by high mobility, introduces Inter-Carrier Interference (ICI), while long multipath delay profiles create Inter-Symbol Interference (ISI) [HT01].

1.2.2 MIMO

A MIMO system is defined as a system with multiple antennas at the receiver and transmitter ends. Traditionally, multiple antennas were employed to shape the radiation diagram of the antenna pattern, using a technique known as beamforming [App76]. However, multiple antennas at the transmitter and receiver may be used to exploit array, diversity, and/or multiplexing gains. In recent years, techniques that transmit over spatially uncorrelated antennas have received broad attention from the research community due to their potential to increase the reliability or the data rate of the wireless link.

Spatial diversity and multiplexing are effective techniques to increase robustness and the data rate in wireless systems requiring low complexity. MIMO transmission schemes that assume channel knowledge at the receiver, but not at the transmitter, mainly deliver spatial diversity or multiplexing gains.

Spatial diversity techniques have been proposed to overcome wireless channel impairments by providing a more reliable transmission link. Spatial diversity can be exploited at the receiver by employing Maximal Ratio Combining (MRC) which uses the knowledge of the channel's coefficients to achieve both array and diversity gains. The technique designed to encode multiantenna transmissions is referred to as Space-Time Coding (STC) [PNG03, GSS+03]. STC schemes map the source symbols to the transmit antennas. These schemes were popularized with the discovery of Space-Time Block Code (STBC). STBC, introduced by [Ala98, TJC99], is an open-loop transmit diversity scheme whose diversity gain is achieved without the knowledge of the channel at the transmitter by employing linear receivers.

As opposed to diversity techniques, the MIMO channel can be used for Spatial Multiplexing (SM), in order to dramatically increase the system throughput [Tel95, Fos96]. The MIMO configuration is applied so as to create parallel streams of data by using SM. This technique boosts the data rate by using the multiple spatial links to transmit more symbols, albeit at the cost of diversity gain.

More recently, the authors in [HH02] have introduced the Linear Dispersion Codes (LDC) framework that generalizes the design of encoding schemes in the space-time or space-frequency domains. This approach provides a linear model of the transmission where spatial diversity and spatial multiplexing may be regarded as particular cases of encoding. Space-time codes that present full diversity and full rate have been proposed. These include rotation of constellations [SP04], non-linear processing [HG03, FB06], or complex-field precoding [MG03].

MIMO-OFDM OFDM itself does not offer any built-in diversity, and in many cases it is desirable to introduce robustness in the wireless link. To obtain a more robust system, multiantenna techniques can be used to deliver array, diversity, and/or multiplexing gains. Since, in OFDM, each subcarrier experiences a flat fading input-output relation, MIMO-OFDM systems can use narrowband multiantenna schemes at each subcarrier by transmitting independent OFDM modulated data through multiple antennas. The spatial domain increases the flexibility of OFDM, thus opening up the way to new allocation and adaptation algorithms [SBM+04].

Interference Nowadays, cellular networks are interference limited, due to an increasing number of users that need to share the spectrum. Multiuser receivers have to cope with interference both in uplink, where a large number of asynchronous users are detected, besides downlink, where the terminal receives a few interfering signals from neighbor Base Stations (BSs) [And05]. The spatial streams created by MIMO transmissions increase interference. For that reason, interference cancelation algorithms have a significant influence on performance. Furthermore, the interference caused by different MIMO techniques

varies as regards their effect on the link performance [Rah07]. Analytical approaches to study the performance of optimum combining and MRC in the presence of interfernce has been followed by the authors in [CFS97].

1.2.3 Adaptation and Scheduling

Adaptive transmission and channel-aware scheduling are techniques that use channel knowledge at the transmitter end. On the basis of available channel sounding techniques, it is fairly common to assume robust channel estimates at the receiver. However, to have the channel estimates at the transmitter is cumbersome in non-reciprocal channels as in Frequency Division Duplex (FDD). In such systems, the channel is estimated at the receiver and a vector with the Channel State Information (CSI) is returned to the transmitter via the feedback channel. Updating the CSI is liable to imperfections such as channel estimation errors, quantization errors, and feedback delays [KVC02]. More specifically, in high mobility scenarios, the rapid channel variation causes the channel information contained in the feedback to become outdated. The effect of outdated estimates in channel statistics affects adaptive techniques [Goe99, NAP04].

Link Adaptation Schemes that adapt the transmission parameters to the varying channel conditions considerably increase the channels's spectral efficiency. More specifically, rate adaptive systems provide substantial gains in performance, along with relatively low complexity and reduced feedback overhead [Gol05, CEGHJ02]. Fast transmission adaptation that reacts at each transmitted frame constitutes a powerful tool insofar as it allows the system to balance the performance according to the signal's strength. Adaptation of the coding rate and modulation allows for a higher degree of flexibility and is referred to as Adaptive Modulation and Coding (AMC).

Adaptive MIMO Link adaptation schemes can be combined with MIMO diversity or multiplexing. A particularly powerful technique, that of adaptation of the rate in SM, independently, at each antenna or stream was proposed in [CLH01], known as Per An-

tenna Rate Control (PARC). As different MIMO techniques provide different performance benefits, e.g., robustness or throughput, the selection of the scheme that is most appropriate to each scenario is a non-trivial task. Although the choice of spatial diversity versus multiplexing is directly related to the Signal to Noise Ratio (SNR), other issues, such as spatial correlation or channel information accuracy have an impact on the choice of the technique. Various authors have addressed MIMO adaptation in recent years, proposing techniques such as switching mechanisms between spatial diversity multiplexing based on the SNR, the MIMO channel eigenvalues, or the condition number of the spatial correlation matrix [HJP05, WSKM06, FPKHJ05]. Another approach is the adaptation of the number of streams and mapping to antennas in a SM system, as proposed in [HJL05].

Multiuser Scheduling In a multiuser scenario, the scheduling algorithms take advantage of independent fading channel conditions observed by the users to increase the system's throughput. This effect is regarded as Multiuser Diversity (MUD), and has received considerable interest from the research community following the theoretical information results first introduced by [KH95].

The use of MIMO techniques with OFDM-based multiuser systems introduces a new dimension to the resource allocation problem, the spatial domain. The authors in [CJS07, NH04] show the fundamental necessity of scaling the quality of the channel knowledge available at the transmitter with the SNR. Optimal algorithms have been proposed for multiuser scheduling and antenna allocation [ZL03, LLC02]. The combination of multiuser allocation of resources with multimode MIMO selection that takes into account service requirements (real-time or non real-time) proves to be a practical approach [MKL06]. In addition, open-loop transmit spatial diversity introduces the channel hardening effect, i.e., it reduces the range of SNR variation [HMT04]. Although spatial diversity provides robustness to the link, the effect is negative in terms of the performance of an opportunistic multiuser scheduler, as the MUD benefits from highly variant channels [BKRM$^+$03]. Therefore, the combination of fading mitigation techniques and opportunistic multiuser schedulers calls for special care in designing the system.

1.3 Challenges and Goals

Although extensive research has been devoted to the topics mentioned in the previous section, several issues still remain a challenge. In the context of the state-of-the-art advances mentioned in the previous section, we list some of the challenges facing future wireless networks.

OFDM poses a broad area of challenges that need to be more efficiently tackled. These include estimation of the timing phase, timing frequency, and frequency offset. Moreover, Peak to Average Power Ratio (PAPR) reduction algorithms are required to obtain enhanced power efficiency. In addition, ICI and ISI effects lead to new issues to be tackled when using OFDM, combined with other techniques, such as multiantenna processing.

Multiantenna processing algorithms continue to be developed in several approaches and present new challenges. In fact, several issues arise in the implementation of MIMO-OFDM systems, such as channel estimation, preamble and packet design, error control coding, and space-time techniques. Closed-loop MIMO systems such as precoding promise significant gains in the system. However, these schemes require new approaches with regard to complexity reduction, and limited feedback.

The design of systems that integrate several advanced adaptive techniques is a prerequisite in future wireless networks that has not yet been fully addressed. For example, although adaptive MIMO switching systems have been proposed, a selection of MIMO that gives due consideration to the reliability of the channel information provided via feedback is still an open issue. Multiuser scheduling with MIMO is another area that raises new challenges, such as the scheduling approach in heterogeneous scenarios in which the terminals use different MIMO techniques.

As adaptive techniques, such as AMC, are regarded as fundamental to future systems, feedback issues arise in systems where the channel is non-reciprocal. The accuracy of the channel knowledge delivered via feedback determines the performance of such techniques and affects each MIMO scheme in different ways. Therefore, the number of antennas

and the MIMO processing must be taken into account when adapting the transmission on the basis of inaccurate CSI. Moreover, there is no analytical framework to evaluate the effect of outdated channel knowledge at the transmitter.

In cellular scenarios, multipath and asynchronous signals produce ISI both in the uplink and the downlink. The effect of signals that arrive after the Cyclic Prefix (CP) length in OFDM requires further study in MIMO channels. Additionally, the Cochannel Interference (CCI), present in single-frequency cellular scenarios, favors implementation of more complex receivers in the uplink with interference cancelation methods.

The scope of this thesis covers the downlink of multiantenna OFDM-based systems. The work presented here sets out to provide an analytical formulation of the effect of feedback delay and interference in rate adaptation for practical MIMO schemes. The analytical approach is applied to evaluate the performance of MIMO schemes with delayed feedback, and to propose closed-form expressions for the adaptation thresholds. Furthermore, simulation results are obtained to support proposed solutions to selected practical problems.

The approach pursued in this thesis to achieve results favors the analytical study of physical layer statistics, and supports the results on simulations for further proof of concepts or where analytical study assumes too complex an approach. The analytical results assume a simplified uncoded system, whereas the simulations target the link-level of a system that incorporates a number of practical issues. The analysis presented does not take into account either channel estimation errors or hardware imperfections. The simulations are performed in MATLAB® [MAT].

1.4 Outline and Contributions

This thesis is organized in four chapters that present the contributions of the work. The list of publications by the author is included in Appendix H.

Chapter 2 compares different perspectives of multiantenna communications and its gains. In our first approach, we discuss the implementation of STBC and beamforming in

OFDM systems and compare the performance in scenarios with different spatial correlation to measure the loss of one system with respect to the other in each case. This study was published in a conference paper [FRM+04]. We then use the LDC framework to investigate the practicality of combining channel coding with spatial diversity and multiplexing. Focus is placed on linear receivers, and the trace orthogonal design space-frequency code is implemented to investigate its strength when combined with AMC in a practical system—the results originated a publication [FLS07b].

Chapter 3, the core contribution of this work, focuses on the reliability of the CSI transmitted via feedback. First, we evaluate the impact of feedback delay in link adaptation, taking into account specific features of future wireless systems. An analytical study of the Bit Error Rate (BER) performance is then presented to show the effect of channel conditions, such as time variability, and spatial diversity. The analysis considers Quadrature Amplitude Modulation (QAM) constellations, MIMO channel statistics in a flat Rayleigh environment, and Jake's model for time selectivity.

Second, we consider a general channel predictor algorithm in combination with STBC, SM, and Antenna Selection (AS). New closed-form expressions for BER performance are obtained for the different MIMO techniques. On the basis of these results, we propose SNR thresholds that depend on the number of antennas for the intervals concerned. These findings were made available in two publications [FCD06, FC06]. The mathematical derivations behind the results of Chapter 3 are presented in Appendix F.

Chapter 4, linked with previous findings on analytical performance in transmission adaptation over time-variant channels, proposes a MIMO switching procedure that selects the appropriate MIMO mode according to channel conditions and the feedback delay experienced by the system. In considering a system whose terminals report the channel quality on a per frame basis, we propose the approach used for the threshold and feedback designs. The description of an integrated system with the proposed MIMO switching mechanism and modulation thresholds led to the development of a patent [CFD+06].

In a cellular environment, Chapter 5 considers the interaction of cochannel signals

in the spatial diversity and OFDM. An analytical model is developed to study of the BER performance of spatial diversity in the presence of multiple interferers. This achievement resulted in the publication [FLS07a]. Then, we analyze the effect of time delayed signals received at the Mobile Station (MS) and compare the degradation in unicast and broadcast transmission modes.

Chapter 6 presents the conclusions and the future work.

Appendices A-E provide the background knowledge required to understand the thesis. More specifically, Appendix A presents the characteristics of slow fading and fast fading, besides an introduction to the channel fluctuations over time, frequency, and space. Appendix B introduces the general features and system model of OFDM. The use of antenna arrays for beamforming is presented in Appendix C. Appendix D introduces the different diversity techniques and describes the channel statistics of diversity and multiplexing. Appendix E details the scheme used in this thesis for rate adaptation, and introduces the basic multiuser scheduling algorithms.

Chapter 2

Beamforming and Space-Time Processing in OFDM

Future wireless systems consider the use of OFDM and MIMO techniques to deliver high-speed data to the users over reliable communication links. This chapter studies an OFDM-based system combined with different multiantenna techniques that process the signal in the space domain. We consider the use of multiple antennas for application of different techniques: beamforming, diversity, and multiplexing.

The implementation of beamforming and spatial diversity in OFDM systems reveals challenges in terms of complexity, feedback, and scenario dependencies. In this chapter, we discuss the differences and limitations of OFDM transmission over scenarios with different angular spread.

Furthermore, the LDC framework generalizes the design of encoding schemes in the space-time or space-frequency domains [HH02]. This framework allows the design of full rate Space-Frequency Coding (SFC) to achieve minimum BER in the class of linear receivers [LZW06], also known as Unitary Trace Orthogonal Design (UTOD) [Bar04]. We investigate the performance of LDC with linear receivers, and the interaction with link adaptation.

The background information on the physical layer techniques treated in this and the

following chapters are presented in Appendices A-E. The remainder of this chapter is organized as follows. Section 2.1 introduces the MIMO space-time linear model. Section 2.2 evaluates the issues arising from the implementation of beamforming and spatial diversity in OFDM systems. Section 2.3 addresses the performance of spatial diversity and spatial multiplexing for multiple antenna wireless communications jointly with link adaptation. Finally, Section 2.4 presents the conclusions of the chapter.

2.1 Space-Time Linear Model

The received signal in a narrowband system affected by fading channel and Additive White Gaussian Noise (AWGN) is represented by a linear model. In OFDM, each subcarrier assumes flat fading and the received signal, as in narrowband systems, can be represented by

$$y = hs + w \ , \tag{2.1}$$

where s is the transmitted symbol, h is the channel response, and w is the noise component.

In multiple antenna processing, the signal model assumes a non-frequency selective channel. Thus, one single complex number characterizes every instant channel realization of each spatial link. The channel of a Single Input Single Output (SISO) configuration is described as one coefficient, $h_{\text{SISO}} = h$, whereas the Multiple Input Single Output (MISO) channel is represented by a row vector

$$\mathbf{h}_{\text{MISO}} = \begin{bmatrix} h_1 & h_2 & \dots & h_{N_t} \end{bmatrix} \ ,$$

and the Single Input Multiple Output (SIMO) channel assumes the form of a column vector:

$$\mathbf{h}_{\text{SIMO}} = \begin{bmatrix} h_1 & h_2 & \vdots & h_{N_r} \end{bmatrix}^T \ .$$

Finally, in the MIMO case, the channel is represented by the matrix:

$$\mathbf{H}_{\text{MIMO}} = \begin{bmatrix} h_{1,1} & h_{1,2} & \dots & h_{1,N_t} \\ h_{2,1} & h_{2,2} & \dots & h_{2,N_t} \\ \vdots & \vdots & \ddots & \vdots \\ h_{N_r,1} & h_{N_r,2} & \dots & h_{N_r,N_t} \end{bmatrix} .$$

In a multiple antenna receiver, the received signal in (2.1) becomes a linear combination of the transmit symbols multiplied by the channel coefficients and added the component of AWGN as follows:

$$\begin{aligned} y_p &= \sum_{q=1}^{N_t} h_{p,q} s_q + w_p \ , \\ \mathbf{y} &= \mathbf{H}\mathbf{s} + \mathbf{w} \ , \end{aligned} \tag{2.2}$$

where the column vectors for transmit, receive and noise signals are defined as

$$\mathbf{s} = \begin{bmatrix} s_1 \\ s_2 \\ \vdots \\ w_{N_t} \end{bmatrix} \ , \ \mathbf{y} = \begin{bmatrix} y_1 \\ y_2 \\ \vdots \\ w_{N_r} \end{bmatrix} \ , \ \mathbf{w} = \begin{bmatrix} w_1 \\ w_2 \\ \vdots \\ w_{N_r} \end{bmatrix} \ .$$

2.2 Beamforming and Spatial Diversity in OFDM Systems

Beamforming and spatial diversity are techniques that use multiple antennas in the downlink of a cellular system. While spatial diversity techniques deliver higher reliability to the wireless link, beamforming increases the signal strength toward a particular user.

In this section, we consider a MISO configuration of the spatial link, with N_t transmit antennas, and a single receive antenna. It is a reasonable choice for downlink cellular systems to place the complexity of handling multiple antennas at the transmitter side, especially for portable receivers, where current drain and physical size are important con-

straints.

The spatial correlation of the channel fading plays an important role in the performance of diversity and beamforming. In fact, the spatial diversity gain degrades when the antennas are correlated, whereas beamforming exploits highly correlated antenna elements.

This section presents an analysis of beamforming and spatial diversity in an OFDM system for different environments. The comparison is based on BER performance for various spatial channel correlations, as a result of angular spread conditions.

2.2.1 Beamforming

Traditionally, beamforming uses antenna arrays to increase the signal power toward the direction of the received or transmitted signal. The array of antenna elements is weighted in order to shape the radiation diagram of the antenna pattern [App76], as described in Appendix C. Here, we focus on transmit beamforming. Thus, the Direction of Departure (DoD), i.e., the direction of propagation of the wave from the transmitter, is the angle of interest. In a multiantenna transmission, data symbols are mapped to the antennas, and the signal at each antenna is weighted by a certain factor. In beamforming, the choice of weights depends on the algorithm used to optimize the radiation pattern. Here, the Minimum Mean Square Error (MMSE) criterion is used to compute the weights of the beamformer.

The computation of weights in beamforming requires the knowledge of the channel coefficients. In slowly time-variant fading, the channel of a downlink Time Division Duplex (TDD) system is estimated in the uplink frame without loss of performance. On the other hand, FDD systems require a feedback channel to obtain the channel estimate at the transmitter side, since the array response is frequency dependent.

In OFDM, downlink beamforming can be implemented either before or after the Inverse Discrete Fourier Transform (IDFT) operation, i.e., either in the frequency or time domain, respectively. The first scheme is referred to as a pre-IDFT downlink beamforming,

and the latter scheme is referred to as a post-IDFT downlink beamforming. Section 2.2.3 discusses the differences in each approach in a multiuser scenario.

The implementation of a beamforming system that tracks each terminal individually in an OFDM system has several constraints in terms of complexity. FDD systems require feedback to obtain the channel knowledge at the transmitter, and the MS mobility determines how frequent the update of the weights should be. Moreover, in frequency domain beamforming, the antenna weights are computed for each subcarrier (or group of subcarriers), greatly increasing the complexity.

A MIMO channel can be accessed through parallel pipes by employing the technique of Singular Value Decomposition (SVD). In such way, a vector of coefficients at the transmitter and at the receiver is used to perform an operation of beamforming. This type of beamforming creates parallel channels used for transmission, and the optimal power allocation is known as *water-filling*.

2.2.2 Spatial Diversity

While beamforming boosts the signal strength in a particular direction using an antenna array, antennas that are physically separated by a few wavelengths experience independent fading channels that can be used for diversity or multiplexing. Appendix D introduces the main space-time processing schemes.

STBC is an open loop transmit diversity scheme, where the diversity is achieved without the knowledge of the channel at the transmitter. STBC maps the data symbols into space-time domain to extract spatial diversity. The spatial rate of a code is defined by the number of symbols transmitted per channel use. Alamouti [Ala98] proposed a full diversity and rate one STBC for two transmit and one receive antennas. At each symbol duration, two data symbols are transmitted through the two transmitting antennas. Tarokh et al. [TJC99] proved that rate one and full diversity code are only achievable for 2×1 MIMO system, i.e., two transmitters and a single receiver, and proposed fractional rate and full diversity codes for four antenna space-time transmit diversity.

Channel use	Ant 1	Ant 2	Ant 3	Ant 4
T_n	s_n	s_{n+1}	s_{n+2}	s_{n+3}
T_n+1	$-s_{n+1}$	s_n	$-s_{n+3}$	s_{n+2}
T_n+2	$-s_{n+2}$	s_{n+3}	s_n	$-s_{n+1}$
T_n+3	$-s_{n+3}$	$-s_{n+2}$	s_{n+1}	s_n
T_n+4	s_n^*	s_{n+1}^*	s_{n+2}^*	s_{n+3}^*
T_n+5	$-s_{n+1}^*$	s_n^*	$-s_{n+3}^*$	s_{n+2}^*
T_n+6	$-s_{n+2}^*$	s_{n+3}^*	s_n^*	$-s_{n+1}^*$
T_n+7	$-s_{n+3}^*$	$-s_{n+2}^*$	s_{n+1}^*	s_n^*

Table 2.1: Half rate space-time encoding scheme

In this section, we apply the 1/2 rate orthogonal code for four antennas that transmits four symbols over eight channel uses. The transmitted symbol block is described in Table 2.1. At the receiver, the four symbols are obtained by combining the eight received signals as detailed in [TJC99].

The STBC algorithms assume a quasi-static fading channel, i.e., the channel is considered constant for the duration of the transmission block. This requirement can be hard to meet in high mobility environments. However, this impairment can be overcome by using the frequency domain, i.e., Space-Frequency Block Code (SFBC), especially designed to be used with OFDM systems, where the orthogonal codes are mapped into consecutive subcarriers. Consequently, the assumption for SFBC is that the subcarriers within the transmitted block have the same channel. SFBC provides diversity over frequency in time selective scenarios where the STBC proves inefficient [LW00]. The performance of SFBC erodes when the transmitted block is longer than the coherence bandwidth of the channel. However, due to the flexibility of the OFDM design, the subcarrier spacing can be shortened, according to the frequency selectivity of the scenario, by increasing the number of subcarriers.

2.2.3 Space-Frequency or Space-Time Processing and Scheduling

This section discusses feasibility issues of the resource allocation of the OFDM frame in multiuser systems, combined with beamforming and spatial diversity. The scheduler assigns the OFDM subcarriers and symbols to the users based on the channel conditions

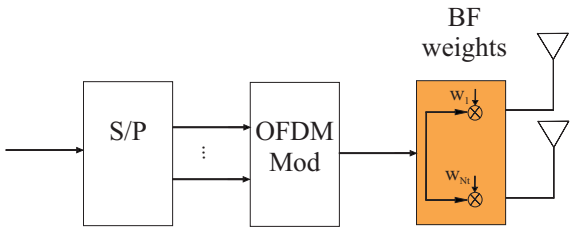

Figure 2.1: Time domain beamforming in OFDM

or on blind hopping patterns.

In time domain scheduling, each OFDM symbol is allocated to one user at a time, Time Division Multiple Access (TDMA). The beamformer determines the radiation pattern to the user allocated to that time slot. In such system, all the subcarriers are used by one user at a given OFDM symbol, thus, a post-IDFT beamformer is recommended. Figure 2.1 shows the block diagram of the time domain beamforming. After the IDFT operation in the transmitter, the time domain signal is transmitted through a wideband beamformer, e.g., a multi-tap beamformer. In order to implement spatial diversity in a TDMA system, the STBC requires that the block of symbols is allocated to one user only. For codes with high number of channel uses, the SFBC permits more flexibility, as it is implemented across OFDM subcarriers [RG97].

In an Orthogonal Frequency Division Multiple Access (OFDMA) system, the scheduler allocates the available subcarriers to the users at each OFDM symbol. The pre-IDFT beamformer allows the system to steer the beams to each user independently in OFDMA. Figure 2.2 shows the frequency domain beamforming implemented on the OFDM subcarriers with blocks of weights for each antenna. Since in OFDM each subcarrier experiences a narrowband single-tap channel, narrowband beamformers can be applied.

However, the number of beams is constrained by the number of transmit antennas that dictate the degrees of freedom of the beamformer. If a large number of users is uniformly distributed over the cell, then the beamforming technique fails at steering the beams toward each user. A possible solution is to create clusters of users who are co-located by spatially grouping the users that are close to each other. In addition to spatial clustering, the scheduling algorithm can also constrain the number of users allocated per

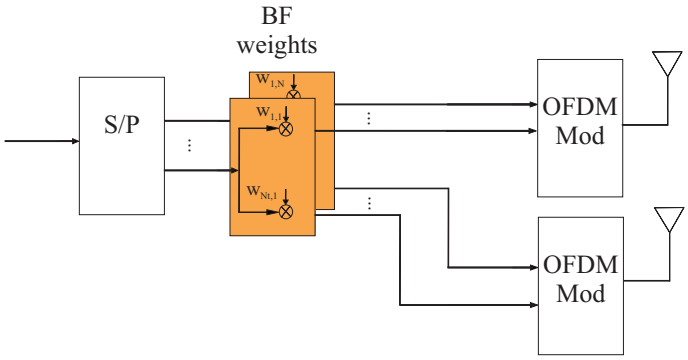

Figure 2.2: Frequency domain beamforming in OFDM

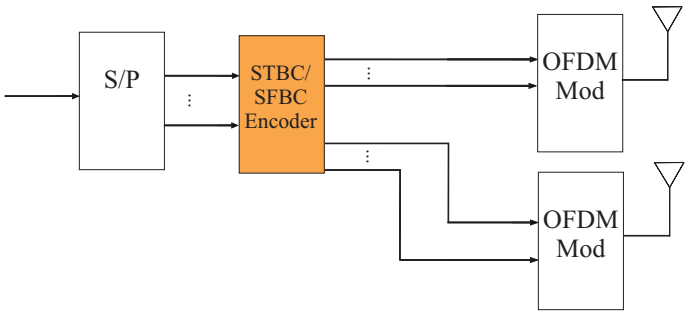

Figure 2.3: STBC and SFBC in OFDM

time slot, and separate the allocation in frequency and time domains. The BS steers the beam that covers the users in that set and avoids interference to other directions in the cell.

If the subcarrier allocation is kept static for at least T OFDM symbols, STBC can be implemented for each narrowband subcarrier. Otherwise, SFBC can also be applied, if the users are allocated contiguous subcarriers, and the number of subcarriers assigned to one user is a multiple of the code block size. Figure 2.3 depicts the implementation of STBC or SFBC encoding in the transmitter of OFDM.

2.2.4 Results

To compare beamforming and spatial diversity, indoor micro-cell and outdoor macro-cell scenarios are considered for the downlink of a single-user scenario. The simulator was developed as an extension of the MATLAB software for OFDM performance simulation

provided in [HT01]. For indoor channel delay profiles, we applied HiperLan/2 channel model A, with a Power Delay Profile (PDP) corresponding to a typical office environment for Non Line of Sight (NLOS) conditions and 50 ns average Root Mean Square (RMS) delay spread [MS98]. For outdoor delay profiles, we use typical urban 12-path channel model [Pat03, Appendix-E].

The parameters selected for simulations are based on the IEEE 802.11a standard. The system bandwidth is 20 MHz at a carrier frequency 5 GHz. The frequency selectivity of the outdoor channel is higher than the indoor channel. Therefore, the OFDM design is adapted to each environment. With a larger coherence bandwidth, the indoor scenario is simulated with an OFDM system with 64 subcarriers, a length of CP of 16 samples, and a symbol duration of 4 μs. For indoor we consider a user velocity of 3 km/h, a maximum delay spread lower than 0.5 μs, and a maximum angular spread of 360° [PP97]. The outdoor scenario uses an OFDM setup of 1024 subcarriers, users with the speed of 50 km/h, maximum delay spread of 5 μs, and maximum angular spread of 20° [PP97]. We assume that the synchronization requirement of the OFDM receiver is perfectly met, and the transmit beamforming weights are computed based on the uplink frame of a TDD system or via a delay and error-free feedback channel in an FDD system.

2.2.4.1 Spatial Correlation

Angular spread is a measure of the angular dispersiveness of the wavefront of the signal between the transmitter and the receiver. The angular spread is usually high in an indoor scenario, owing to the proximity of scatterers, and low in an urban scenario.

A low angular spread limits the available spatial diversity, therefore beamforming is more appropriate to use. On the other hand, in indoor channels, due to a broader angular spread, spatial diversity can effectively exploit the uncorrelated signals.

For transmit diversity, the physical separation between antenna elements is assumed five times the wavelength, 5λ. A large separation makes the antenna elements uncorrelated, and it is feasible at the BS due to lower constraints on size. The implementation of

beamforming requires the antenna elements to be placed closely, i.e., the wavefront should be phase-coherent over the antenna aperture. Hence, we use a spacing of $\lambda/4$, which is a common value considered in literature within the correlation condition of $d < \lambda/2$.

In the wideband signal, the L multipath signals depart from the array with different angles. As shown in Appendix C, the signal vector representation is the sum of all signals shaped by the steering vector, $\mathbf{a}(\theta_l)$, in (C.1) [Ven03].

The spatial-temporal fading channel is modeled with the correlated fading coefficients of the N_t antenna elements of the l tap in accord with [SLWR01]

$$\mathbf{h}_l^R = \mathbf{R}^{1/2}\mathbf{h}_l \ ,$$

where $\mathbf{h}_l$ is the channel vector with N_t independent coefficients. The spatial covariance matrix $\mathbf{R}$ is given by

$$\begin{aligned} \mathbf{R} &= \frac{1}{L}\sum_{l=1}^{L}\mathbf{a}^H(\theta_l)\mathbf{a}(\theta_l) \ , \\ \mathbf{a}(\theta_l) &= [1, \exp(j\alpha_l), \ldots, \exp(j(N_t-1)\alpha_l)] \ , \\ \alpha_l &= \frac{2\pi}{\lambda} d \sin\theta_l \ , \end{aligned}$$

where $\mathbf{a}(\theta_l)$ is the steering vector dependent on azimuth direction θ_l of the l^{th} signal. The steering vector is the N_t-dimensional complex vector containing the responses of the antenna elements to a narrowband source of unit power [God04].

2.2.4.2 BER Performance

This section presents the results of uncoded BER for transmit diversity and frequency domain beamforming for various values of angular spread in a single-user OFDM system. Spatial diversity is obtained with the orthogonal half rate STBC for four antennas. STBC is used in the indoor scenario, while the diversity for outdoor scenario is obtained with SFBC. The results are obtained with Quadrature Phase Shift Keying (QPSK). The

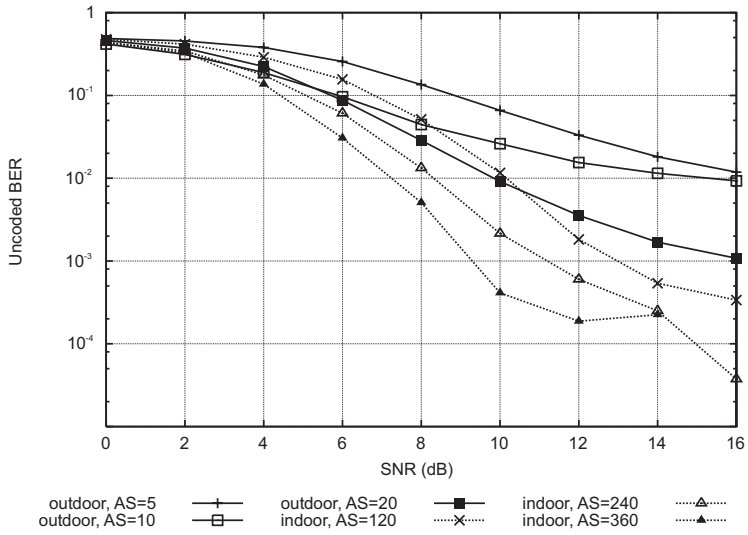

Figure 2.4: BER performance of transmit diversity for different angular spread

angular spread considered for indoor environment is 120°, 240°, and 360°, whereas for outdoor environment is 5°, 10°, and 20°.

Figure 2.4 illustrates the BER curves for the transmit diversity configuration in outdoor (SFBC) and indoor (STBC) scenarios. The high angular spread of indoor scenarios, combined with the low mobility, presents STBC as the best technique. In fact, the high angular spread induces a low correlation of the antennas, and the low mobility makes the channel quasi-static, necessary conditions for the STBC to exploit diversity. In outdoor scenarios, owing to a high mobility of the MS, STBC is not effective due to the loss of quasi-static characteristic of the channel. Therefore, SFBC is used for outdoor. In outdoor, the BER curve presents an error floor at high SNR on account of the high frequency selectivity of the channel.

Figure 2.5 shows the BER performance of transmit diversity and beamforming techniques in indoor scenarios, while Figure 2.6 presents the results for outdoor scenarios. Beamforming provides a robust performance at lower angular spread values. The spatial diversity increases consistently the performance in terms of BER as the angular spread widens both in indoor and outdoor environments. Transmit diversity outperforms beamforming in indoor scenarios with very high angular spread, but otherwise the array gain of

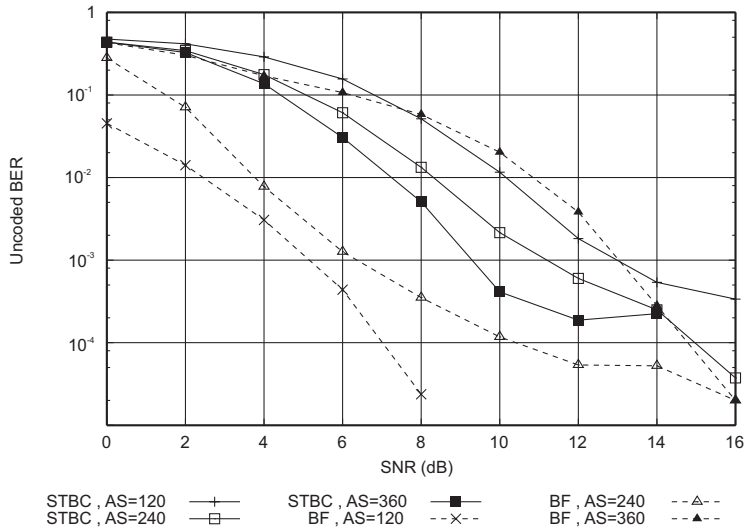

Figure 2.5: BER performance of beamforming and STBC for indoor channel

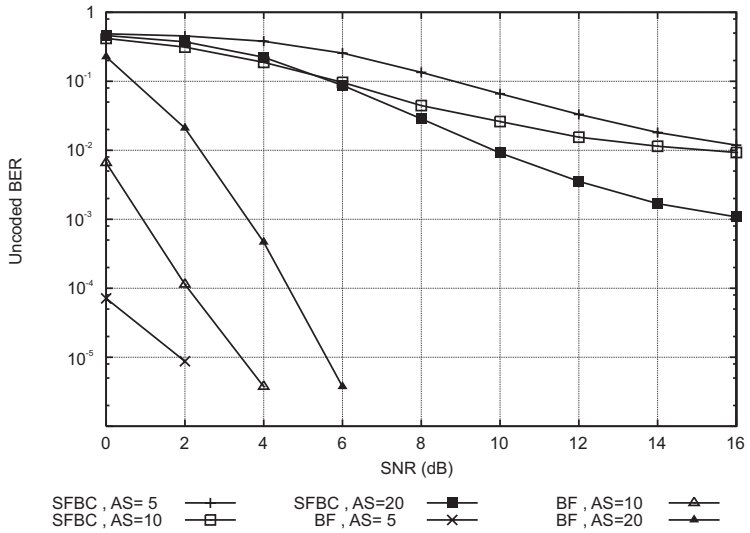

Figure 2.6: BER performance of beamforming and SFBC for outdoor channel

beamforming delivers better performance. Although the strength of beamforming comes at the cost of a higher complexity, the advantage in outdoor scenarios suggests its implementation in macro cells.

2.2.5 Summary

This section provided an insight into the performance of spatial diversity and beamforming in different wireless environments. We have discussed frequency and time domain approaches for transmit diversity and beamforming in OFDM-based systems. Results show that STBC is more suitable for indoor environments with high angular spread, whereas in outdoor scenarios, the array gain of beamforming is more effective than diversity.

2.3 MIMO and Rate Adaptation in OFDM

This section presents a general framework for space-frequency coding in OFDM systems and analyzes the potential of link adaptation over such systems. As discussed before, in OFDM systems, the same design applied to STBC can be used to encode signals in space and frequency domains (SFBC).

SM is a simple technique to transmit parallel streams over a MIMO link that achieves full spatial rate, i.e., the symbols transmitted per channel use equal the number of transmit antennas. However, SM does not include any sort of transmit diversity, and the number of receive antennas must be higher than the number of transmit antennas for the decoder to recover the streams. Linear Dispersion Codes (LDC) are high rate coding schemes that can handle any configuration of transmit and receive antennas and have SM and STBC as special cases. LDC uses a linear matrix formulation framework to transmit codewords that are a linear combination of dispersion matrices [HH02]. Many authors have studied LDC potential given the freedom of the code design [HJP02]. The authors in [Bar04] and [LZW06] have independently derived necessary and sufficient conditions for a full rate LDC to achieve minimum BER with linear receivers, also known as Unitary Trace Orthogonal Design (UTOD).

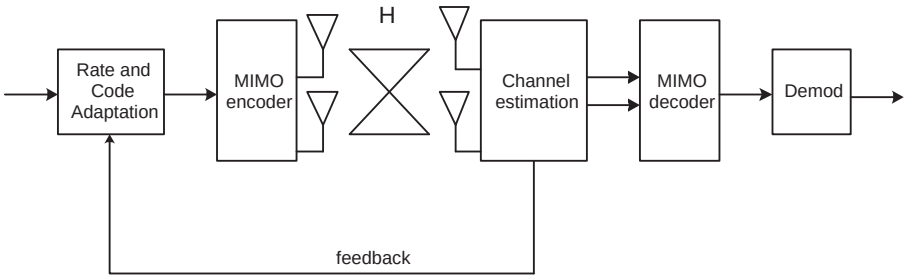

Figure 2.7: System model with MIMO and AMC

Schemes that adapt the transmission parameters to the varying channel conditions considerably increase the spectral efficiency of the channel, and have as well received special attention from researchers in recent years [CG01, CEGHJ02]. AMC systems, in particular, provide substantial gains in performance with relatively low complexity and reduced feedback overhead.

Although AMC and MIMO techniques have been proposed for several systems, e.g., 3GPP E-UTRA air interface [3GP06a], the interaction between the new MIMO encoding schemes and link adaptation is still an open issue. In this section, we study the performance and impact of an LDC design in a practical system. In particular, we focus on the effect of linear receivers and link adaptation in the performance of the class of UTOD. The results are compared against two well-known open-loop multiantenna techniques that exploit spatial diversity, SFBC, and multiplexing, SM.

2.3.1 System Model

The system model considered in this section consists of an OFDM-based system combined with a MIMO and AMC blocks, as shown in Figure 2.7. The system is implemented with the simulator described in Appendix G. The MIMO configuration considers N_t transmit antennas and N_r receive antennas. We assume the downlink channel and an SFC encoder that maps the data symbols to antennas and OFDM data subcarriers at the transmitter. Section 2.3.2 describes the set of encoding schemes considered for the multiple antenna system following an LDC framework.

The system works at a carrier frequency of 2 GHz, and uses 10 MHz bandwidth.

The PDP of the channel is modeled with the Six Taps Vehicular A Channel described in [3GP07], and the speed of 3 km/h. The link adaptation scheme selects the Modulation Code Schemes (MCS) level based on the long term average channel gain, assumed known at the transmitter. The implementation of the link-level simulator is described in Appendix G.

2.3.2 Linear Dispersion Codes Model

The data stream of N_s symbols is transmitted over T channel uses. In this case, the MIMO encoding is performed over consecutive subcarriers, i.e., SFC. When dealing with linear dispersion processing, each symbol $\mathbf{s}_v$ is encoded with a matrix C_v of size $[N_t \times T]$, as follows [HH02]:

$$\mathbf{S} = \sum_{v=1}^{N_s} \mathbf{s}_v C_v \ .$$

The encoding matrices can also be decoupled into real and imaginary parts to allow a higher degree of freedom,

$$\mathbf{s}_v = \alpha_v + j\beta_v \ ,$$
$$\mathbf{S} = \sum_{v=1}^{N_s} \alpha_v A_v + j\beta_v B_v \ .$$

We assume a flat fading wireless channel at each subcarrier, and that the channel coefficients remain constant over the N_s subcarriers of the encoding block. By extending the MIMO linear model in (2.2), the received signal can be constructed by grouping in the same received signal matrix, $\mathbf{Y}_{[N_r \times T]}$, the T consecutive received signal vectors of size $[N_r \times 1]$. The block fading channel MIMO model can be expressed by

$$\mathbf{Y} = \sqrt{\frac{E_s}{N_t}}\mathbf{H}\mathbf{S} + \mathbf{W} \ , \tag{2.3}$$

where E_s is the transmitted signal power, $\mathbf{H}$ is the channel coefficients matrix, and $\mathbf{W}$ is the matrix with T noise vectors.

Such system model generalizes the design of space-frequency transmission schemes, such that it is possible to represent the well known Alamouti or SM schemes in the same framework. The 2×2 MIMO configuration for Alamouti scheme is obtained with the following dispersion matrices:

$$A_1 = \begin{bmatrix} 1 & 0 \\ 0 & 1 \end{bmatrix}, \quad B_1 = \begin{bmatrix} 1 & 0 \\ 0 & -1 \end{bmatrix},$$
$$A_2 = \begin{bmatrix} 0 & 1 \\ -1 & 0 \end{bmatrix}, \quad B_2 = \begin{bmatrix} 0 & 1 \\ 1 & 0 \end{bmatrix},$$
$$\mathbf{S} = \begin{bmatrix} \mathbf{s}_1 & \mathbf{s}_2 \\ -\mathbf{s}_2 * & \mathbf{s}_1^* \end{bmatrix},$$

while SM is represented by

$$C_1 = \begin{bmatrix} 1 & 0 \\ 0 & 0 \end{bmatrix}, \qquad C_2 = \begin{bmatrix} 0 & 1 \\ 0 & 0 \end{bmatrix},$$
$$C_3 = \begin{bmatrix} 0 & 0 \\ 1 & 0 \end{bmatrix}, \qquad C_4 = \begin{bmatrix} 0 & 0 \\ 0 & 1 \end{bmatrix},$$
$$\mathbf{S} = \begin{bmatrix} \mathbf{s}_1 & \mathbf{s}_2 \\ \mathbf{s}_3 & \mathbf{s}_4 \end{bmatrix}.$$

The equivalent form of the encoded symbol matrix can be simplified with the vector operation for matrices, as follows:

$$\text{vec}(\mathbf{S}) = \mathbf{F}\mathbf{s},$$
$$\mathbf{F} = \begin{bmatrix} \text{vec}(C_1) & \dots & \text{vec}(C_{N_s}) \end{bmatrix}.$$

Applying this representation to the block fading model (2.3), one obtains:

$$\begin{aligned}\mathbf{y} &= \sqrt{\frac{E_s}{N_t}}\left(\mathbf{I}_T \otimes \mathbf{H}\right)\mathbf{F}\mathbf{s} + \mathbf{w} \\ &= \sqrt{\frac{E_s}{N_t}}\mathbf{H}_{eq}\mathbf{s} + \mathbf{w} \ , \end{aligned} \tag{2.4}$$

where $\mathbf{y} = \mathrm{vec}(\mathbf{Y})$, $\mathbf{w} = \mathrm{vec}(\mathbf{W})$, $\mathbf{H}_{eq} = \left(\mathbf{I}_T \otimes \mathbf{H}\right)\mathbf{F}$, and $\otimes$ denotes the Kronecker product.

The design of the encoding matrices that process the data symbols to the transmit antennas affects the performance of the MIMO system. We consider that instantaneous and complete channel knowledge is not available at the BS, hence the focus is given to blind techniques.

An LDC design is referred to as UTOD when satisfies the conditions:

$$\begin{aligned}\mathrm{tr}\left(A_k^* A_l\right) &= \delta_{kl} \ , \\ A_k^* A_l &= \frac{1}{N_t}\mathbf{I}_{N_t} \ , \end{aligned}$$

where the trace of a matrix is denoted by tr(.). These codes are capacity lossless, i.e., deliver full spatial rate, and ensure the minimum BER performance in the class of linear receivers [Bar04].

Various methods to generate matrices that satisfy these conditions have been proposed in literature [DTB02, HH02, Bar04]. Here, we use the method given in [HH02], where a generalization to any number of transmit antennas is obtained by defining the encoding matrices as

$$C_{N_t(k-1)+l} = \frac{1}{\sqrt{N_t}} D^{k-1}\Pi^{l-1}, \qquad k = 1, \ldots, N_t, \quad l = 1, \ldots, N_t \ ,$$

where

$$D = \begin{bmatrix} 1 & 0 & \dots & 0 \\ 0 & e^{j\frac{2\pi}{N_t}} & & \\ \vdots & & \ddots & \\ 0 & & & e^{j\frac{2\pi(N_t-1)}{N_t}} \end{bmatrix} \quad , \quad \Pi = \begin{bmatrix} 0 & \dots & & 0 & 1 \\ 1 & 0 & & & \vdots \\ 0 & 1 & 0 & & \\ \vdots & & \ddots & \ddots & \vdots \\ 0 & \dots & 0 & 1 & 0 \end{bmatrix} .$$

The spatial streams of the LDC can be decoded if the system of equations of the linear model in (2.4) is determined. This condition is met if $N_s \leq N_t T$. Thus, any MIMO decoding technique can be employed, such as linear or iterative techniques. In this work, the focus is given to linear techniques, in particular to the MMSE receiver that estimates the transmitted symbol as

$$\tilde{\mathbf{s}} = \sqrt{\frac{N_t}{\rho^a}} \left(\mathbf{H}_{eq} \mathbf{H}_{eq}^H + \frac{N_t}{\rho^a} \mathbf{I}_{N_t} \right)^{-1} \mathbf{H}_{eq}^H \mathbf{y} \ , \tag{2.5}$$

where ρ^a is the SNR per receive antenna.

2.3.3 Performance of LDC

The assumptions for the simulations are based on the 3GPP LTE specifications for the physical layer [3GP06a]. We consider a MIMO baseline configuration of two antennas at transmitter and receiver. The multiantenna techniques taken into account are Orthogonal SFC (Alamouti), LDC-UTOD, and SM. The receiver in SM and LDC modes is a linear MMSE detector. In this approach, a point-to-point MIMO environment is assumed for the simulations, leaving the scheduler interactions at an independent layer.

The comparison of full spatial rate MIMO encoding schemes (SM and LDC) with rate one Alamouti scheme under fair throughput is essential to understand the potential of LDC. Considering a MIMO 2×2 configuration, a full rate scheme encodes twice the number of bits than a rate one technique. Thus, for a fair throughput comparison, when LDC and SM schemes use a 2-bit modulation, QPSK, Alamouti scheme needs to employ a

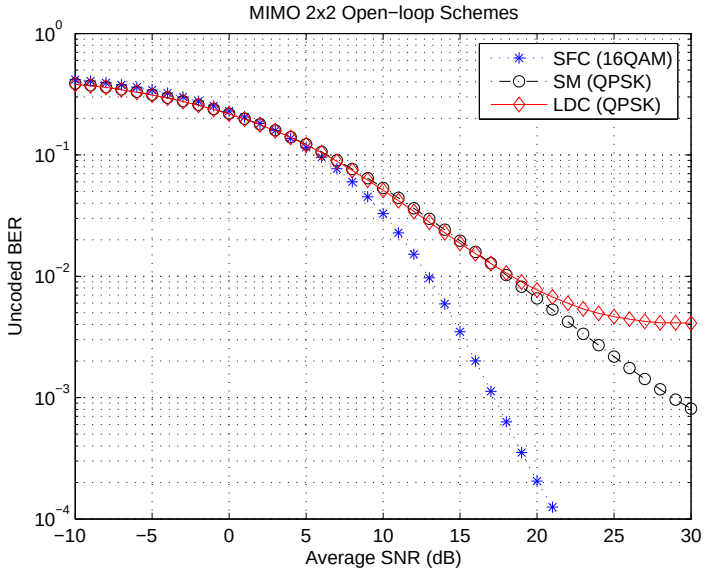

Figure 2.8: Uncoded BER in MIMO 2×2 configuration. SFC uses 16QAM, while LDC and SM use QPSK

4-bit modulation, 16-QAM, to achieve the same number of bits transmitted in one resource block. The following results are obtained using a fixed modulation order for each MIMO scheme.

Figure 2.8 depicts the performance in terms of uncoded BER. Although LDC is superior to SFC in the low SNR range, it shows no diversity effect in the slope of the curve. In fact, the diversity order of the MMSE receiver is $N_t - N_r + 1$ [FB06]. Furthermore, at high SNR range LDC suffers a BER floor, being outperformed by the two other techniques in this region. The LDC transmits a linear combination of two symbols at a given resource block, antenna and subcarrier. This inter-stream interference, not present in the other schemes, is contributing for the BER floor observed in LDC performance.

Taking into account the channel coding and a target Block Error Rate (BLER) of 20%, Figure 2.9 depicts the spectral efficiency of the system. LDC shows a performance tradeoff between SFBC and SM, suggesting that it can be a good compromise for a robust high rate MIMO encoding scheme. However, this is true only for low order modulations.

The BER floor observed for LDC with linear receiver at high SNR has higher impact on large and more dense modulations. Thus, it is important to study the spectral efficiency

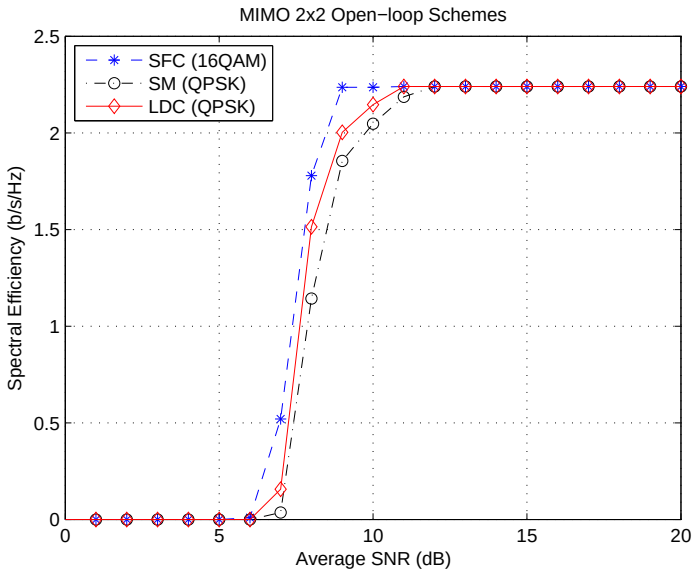

Figure 2.9: Spectral efficiency in MIMO 2×2 with fixed modulation. SFC uses 16-QAM, while LDC and SM use QPSK

in scenarios where larger modulations are available for transmission, such as the link adaptation case.

Figure 2.10 shows the spectral efficiency obtained for a MIMO 2×2 with nine MCS. Comparing SFC and SM, we verify that SFC achieves the best performance at poor channel conditions, but at higher SNR, SM outperforms in terms of throughput due to the full spatial rate feature. Although LDC follows the performance of SFBC at low SNR, and achieves higher throughput at higher SNR; unlike SM, LDC fails to deliver full spatial rate in good channel conditions. To sum up, in a system with equal number of receive and transmit antennas while employing a linear receiver, LDC suffers a significant drawback due to the BER floor.

The loss in performance of LDC at high modulation orders can be compensated by increasing the number of receive antennas, thus allowing gains in the diversity order, and reducing the BER floor level. Figure 2.11 shows the BER for a 2×4 MIMO system. Due to lower modulation and increased diversity, LDC outperforms both SFBC and SM in the same region of analysis as seen in Figure 2.8. In order to show this effect in link adaptation, Figure 2.12 presents the spectral efficiency curve for a system with four receive

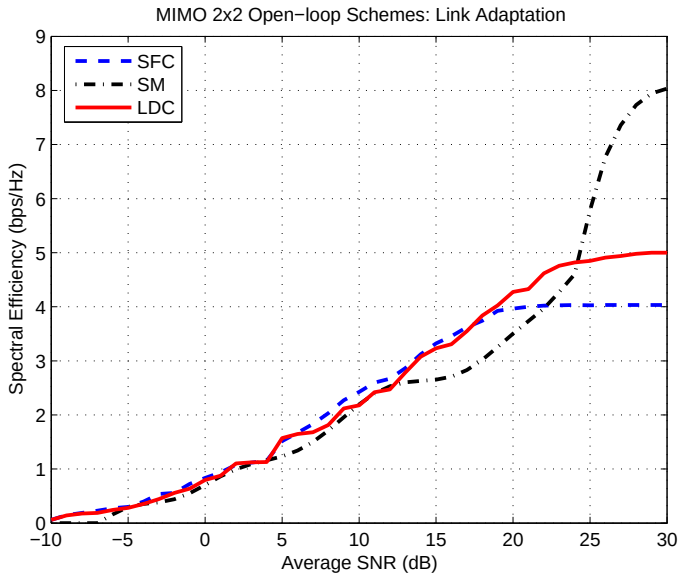

Figure 2.10: Spectral efficiency in MIMO 2×2 with link adaptation

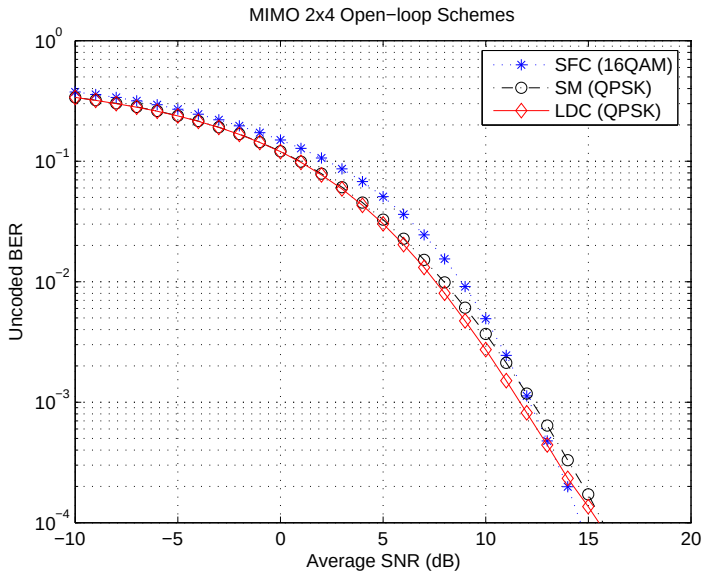

Figure 2.11: Probability of bit error of an uncoded system in MIMO 2×4 with fixed modulation. SFC uses 16QAM, while LDC and SM use QPSK

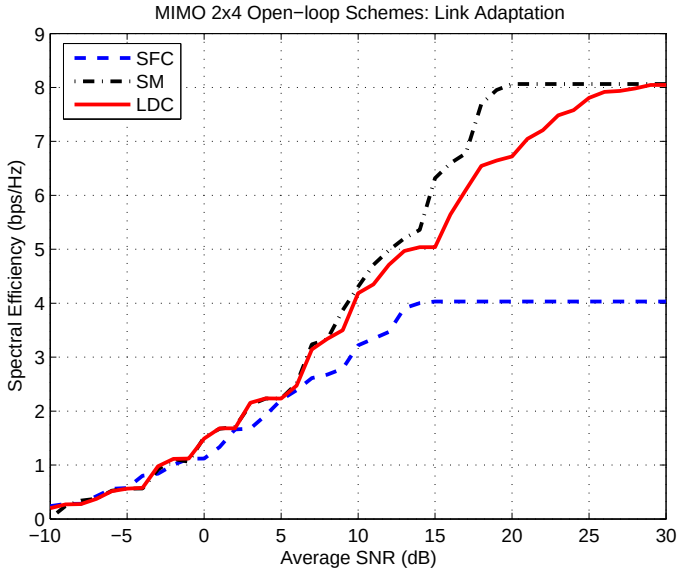

Figure 2.12: Spectral efficiency in MIMO 2×4 with link adaptation

antennas. Although LDC now achieves the full spatial rate at high SNR, it still suffers a loss compared to SM at high modulation orders.

2.3.4 Summary

This section evaluated the potential of LDC in a practical MIMO implementation. We compared the spectral efficiency of different MIMO techniques and AMC in terms of diversity and multiplexing. LDC increases the degrees of freedom to develop MIMO mapping schemes aiming at multiplexing and diversity gains. However, with linear receivers these designs have constraints that need to be evaluated. In particular, we compare the performance of full rate LDC-UTOD with Alamouti and SM, under fair throughput conditions, in order to assess the interaction between link adaptation and LDC. Results show that UTOD is optimized for low modulation orders and higher number of receive antennas, slightly outperforming the other schemes studied in low SNR conditions. Whereas for dense modulations, SM outperforms UTOD at high SNR. Nevertheless, we show that an increase in the number of receive antennas can dramatically improve the spectral efficiency of the system in strong channel conditions.

2.4 Conclusions

This chapter compared different approaches and gains of multiantenna techniques in OFDM transmissions and combined them with link adaptation. Beamforming and spatial diversity are designed for different channel characteristics and special issues need to be considered when implementing each technique with OFDM.

Although LDC potentially provides higher gains with complex receivers, we combine the full rate LDC code UTOD with a linear receiver to obtain a practical tradeoff between spatial diversity and multiplexing. In this context, we show that UTOD, combined with channel coding and AMC, proves to be a robust MIMO technique at low and mid-range SNR, below 20 dB. However, the UTOD scheme only achieves the high SNR throughput of SM by increasing the number of receivers in a MIMO configuration 2×4.

The link adaptation used in the second part of this chapter requires a CSI which was considered to be error-free. In a practical scenario, however, the channel knowledge obtained via feedback is not perfect. Chapter 3 focuses on the downlink adaptive transmission of a MIMO spatial link for further investigation on the inaccuracy of feedback channel information due to delay.

Chapter 3

Feedback Delay in Rate Adaptive MIMO

Schemes that adapt the transmission parameters to the varying channel conditions increase significantly the spectral efficiency of the channel. Particularly, rate adaptive systems provide substantial gains in performance with relatively low complexity, and reduced feedback overhead [CEGHJ02, CG01].

In recent years, several authors have dedicated their research to analytical studies of the performance of rate adaptive systems under feedback delay. Increasing the number of bits in the modulated symbol boosts the data rate, thus it is wise to choose a more dense modulation in favorable channel conditions. An adaptive multi-level QAM mechanism is of interest for a system that adjusts the data rate based on CSI [AG00]. The recent surge of interest in multiple antenna techniques rose the importance of studying the analytical performance of adaptive M-QAM systems combined with STBC, as in [KT03], or SM, as in [DB05].

Although rate adaptation provides performance gains in varying channel conditions, the channel information required by this technique becomes outdated when the channel is changing rapidly. A study on channel prediction and impact of outdated estimates in time-varying channels is presented in [Goe99].

In scenarios where the feedback is subject to delays, channel prediction uses the fading statistics to increase the reliability of the CSI. The authors in [Ekm02, Hol02] derived closed-form approximations of the BER performance in SISO systems with a power predictor.

This chapter studies the impact of feedback delay in discrete rate adaptation. We obtain new closed-form analytical expressions for BER, and propose SNR switching thresholds that take into account the channel uncertainty. Furthermore, we derive closed-form expressions for the BER performance of the system for MIMO diversity and multiplexing, as well as a tractable BER expression for AS.

The chapter is outlined as follows. Section 3.1 describes the system model and evaluates the performance of rate adaptation combined with different antenna diversity methods over Rayleigh channel through a statistical perspective. In the light of the feedback delay, Section 3.2 derives analytical performance measures to analyze the effect of outdated channel information and proposes an approach to calculate switching thresholds for the rate adaptive system. Section 3.3 analyzes the impact of channel prediction error on the BER performance for MIMO diversity, multiplexing, and Antenna Selection (AS). Section 3.4 shows the loss when the adaptation does not take into account the delay or MIMO scheme employed for transmission. Finally, Section 3.5 presents the conclusions of the chapter.

3.1 Link and System Implications from Outdated Feedback

This section describes the rate adaptive system for a multimode MIMO system over a Rayleigh fading channel. This system is assumed in Sections 3.2, 3.3, and 3.4.

The system model in Figure 3.1 represents the link-level of the downlink of a cellular system. The transmitter selects the QAM level to modulate data, as described in Appendix E.1, and maps the symbols to the available antennas in the MIMO encoder. The channel estimation is assumed to be perfect at the receiver. Then the terminal communicates the SNR in the CSI format via the feedback channel to the transmitter. On the

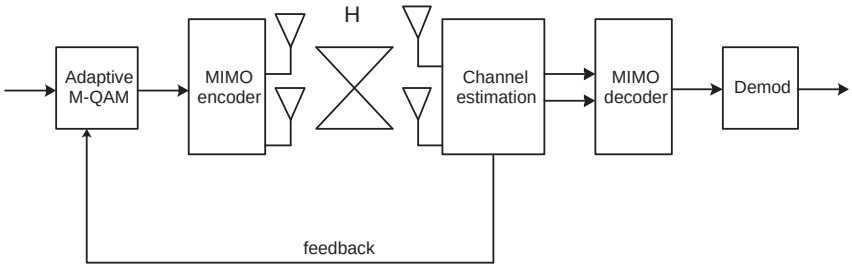

Figure 3.1: System model of MIMO and adaptive modulation

basis of the CSI, the system selects the rate, i.e., the constellation size of the modulation to be transmitted.

The wireless channel is characterized by a flat Rayleigh fading channel. A different number of antennas at transmitter and receiver ends is assumed according to the MIMO configuration. The spatial links experience independent fading; thus, no correlation exists between channel gains. The MIMO diversity mode considers STBC at the transmitter and MRC at the receiver side. The SM mode employs a Zero Forcing (ZF) receiver to decode the parallel streams, and the AS mode applies feedback information to choose the proper transmit antenna.

As seen in Section 2.1, the narrowband linear model of the received signal is represented by

$$\mathbf{y} = \mathbf{H}\mathbf{s} + \mathbf{w} \ ,$$

where $\mathbf{H}$ is the $[N_r \times N_t]$ matrix of complex Gaussian channel coefficients with variance $\sigma^2_{\mathbf{h}}$, $\mathbf{s}$ is the transmitted signal with energy E_s, and $\mathbf{w}$ is the AWGN vector with power N_0.

For the SISO configuration, the CSI feedback is based on the SNR measured at the receive antenna. However, due to the independency of the MIMO channels, the SNR at each receive antenna provides insufficient information for the rate adaptation of the transmission. The decision must be based on the post-processing SNR, i.e., after the MIMO decoding, to account for the type of MIMO scheme. The post-SNR statistics of the MIMO techniques are described in Appendix D.3.

The delay between the time that the MS measures the channel and the time that the BS applies that information to send the signal in downlink is referred to as feedback delay.

The rate adaptive scheme consists of a discrete M-QAM adaptation with a constant transmit power and a BER constraint of BER_t as described in Appendix E.1. In a practical system, the SNR thresholds are found through measurements and building an extensive look-up table, compensating for the effect of outdated CSI. However, this approach not only increases the complexity of the system, but it also loses the generalization of the model. This chapter aims at providing an analytical framework of the feedback delay effect in Rayleigh fading channels. Therefore, we opt for analytical performance measures to assess the degradation of the rate adaptive system combined with MIMO.

In order to reduce the uncertainty of the CSI in the presence of feedback delay, Section 3.3 considers a prediction algorithm for the rate adaptive system. As detailed in Appendix F.1, the predictor estimates the channel power within a time horizon based on a regressor vector, i.e., a buffer with the observed past channel coefficients.

In the following, we present a preliminary evaluation of the outdated channel knowledge received via feedback on different multiantenna techniques and multiuser scheduling.

3.1.1 Preliminary Evaluation of Outdated Channel

This section presents a preliminary study about the outdated CSI based on the time correlation statistics. We evaluate the analytical throughput of a two level M-QAM adaptation combined with different multiple antenna techniques over Rayleigh fading channel.

In a time-varying channel, the time correlation is a measure that describes the variation of the channel coefficients at time n and after a time delay of τ. As described in Appendix A.2.1, when considering the Jakes model [JC94], the correlation between two channel samples separated by a delay of τ is given by $\rho = J_0(2\pi f_d \tau)$, where f_d is the maximum Doppler frequency. One can calculate the distribution of the delayed channel, $\mathbf{h}_\tau = \mathbf{h}(n+\tau)$, based on $\mathbf{h} = \mathbf{h}(n)$. In [Goe99], the author shows that for a Rayleigh

channel, where the channel coefficients follow a complex Gaussian distribution with mean μ and variance σ^2, the delayed channel $\mathbf{h}(n+\tau)|\mathbf{h}(n)$ also has a complex Gaussian distribution with mean $\mu = \rho\mathbf{h}(n)$ and variance $\sigma^2 = 1-\rho^2$. In this preliminary approach, this distribution is then used to generate the delayed channel coefficients available through feedback, i.e., the value of the channel gain at the time n_2 assuming that the channel information available was measured at instant $n_1 = n_2 - \tau$.

The rate adaptation module considers two M-QAM levels, namely QPSK and 16-QAM, and the average SNR at the transmitter is 10 dB. The Rayleigh channel coefficients are generated independently for each spatial link.

This link-level approach considers a single cell scenario and a point-to-point MIMO link. The multiantenna techniques analyzed are STBC, AS, and MRC. The post-processing SNR, defined by γ, is described for each considered MIMO scheme in Appendix D.3.

On the basis of the post-processing SNR, we compute analytically the spectral efficiency of an uncoded M-QAM transmission and a packet size of $L_p = 50$ symbols, according to $\eta = \log_2(M)(1 - BER(\gamma))^{L_p}$. As mentioned in Appendix B, the expression for uncoded BER performance of square M-QAM with Gray bit mapping over AWGN is approximated with [Pro01]

$$BER(M,\gamma) \approx \frac{2}{\log_2 M}\left(1 - \frac{1}{\sqrt{M}}\right)\operatorname{erfc}\left(\sqrt{1.5\frac{\gamma}{M-1}}\right) \quad , \tag{3.1}$$

where $\operatorname{erfc}(z) = \frac{2}{\sqrt{\pi}}\int_z^\infty e^{-t^2}dt$.

A multiuser scheduler based on CSI is sensitive to the feedback delay. We use a max-SNR scheduler that assigns the transmission to the user with the highest SNR at a given slot, as described in Appendix E.2. Although the fast fading experienced by each user is independent, we assume that all users have the same average SNR level, thus avoiding fairness issues.

Based on the time length considered for frame duration, in the order of 1 ms, two lengths for the feedback delay are considered, *regular* and *fast feedback*. The regular feed-

back channel suffers a delay within 0.5 and 1 ms, and is employed in the rate adaptation. On the other hand, AS utilizes a fast feedback channel with delays between 0.1 and 0.5 ms. Behind this assumption lies the fact that in the system perspective, it is not feasible to change the modulation of a transmission within a shorter period than a frame duration, since the receiver has to be aware of the change to decode the modulated symbols. On the other hand, a change in the transmitting antenna can be done at the BS without the need of informing the receiver; thus, it is transparent to the terminal and can be performed faster.

3.1.1.1 Results

Results for a single-user system are presented in Figure 3.2. Figure 3.2(a) depicts the spectral efficiency versus user mobility when ideal CSI is available at the BS, i.e., no feedback delay. The user speed does not affect performance, since the delay is assumed instantaneous. As the results are statistical observations of the SNR distribution, the degradation of STBC due to variation of the channel in consecutive symbols is not observed. The scheme with two receivers implements MRC and achieves the highest performance, due to the combination of array and diversity gains. The transmit diversity schemes with two and four antennas apply STBC, and exploit diversity gain. AS scheme outperforms both STBC configurations due to the gain obtained by the use of the feedback information.

Considering a fast feedback channel with 0.5 ms delay and a regular feedback of 1 ms, Figure 3.2(b) shows the degradation in performance due to an increase in speed for the same multiantenna techniques. In fact, at higher speed, the channel becomes more time-variant, and the probability of choosing a modulation not appropriate for the channel quality increases. In this case, we observe a stronger effect of mobility in the AS scheme due to its sensitivity to feedback delays, and the transmit diversity as more robust technique.

Figure 3.3 shows the spectral efficiency of a system with ten users at the same average SNR of 10 dB. It is significant to note that when the delay is low, Figure 3.3(a)

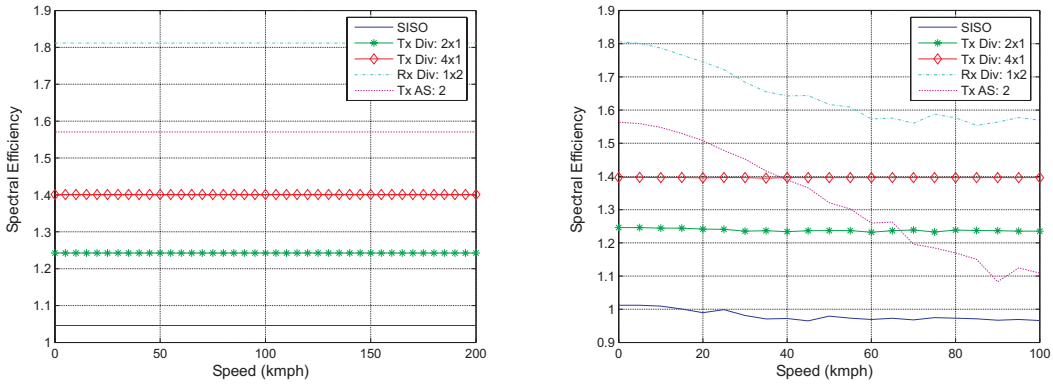

(a) no delay feedback (ideal) (b) fast feedback: 0.5 ms, regular feedback: 1 ms

Figure 3.2: Single-user scenario

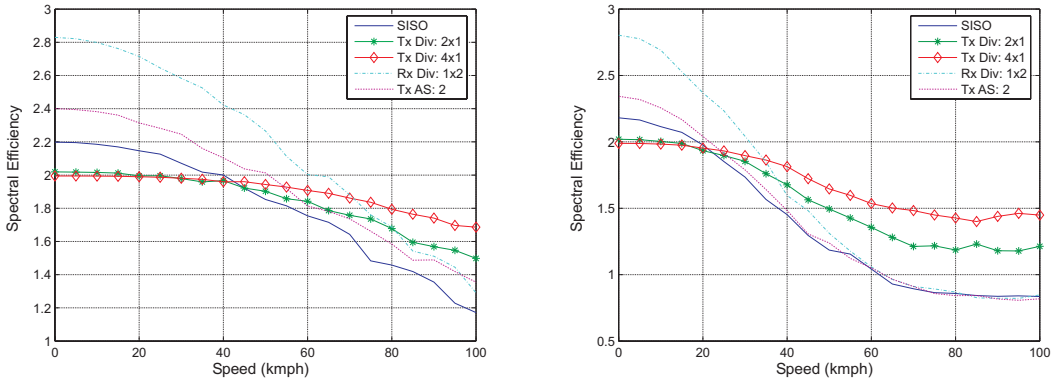

(a) fast feedback: 0.1 ms, regular feedback: 0.5 ms (b) fast feedback: 0.5 ms, regular feedback: 1 ms

Figure 3.3: Ten users scenario with scheduler max-SNR

shows that the MUD gain available at low speed is higher for a SISO configuration than for transmit diversity. This effect is explained by an incompatibility of diversity techniques, i.e., the scheduler provides no benefit in a constant channel. In other words, the MUD gain is significantly diminished when combined with spatial diversity. In fact, while the opportunistic scheduling exploits the channel variability allocating users at peaks of channel power, STBC introduces channel hardening, i.e., reduces the range of the SNR [HMT04, BKRM$^+$03]. However, when feedback delays are considered in the system and the speed increases, the scheduler and AS lose part of their gain, due to outdated feedback, as depicted in Figure 3.3(b).

3.1.2 Summary

Closed-loop schemes provide performance gains in low mobility scenarios, but suffer degradation due to feedback delay as the speed of the terminal increases. Although open-loop spatial diversity proves to be incompatible with multiuser scheduling, it makes the system more robust at high mobility.

The selection of MIMO techniques in systems on the basis of CSI obtained via feedback must consider the variability of the channel. Hence, next sections derive and look into the analytical expressions of the performance of adaptive rate schemes with MIMO.

3.2 Analytical Performance of Rate Adaptation

This section describes and derives the analytical expressions for the BER and throughput of the rate adaptation mechanism combined with spatial diversity.

The expression (3.1), for the uncoded BER, is not easily invertible. Therefore, as described in Appendix E.1, the up-coming derivations we use the approximation proposed in [CG01]:

$$BER(M,\gamma) \approx 0.2 \exp\left(\frac{-1.6\gamma}{M-1}\right) \quad . \tag{3.2}$$

This approximation is shown in [CG01] to be tight within 1 dB for $BER \leq 10^{-3}$ and $M \geq 4$.

The system emplys an adaptive discrete modulation, i.e., M is restricted to 2^i, where i is an integer, adapted by the system according to the measured γ. Moreover, the power at the transmitter is kept constant and not adapted. It has been shown in [CG01] that the adaptation of both rate and power does not bring significant advantage over the adaptation of only rate.

In this adaptive scheme, for R available constellation sizes, the SNR is divided into $R+1$ regions. The M_i order of QAM is transmitted once the SNR falls into region i delimited by SNR thresholds (or switching thresholds). To define the SNR thresholds,

we apply an instantaneous BER constraint, such that the BER is always smaller than a target value, i.e., $BER \leq BER_t$; thus obtaining the SNR threshold γ_i for region i,

$$\gamma_i = \frac{M_i - 1}{-1.6} \ln\left(\frac{BER_t}{0.2}\right) \quad . \tag{3.3}$$

In the discrete adaptive M-QAM system, the average BER within one SNR region i is obtained by averaging (3.2) over the SNR distribution. The average BER is represented by the sum of the BER of each region weighted with the number of bits of the modulation [AG00] as follows:

$$\overline{BER} = \frac{\sum_{i=0}^{R} \log_2(M_i) \int_{\gamma_i}^{\gamma_{i+1}} BER(M_i, \gamma) f(\gamma) d\gamma}{\sum_{i=0}^{R} \log_2(M_i) \int_{\gamma_i}^{\gamma_{i+1}} f(\gamma) d\gamma} \quad . \tag{3.4}$$

Given this adaptive modulation scheme, the average spectral efficiency is given by the probability that the SNR lies within the boundaries of each fading region and takes into account the errors on the link; thus, for an uncoded system, it is given by

$$\eta_{eff} = \sum_{i=0}^{R-1} \log_2(M_i) \int_{\gamma_i}^{\gamma_{i+1}} f(\gamma) d\gamma \left(1 - \log_2(M_i) \int_{\gamma_i}^{\gamma_{i+1}} BER(\gamma) f(\gamma) d\gamma\right) \quad . \tag{3.5}$$

When the value of SNR used to adapt the transmission at the BS contains an error, the predicted SNR, $\hat{\gamma}$, is different from the true SNR experienced, γ, thus the approximated BER can be re-written as

$$BER(\gamma, \hat{\gamma}) = BER(M_i, \gamma) \approx 0.2 \exp\left(\frac{-1.6\gamma}{M_i(\hat{\gamma}) - 1}\right) \quad .$$

Note that the order $M_i(\hat{\gamma})$ is adapted on the basis of the predicted SNR at the BS, $\hat{\gamma}$. However, in the notation, we will drop this dependence and use hereon only M_i. The instantaneous BER of the system as a function of $\hat{\gamma}$ is

$$BER(\hat{\gamma}) = \int_0^{\infty} BER(\gamma, \hat{\gamma}) f(\gamma|\hat{\gamma}) \, d\gamma \quad , \tag{3.6}$$

and new SNR thresholds have to be computed for the system to meet the BER constraint.

In an adaptive rate system based on predicted values of the SNR, the average BER for discrete rate adaptation with R constellations and the average spectral efficiency are

$$\overline{BER} = \frac{\sum_{i=0}^{R-1} \log_2(M_i) \int_{\gamma_i}^{\gamma_{i+1}} BER(\hat{\gamma}) f(\hat{\gamma}) d\hat{\gamma}}{\sum_{i=0}^{R-1} \log_2(M_i) \int_{\gamma_i}^{\gamma_{i+1}} f(\hat{\gamma}) d\hat{\gamma}} \quad , \tag{3.7}$$

$$\eta_{eff} = \sum_{i=0}^{R-1} \log_2(M_i) \int_{\gamma_i}^{\gamma_{i+1}} f(\hat{\gamma}) d\hat{\gamma} \left(1 - \log_2(M_i) \int_{\gamma_i}^{\gamma_{i+1}} BER(\hat{\gamma}) f(\hat{\gamma}) d\hat{\gamma} \right) \quad . \tag{3.8}$$

3.2.1 Evaluation of Analytical Performance

This section details the closed-form expressions of the BER performance analytical measures for rate adaptation in the context of MIMO diversity. Assuming no feedback delay, Section 3.2.1.1 deals with the instantaneous BER approximation in (3.2) and the thresholds in (3.3). Section 3.2.1.2 analyzes the case with feedback delay applying the BER definition of (3.6).

3.2.1.1 Analytical Measures for Ideal Feedback

In the context of the statistics of the MIMO diversity channel as described in Appendix D.3.1, we derive closed-form expressions of the average performance measures for MIMO diversity scheme with rate adaptation.

As used in [AG00], the probability of i^{th} fading region in a Rayleigh channel can be expressed as follows:

$$\int_{\gamma_i}^{\gamma_{i+1}} f(\gamma) d\gamma = \frac{\Gamma(N_t N_r, \frac{N_t}{\bar{\gamma}} \gamma_i) - \Gamma(N_t N_r, \frac{N_t}{\bar{\gamma}} \gamma_{i+1})}{\Gamma(N_t N_r)} \quad , \tag{3.9}$$

where $\Gamma(.)$ is the complete gamma function, and $\Gamma(.,.)$ is the incomplete gamma function. From this closed-form expression, we obtain the average spectral efficiency, applying (3.5), of the adaptive rate system shown in Section 3.2.1.1.

The average BER within a single fading region can be expressed for MIMO diversity

scheme as

$$\begin{aligned}\overline{BER}_i &= \int_{\gamma_i}^{\gamma_{i+1}} BER(M_i,\gamma) f(\gamma) d\gamma \\ &= 0.2\left(\frac{N_t}{\bar{\gamma}}\frac{1}{b_i}\right)^{N_t N_r} \frac{\Gamma(N_t N_r, b_i\gamma_i) - \Gamma(N_t N_r, b_i\gamma_{i+1})}{\Gamma(N_t N_r)} \ , \end{aligned} \tag{3.10}$$

where $b_i = \frac{N_t}{\bar{\gamma}} + \frac{1.6}{M_i - 1}$. Using (3.9) and (3.10) in (3.4), one can derive the average BER of the adaptive rate system.

The thresholds defined by (3.3) are addressed to as generic thresholds. These thresholds assume an instantaneous delay-free feedback situation, i.e., no delay is taken into account in the SNR thresholds design.

3.2.1.2 Analytical Measures for Delayed Feedback

In this section, we introduce a delay τ between the time the SNR is measured and the time it is employed at transmitter, and derive closed-form expressions of the average performance measures for MIMO diversity scheme with rate adaptation.

It should be noted that the time delay, τ, of the feedback in a time-varying channel affects the BER performance, but not the attempted throughput. For a signal transmitted at instant n, with channel SNR, γ_n, the decision about the modulation size is taken at instant $n-\tau$, i.e., the adaptation is performed based on $\gamma_{n-\tau}$. As no prediction algorithm is assumed here, the prediction SNR is the outdated SNR, $\hat{\gamma} = \gamma_{n-\tau}$.

Consider γ and $\hat{\gamma}$, as the SNR at instants n and $n-\tau$, respectively. Then, for a MIMO diversity link, it is possible to prove that the conditional Probability Density Function (PDF) of γ given $\hat{\gamma}$ is

$$\begin{aligned} f(\gamma|\hat{\gamma}) = &\frac{N_t}{(1-\rho)\bar{\gamma}} (\gamma)^{\frac{N_t N_r - 1}{2}} (\rho\hat{\gamma})^{-\frac{N_t N_r - 1}{2}} \exp\left(-\frac{N_t(\rho\hat{\gamma}+\gamma)}{(1-\rho)\bar{\gamma}}\right) \\ &\times I_{N_t N_r - 1}\left(\frac{2N_t\sqrt{\rho}}{(1-\rho)\bar{\gamma}}\sqrt{\hat{\gamma}\gamma}\right) \ , \end{aligned}$$

where, assuming Jakes model for time variation, the time correlation factor is $\rho = J_0^2(2\pi f_d \tau)$,

and $I_\beta(z)$ is the modified Bessel function of order β.

With the knowledge of the conditional PDF of the SNR, the instantaneous BER based on the delayed SNR in (3.6) is

$$\begin{aligned} BER(\hat{\gamma}) &= \int_0^\infty BER(\gamma,\hat{\gamma}) f(\gamma|\hat{\gamma}) d\gamma \\ &= 0.2 \left(\frac{1}{1+\frac{1.6}{M_i-1}\frac{\bar{\gamma}(1-\rho)}{N_t}} \right)^{N_t N_r} \exp\left(\frac{\hat{\gamma}\rho\frac{1.6}{M_i-1}}{1+\frac{1.6}{M_i-1}\frac{\bar{\gamma}(1-\rho)}{N_t}} \right) \quad . \end{aligned} \tag{3.11}$$

In this case, the generic thresholds shown in (3.3) are not accurate; thus, introducing updated thresholds that consider feedback delay is necessary for a correct selection of rate. The updated thresholds are obtained by inverting the equation (3.11), and can be written as

$$\gamma_i = \frac{1+\frac{1.6}{M_i-1}\frac{\bar{\gamma}(1-\rho)}{N_t}}{\rho\frac{1.6}{M_i-1}} \ln\left[5BER_t \left(1+\frac{1.6}{M_i-1}\frac{\bar{\gamma}(1-\rho)}{N_t} \right)^{N_t N_r} \right] \quad . \tag{3.12}$$

Similar to (3.10), the closed-form expression for the average BER within fading region i reads

$$\begin{aligned} \overline{BER}_i^\rho &= \int_{\gamma_i}^{\gamma_{i+1}} BER(\hat{\gamma}) f(\hat{\gamma}) d\hat{\gamma} \\ &= 0.2 \left(\frac{N_t}{\bar{\gamma} b_i} \right)^{N_t N_r} \frac{\Gamma(N_t N_r, b_i^\rho \gamma_i) - \Gamma(N_t N_r, b_i^\rho \gamma_{i+1})}{\Gamma(N_t N_r)} \quad , \end{aligned}$$

where $b_i^\rho = \frac{N_t}{\bar{\gamma}} + \frac{1.6 N_t \rho}{1.6(1-\rho)+N_t(M_i-1)}$.

3.2.2 Results and Discussion

This section presents the results for an adaptive M-QAM system with constellation sizes $M = 4, 16, 64, 256$, and with $BER_t = 10^{-3}$. The receiver tracks continuously the post-processing SNR, and the M-QAM order is computed based on the SNR thresholds.

Figure 3.4 depicts the analytical curves of the average BER performance of a delay-free SISO and MRC system. Notice that the average BER is always below BER_t, due to the instantaneous constraint $BER \leq BER_t$. In the same plot, the simulation curves

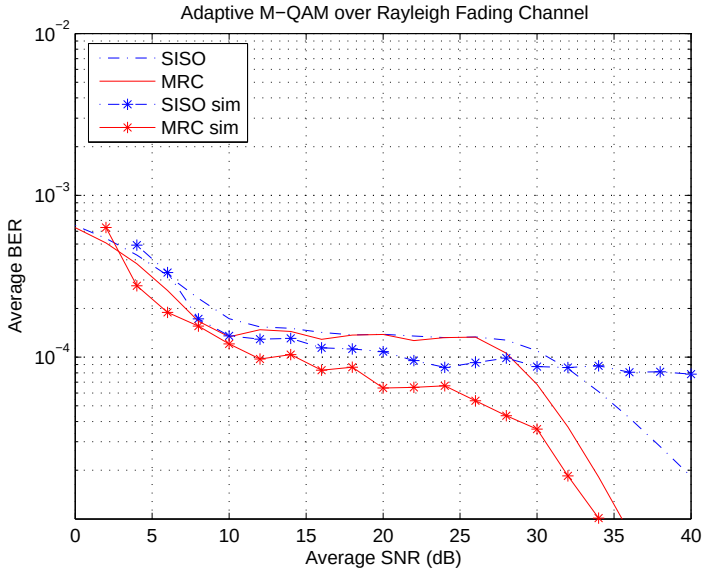

Figure 3.4: Average BER of a discrete M-QAM adaptive system. The lines without marker represent the analytical results, whereas the star corresponds to the simulation results for the case with no feedback delay

for the situation without feedback delay are plotted. The difference between analytical and simulated curves resides in the fact that the BER approximation is not exact and the inaccuracy increases in adaptive rate system for higher modulation orders.

The performance of the system in the presence of feedback delay is shown to be affected by the use of generic thresholds (3.3) or updated thresholds (3.12). In fact, Figure 3.5 shows that the BER degradation is significant when generic thresholds are used with a normalized time delay experienced by the feedback of $f_d\tau = 0.06$. In SISO with generic thresholds, the BER constraint is not fulfilled for a long range of channel conditions ($15 \leq \bar{\gamma} \leq 38$ dB), whereas the updated thresholds maintain the BER performance under the required BER constraint. Also for MRC scheme, which is generally more robust, the average BER performance is improved by employing the updated thresholds.

3.2.3 Summary

This section evaluated the performance of a rate adaptive system combined with spatial diversity in a time-variant channel. Closed-form expressions of the BER were derived

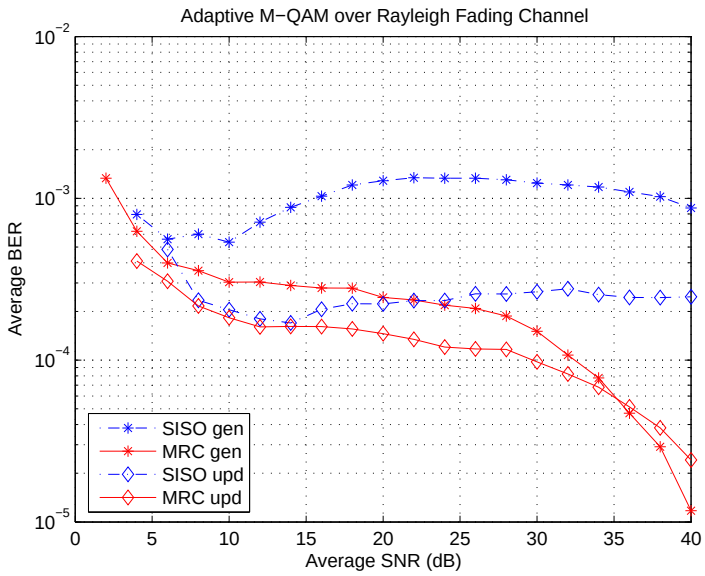

Figure 3.5: Average BER of a discrete M-QAM adaptive system with delay. Normalized feedback delay is $f_d\tau = 0.06$. The star corresponds to generic and the diamond to updated thresholds

for a M-QAM scheme with spatial diversity over flat Rayleigh fading channels and with feedback delay. More conservative thresholds that take into account the feedback delay were derived, and compared with generic thresholds.

3.3 Channel Power Prediction

Section 3.2 showed the impact of feedback delay in the rate adaptation performance. However, prediction methods have been proposed to reduce the uncertainty of the CSI obtained via feedback in time-variant channels. This section presents the analytical study on the BER performance of an adaptive M-QAM with channel power prediction for various MIMO schemes.

On the basis of the power predictor proposed in [Ekm02], this section derives new closed-form expressions for the BER performance of different MIMO schemes. Analytical SNR thresholds are then obtained from the closed-form expressions.

3.3.1 Power Prediction

In [Ekm02, ESA02], a prediction based on linear regression is analyzed in the context of a Rayleigh fading channel. The predictor is detailed in Appendix F.1. The channel coefficients are predicted L symbols ahead using a regressor vector and Mean Square Error (MSE) optimal weights. On the basis of the prediction of coefficients, $\hat{\mathbf{h}}$, the unbiased power predictor was shown to be

$$\hat{p}_{n|n-L} = |\hat{\mathbf{h}}_{n|n-L}|^2 + \sigma^2_{\epsilon_\mathbf{h}} \ .$$

The prediction of the instantaneous SNR is then obtained from the predicted power with $\hat{\gamma} = \hat{p}\frac{E_s}{N_0}$.

3.3.2 MIMO Diversity

Appendix F.2 shows the derivation of the distribution functions of the SNR, and Appendix F.3 the closed-form expressions for the BER performance. The main results are presented for MIMO diversity. The PDF of the SNR conditioned on the predicted SNR for a MIMO diversity scheme, (F.16), is

$$\begin{aligned} f(\gamma|\hat{\gamma}) = U(\gamma)U(\hat{\gamma} - N_r\bar{\gamma}\upsilon_{\mathbf{h}\epsilon_\mathbf{h}})\frac{N_t}{\bar{\gamma}\upsilon_{\mathbf{h}\epsilon_\mathbf{h}}}\gamma^{\frac{N_tN_r-1}{2}}(\hat{\gamma} - N_r\bar{\gamma}\upsilon_{\mathbf{h}\epsilon_\mathbf{h}})^{-\frac{N_tN_t-1}{2}} \\ \times \exp\left[-\frac{\gamma + \hat{\gamma} - N_r\bar{\gamma}\upsilon_{\mathbf{h}\epsilon_\mathbf{h}}}{\frac{\bar{\gamma}}{N_r}\upsilon_{\mathbf{h}\epsilon_\mathbf{h}}}\right] I_{N_tN_r-1}\left(\frac{2N_t}{\bar{\gamma}\upsilon_{\mathbf{h}\epsilon_\mathbf{h}}}\sqrt{\gamma(\hat{\gamma} - N_r\bar{\gamma}\upsilon_{\mathbf{h}\epsilon_\mathbf{h}})}\right) \ , \end{aligned}$$

where $\upsilon_{\mathbf{h}\epsilon_\mathbf{h}}$ is the relative prediction error variance, and includes the effect of both the feedback delay and the prediction error.

The instantaneous BER as a function of $\hat{\gamma}$, (F.24), is obtained as follows:

$$\begin{aligned} BER(\hat{\gamma}) &= \int_0^\infty BER(\gamma,\hat{\gamma}) f(\gamma|\hat{\gamma}) d\gamma \\ &= U(\hat{\gamma} - N_r\bar{\gamma}\upsilon_{\mathbf{h}\epsilon_\mathbf{h}}) 0.2 \left(\frac{N_t}{\bar{\gamma}\upsilon_{\mathbf{h}\epsilon_\mathbf{h}} b(i)}\right)^{N_t N_r} \exp\left[\frac{\hat{\gamma} - N_r\bar{\gamma}\upsilon_{\mathbf{h}\epsilon_\mathbf{h}}}{\frac{\bar{\gamma}}{N_t}\upsilon_{\mathbf{h}\epsilon_\mathbf{h}}} \left(\frac{N_t}{\bar{\gamma}\upsilon_{\mathbf{h}\epsilon_\mathbf{h}} b(i)} - 1\right)\right] , \end{aligned} \tag{3.13}$$

where $b(i) = \frac{N_t}{\bar{\gamma}\upsilon_{\mathbf{h}\epsilon_\mathbf{h}}} + \frac{1.6}{M_i - 1}$.

The generic SNR thresholds in (3.3) are applicable when the feedback is assumed delay-free, i.e., a constant channel in the window of time where the adaptation takes place. When the channel is time-variant, the feedback delay introduces a level of uncertainty in the information of the channel quality. The updated SNR thresholds take into account both the relative prediction error variance and the receiver combining technique to compensate the mismatch.

For a system with instantaneous BER constraint $BER \leq BER_t$, and constant transmit power, the updated SNR thresholds, (F.25), are given by

$$\gamma_i = N_r\bar{\gamma}\upsilon_{\mathbf{h}\epsilon_\mathbf{h}} + \frac{\bar{\gamma}\upsilon_{\mathbf{h}\epsilon_\mathbf{h}}}{N_t\left(\frac{N_t}{\bar{\gamma}\upsilon_{\mathbf{h}\epsilon_\mathbf{h}} b(i)} - 1\right)} \ln\left[\frac{BER_t}{0.2}\left(\frac{\bar{\gamma}\upsilon_{\mathbf{h}\epsilon_\mathbf{h}} b(i)}{N_t}\right)^{N_t N_r}\right] . \tag{3.14}$$

3.3.3 MIMO Multiplexing

Similar to the previous section, Appendix F.2 shows the derivation of the distribution functions of the SNR, and Appendix F.3 the closed-form expressions for the BER performance. The PDF of the SNR conditioned on the predicted SNR for SM, (F.9), is

$$f(\gamma|\hat{\gamma}) = \frac{U(\gamma)U(\hat{\gamma} - \bar{\gamma}\upsilon_{\mathbf{h}\epsilon_\mathbf{h}})}{\frac{\bar{\gamma}}{N_a}\upsilon_{\mathbf{h}\epsilon_\mathbf{h}}} \exp\left[-\frac{\gamma + \hat{\gamma} - \bar{\gamma}\upsilon_{\mathbf{h}\epsilon_\mathbf{h}}}{\frac{\bar{\gamma}}{N_a}\upsilon_{\mathbf{h}\epsilon_\mathbf{h}}}\right] I_0\left(\frac{2N_a}{\bar{\gamma}\upsilon_{\mathbf{h}\epsilon_\mathbf{h}}}\sqrt{\gamma(\hat{\gamma} - \bar{\gamma}\upsilon_{\mathbf{h}\epsilon_\mathbf{h}})}\right) .$$

The instantaneous BER as a function of $\hat{\gamma}$, (F.22), is obtained as follows:

$$\begin{aligned} BER(\hat{\gamma}) &= \int_0^\infty BER(\gamma,\hat{\gamma}) f(\gamma|\hat{\gamma}) d\gamma \\ &= U(\hat{\gamma} - \bar{\gamma}\upsilon_{\mathbf{h}\epsilon_\mathbf{h}}) \frac{0.2N_a}{\bar{\gamma}\upsilon_{\mathbf{h}\epsilon_\mathbf{h}} b(i)} \exp\left[\frac{\hat{\gamma} - \bar{\gamma}\upsilon_{\mathbf{h}\epsilon_\mathbf{h}}}{\frac{\bar{\gamma}}{N_a}} \left(\frac{N_a}{\bar{\gamma}\upsilon_{\mathbf{h}\epsilon_\mathbf{h}} b(i)} - 1 \right) \right] , \end{aligned} \tag{3.15}$$

where $b(i) = \frac{N_a}{\bar{\gamma}\upsilon_{\mathbf{h}\epsilon_\mathbf{h}}} + \frac{1.6}{M_i - 1}$.

Finally, as opposed to the generic thresholds in (3.3), the updated SNR thresholds for SM, (F.23), are given by

$$\gamma_i = \bar{\gamma}\upsilon_{\mathbf{h}\epsilon_\mathbf{h}} + \frac{\bar{\gamma}\upsilon_{\mathbf{h}\epsilon_\mathbf{h}}}{N_a \left(\frac{N_a}{\bar{\gamma}\upsilon_{\mathbf{h}\epsilon_\mathbf{h}} b(i)} - 1 \right)} \ln\left[\frac{BER_t}{0.2} \frac{\bar{\gamma}\upsilon_{\mathbf{h}\epsilon_\mathbf{h}} b(i)}{N_a} \right] . \tag{3.16}$$

3.3.4 Antenna Selection

For AS, the expression obtained for conditional PDF of the SNR is presented in Appendix F.2 and the BER in Appendix F.3, but no closed-form is found for the updated thresholds. Nevertheless, the tractable equation for the BER performance allows for a numerical evaluation.

3.3.5 Evaluation of Analytical Performance

In order to plot the analytical curves of BER and average effective throughput, the system described in Section 3.1 is assumed with four M-QAM levels and an unbiased power predictor. The instantaneous BER curves in AWGN channel, expressed by (3.2), for the four M-QAM levels using SISO in a delay-free scenario are depicted in Figure 3.6. In the discrete rate adaptive system, the region of interest in the curves is below the target BER.

The average BER, expressed by (3.4), depends on the fading channel assumed. To obtain a Rayleigh channel performance, the average BER is computed over 10^6 symbols for each SNR value. The link experiences a constant channel realization within each symbol. We have chosen a target BER of 10^{-3}, thus the system uses the largest modulation that has

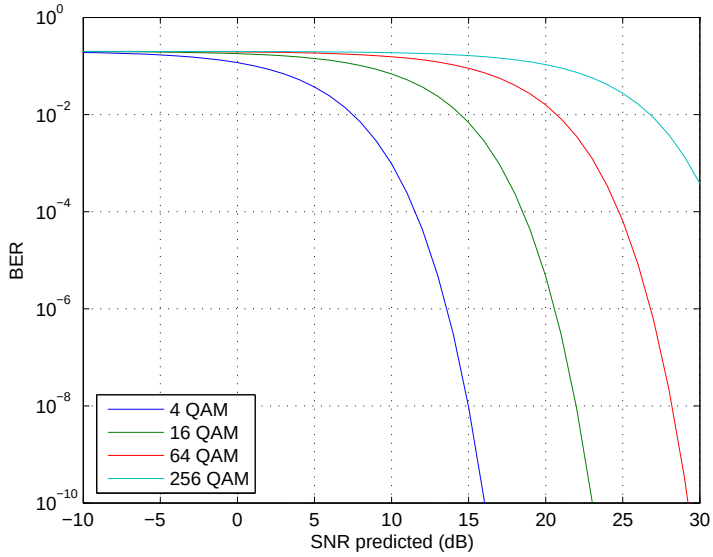

Figure 3.6: BER for different M-QAM levels

a BER below 10^{-3}. Figure 3.7 depicts the average BER, for the adaptive M-QAM without feedback delay applied to SISO, STBC, MRC, and SM. The AS scheme is not represented in these results, since no closed-form of the instantaneous BER was obtained. Note that the average BER is always below the instantaneous constraint, i.e., $BER \leq BER_t$, and the diversity and array gains are visible at higher SNR values.

In the presence of feedback delay, the instantaneous BER expression assumes the form of (3.13) for MIMO diversity and (3.15) for MIMO spatial multiplexing. In a SISO system, Figure 3.8 depicts the instantaneous BER in terms of predicted SNR for QPSK and increasing relative prediction error variance, $\upsilon_{\mathbf{h}\epsilon_\mathbf{h}}$. The prediction error variance is affected by the prediction horizon and the time variance of the channel. Thus, in a delay-free feedback scenario, or in a time constant channel, the prediction error variance tends to zero. Due to this effect, the SNR thresholds, valid in the delay-free case, fail at high prediction error and need to be updated according to the new BER curve, as Figure 3.8 illustrates.

Evaluating (3.13) and (3.15) for configurations with more than one antenna, Figures 3.9(a) and 3.9(b) show the analytical curves for the MIMO techniques under consid-

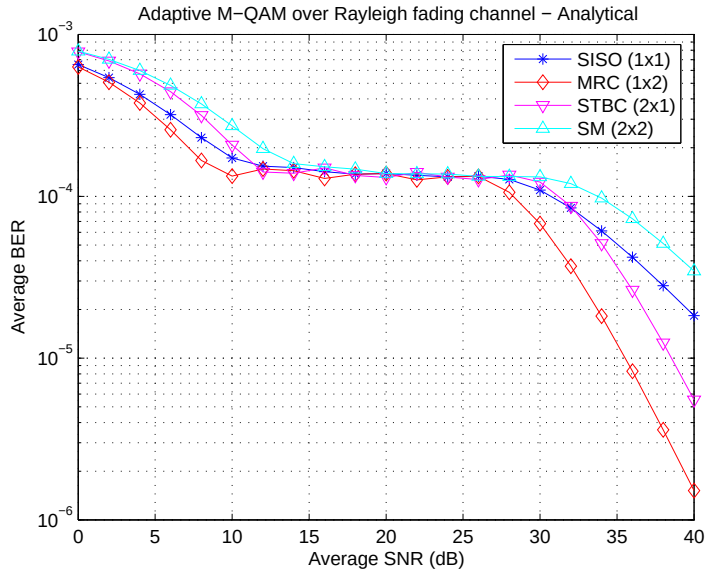

Figure 3.7: Adaptive M-QAM (M=0,4,16,64,256) over Rayleigh fading channel. $BER_t = 10^{-3}$

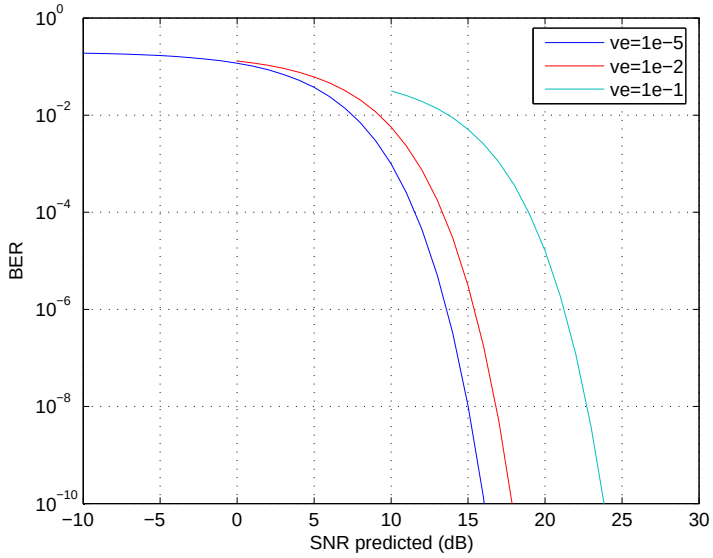

Figure 3.8: BER curves of SISO for different values of relative error variance. Using QPSK and $\bar{\gamma} = 20$ dB

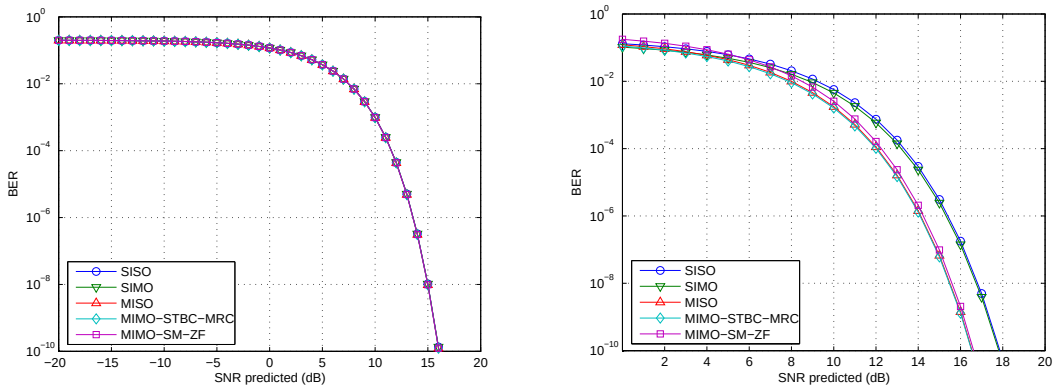

(a) low prediction error variance ($\upsilon_{\mathbf{h}\epsilon_\mathbf{h}} = 10^{-4}$) (b) high prediction error variance ($\upsilon_{\mathbf{h}\epsilon_\mathbf{h}} = 10^{-2}$)

Figure 3.9: BER curves for different MIMO techniques. Using QPSK and $\bar{\gamma} = 20$ dB

eration for two cases of prediction error, low relative prediction error variance and high prediction error variance, respectively. While all MIMO modes follow the same instantaneous BER performance in an error-free CSI scenario, as shown in Figure 3.9(a), the differences appear at higher prediction error variance, and are more evident in MIMO diversity configuration.

The average BER in the case with prediction error is obtained by using the instantaneous BER, (3.13) and (3.15), in (3.4). Figure 3.10 shows the average BER curve for the discrete SNR, when delay is considered for different MIMO schemes. The degradation in performance is more significant for values of relative prediction error of $\upsilon_{\mathbf{h}\epsilon_\mathbf{h}} \geq 10^{-1}$.

Figure 3.11 depicts the average effective throughput for the same set of schemes. In the case of a higher prediction error, the performance degradation is significant, and the trend is more evident and pronounced in the case of SISO and SM schemes.

3.3.6 Summary

In this section, we presented closed-form expressions for the BER performance of MIMO diversity and SM techniques when a rate adaptive system employs a predictor for the SNR. Although for AS no closed-form of the BER was achieved, a tractable expression was derived, which permits a numerical analysis of performance to be applied in Chapter 4. The feedback delay and the prediction error were shown to have different impact on the

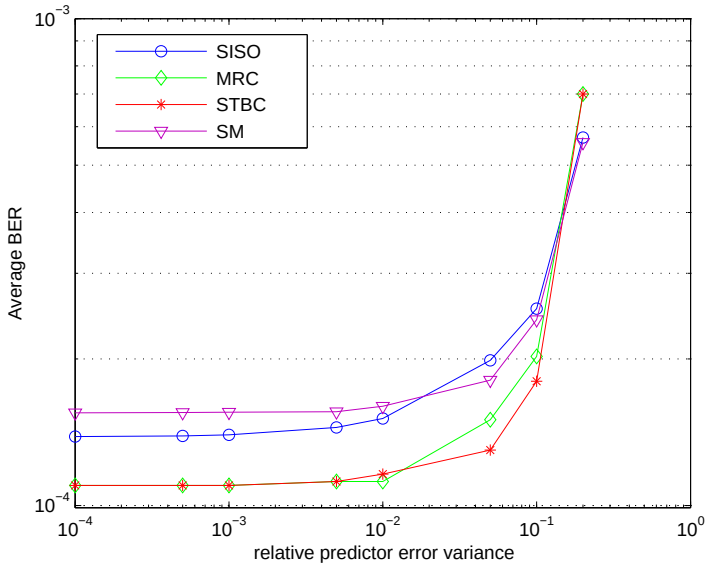

Figure 3.10: Average BER for different MIMO techniques. $\bar{\gamma} = 20$ dB and $BER_t = 10^{-3}$

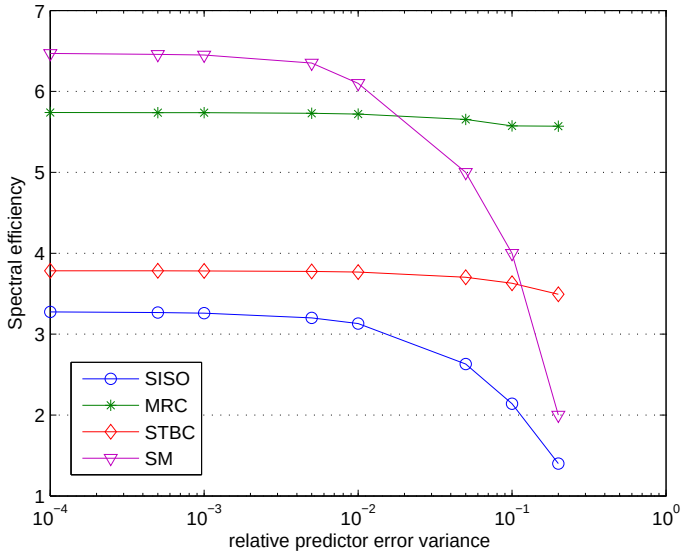

Figure 3.11: Average effective throughput for different MIMO techniques. $\bar{\gamma} = 20$ dB and $BER_t = 10^{-3}$

instantaneous BER of each MIMO scheme.

3.4 Practical System Aspects

The SNR thresholds for rate selection depend on the SNR distribution of the MIMO transmission scheme as well as on the number of antennas. Moreover, in the presence of feedback delay, the SNR thresholds also depend on the relative prediction error variance, $\upsilon_{\mathbf{h}\epsilon_{\mathbf{h}}}$.

The results presented so far assume that the SNR thresholds of the system are updated according to the prediction error and the MIMO technique. However, since these thresholds require a higher complexity in the system to obtain the estimate of the prediction error variance, a simpler version of a rate adaptive system would use generic thresholds (not updated). The generic thresholds can also be applied when the information about the channel variability is unknown, or when the feedback message does not allow to include information about the MIMO scheme and the prediction error variance. This section shows the degradation that arises from SNR thresholds that are not updated (or updated incorrectly) to the channel conditions.

The SNR thresholds with incorrect values are analyzed for two parameters: transmission technique and value of prediction error variance. This work identifies two plausible situations that occur in a simplified rate adaptive system. The system uses a feedback message with the SNR measured in the symbol received, but neither the MIMO mode nor the prediction error variance are taken into account. The first case applies SISO thresholds for any MIMO technique, and is presented in Section 3.4.1. The second case considers generic thresholds (not considering delay effect) instead of updated thresholds, and is presented in Section 3.4.2.

3.4.1 SISO thresholds for MIMO

When the rate adaptation system is unaware of the different multiple antenna techniques, the system assumes a SISO link. Figure 3.12 depicts the loss in throughput for other MIMO techniques. The results show that the use of SISO thresholds for other MIMO

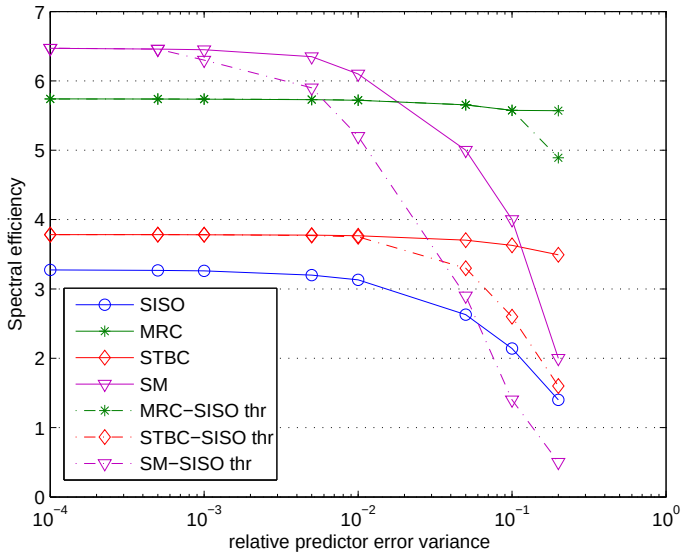

Figure 3.12: Average effective throughput for different MIMO techniques. Updated versus SISO thresholds. $\bar{\gamma} = 20$ dB and $BER_t = 10^{-3}$. The 'solid lines' represent the updated thresholds, and the 'dotted lines' represent the SISO thresholds

configurations creates a substantial loss in performance, but the effect is very different depending on the technique. The SM scheme reveals to be more sensitive to prediction error when compared to the diversity schemes. More specifically, even at $\upsilon_{\mathbf{h}\epsilon_\mathbf{h}} \leq 10^{-2}$, the performance loss is significant. On the other hand, MRC has an almost negligible degradation in performance.

3.4.2 Generic versus Updated Thresholds

In previous sections, two types of SNR thresholds, the generic and the updated thresholds, were defined. While the generic thresholds do not take into account the delay and prediction errors, the updated thresholds consider the statistics of the predicted SNR accordingly. Here, we analyze the impact of the generic thresholds that are not updated with the prediction error. The system suffers a delay in the feedback between receiver and transmitter, but the thresholds assume zero delay feedback.

Figure 3.13 depicts the loss in BER performance against the relative predictor error variance. Updated thresholds are more conservative, as these compensate the uncertainty

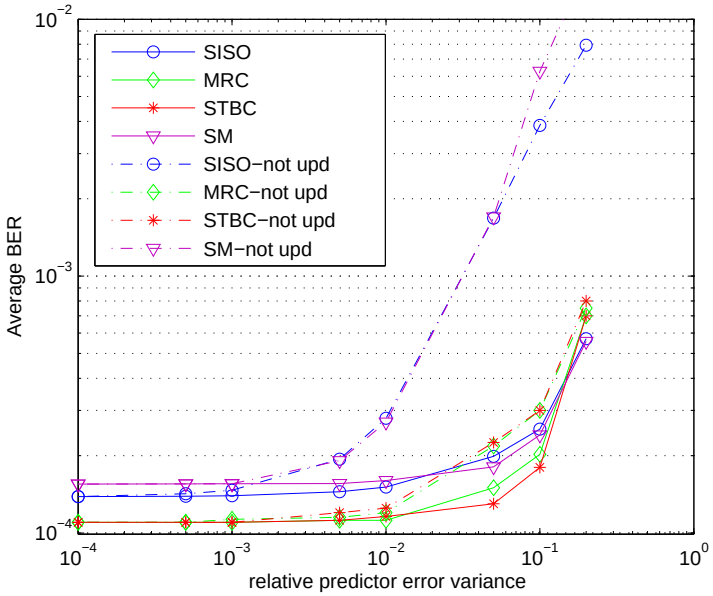

Figure 3.13: Average BER for MIMO techniques. Updated versus generic thresholds. $\bar{\gamma} = 20$ dB and $BER_t = 10^{-3}$. The 'solid lines' represent the updated thresholds, and the 'dotted lines' represent the generic thresholds

in the feedback CSI by increasing the SNR threshold. However, while the difference of performance in SISO and SM is substantial, MRC and STBC updated thresholds have lower impact in the BER. In fact, the BER for SISO and SM is only kept under the constraint if updated thresholds are used, confirming these schemes as the less robust techniques to prediction errors.

3.4.3 Summary

This section presented the analysis of the effect of the prediction error in the CSI obtained with a feedback channel that experiences delay. We have separately studied the case of updated SNR thresholds that do not take the MIMO mode into account, as well as the case of updated SNR thresholds that do not consider the delay.

3.5 Conclusions

This chapter addressed the impact of feedback delay in the performance of adaptive systems. The goal was to find the extent to which a system affected by delay can be tuned while meeting the BER constraints.

The statistics of the post-processing SNR can be used to evaluate the effect of feedback delay, as well as they can be used to design SNR thresholds. To assess the sensitivity of different multiantenna techniques under a time-variant channel, we have studied the average BER over flat Rayleigh fading channels.

The channel prediction reduces the uncertainty of channel information at transmitter caused by feedback delay. In addition, with an unbiased channel power predictor, we have identified a measure for the reliability of the CSI in feedback directly related with the normalized delay and the predictor regressor.

On the basis of the analytical study, this chapter presented closed-form expressions for the BER of MIMO diversity and SM, and it also proposed SNR thresholds updated according to the CSI inaccuracy due to delay. Simulation results show that these thresholds fulfill the BER constraint in the presence of delayed feedback.

The feedback delay and the time variability of the channel are factors that need to be considered both in the design of a rate adaptive system and in the choice of MIMO. The selection of the best scheme according to the channel conditions and feedback delay is determinant for receivers that are able to use different MIMO modes. These results are applied in Chapter 4 to propose such MIMO switching mechanism.

Chapter 4

Adaptive MIMO-OFDMA Mechanisms

The reliability of the CSI available at the transmitter is a determinant factor in a link adaptation system based on feedback. In Chapter 3, we derived new thresholds for a rate adaptive scheme. These thresholds take into account the channel prediction error variance and the MIMO technique. On the basis of that background, this chapter presents a general framework of a system with multiple MIMO capabilities. In addition, we aim at tackling some of the more practical issues for implementation in a multiuser system. As a result, the present chapter proposes a transmit strategy for a multimode MIMO system with a generic OFDMA allocation, and focuses on the choice of MIMO modes in an integrated MIMO switching system.

The previous chapters showed how different MIMO techniques provide various performance benefits, e.g., robustness and throughput. Several authors have addressed the MIMO adaptation issue in recent years, such as switching mechanisms between spatial diversity and multiplexing based on the SNR, the MIMO channel eigenvalues, and the condition number of the spatial correlation matrix [HJP05, WSKM06, FPKHJ05]. However, to the author's knowledge, schemes incorporating the reliability of CSI feedback of the MS have not been proposed to date. Moreover, the combination of multiuser alloca-

tion of subchannels in OFDM with multimode MIMO selection reveals to be a practical approach for integrated systems. In [MKL06], the authors present an integrated allocation scheme for the transmission parameters of real-time and non real-time services to the users in the cell center or the cell-edge. This chapter proposes a concept for an integrated system based on the reliability of the CSI.

The remainder of this chapter is organized as follows. Section 4.1 describes the general system structure and presents a preliminary evaluation of feedback delay and SNR thresholds in a simplified link adaptation system. Section 4.2 proposes the strategy for the switching mechanism to optimize the performance of the feedback in the presence of delay, and it proposes a MIMO look-up table for two transmit antennas. Based on the different approach required for frame-based communications, Section 4.3 presents an analysis of different options for setting the thresholds in this case and proposes a tradeoff solution. Finally, Section 4.4 points out the main conclusions of the chapter.

4.1 System Description

This section presents the structure of the general framework for an OFDM-based system with MIMO and link adaptation capabilities. We consider the downlink of a single cell OFDMA system with carrier frequency at 2 GHz. The BS possesses two or more antennas and can switch between different transmit modes. Moreover, the BS schedules the users by allocating the available subchannels, based on CSI sent via a feedback channel from the MS. As the users are given different subcarriers, we consider that there is no inter-user interference at the receiver.

The wireless channel is frequency selective over the system bandwidth, but the simulations consider the performance of a flat fading single OFDM subcarrier. The channel is quasi-static varying in time according to the classical Doppler, such that it is approximately constant over two consecutive symbols. The spatial links of the MIMO configuration are uncorrelated, and a limited signalling overhead is considered for the feedback channel. Based on these conditions, the MIMO transmission modes selected for analysis were the

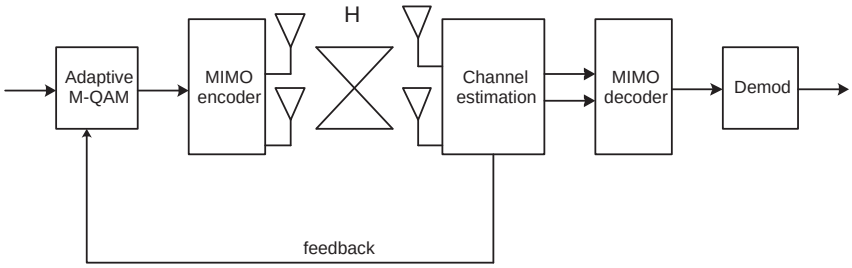

Figure 4.1: System model of MIMO and adaptive modulation

single antenna (SISO), the open-loop schemes STBC and SM, and the closed-loop AS. Following the analytical study of Chapter 3, we consider a simple ZF detector for SM. The average transmit energy is assumed the same for all MIMO options.

The BS supports a rate adaptation system that selects the current modulation for each user in the downlink frame on the basis of feedback CSI. The available constellations are QPSK, 16-QAM, 64-QAM, and 256-QAM. The system model of a channel allocated to one user is represented in Figure 4.1.

The channel estimation at the MS is assumed perfect. The MS tracks the channel quality on its allocated subchannels and sends the feedback information on an uplink channel to the BS. The tracking process is performed on one antenna when AS mode is selected for transmission or over the two transmit antennas for STBC or SM.

The delay between the channel measure at MS and the frame transmitted from BS adapted according to the CSI is the feedback delay, τ. The normalized value of feedback delay is $f_d\tau$. The BS tracks the channel time variability by means of stored past information in a CSI buffer, and uses it to determine the reliability measure of the link. Channel prediction is embedded at the MS to compensate for the time variability of the channel. On the basis of the prediction error variance, the BS selects the appropriate transmission mode. The SNR thresholds derived in Chapter 3 are implemented to select the rate by taking into account the MIMO mode and the prediction error.

The BS schedules the transmission to different users based on the CSI sent via feedback. The decision on the subchannel and transmit strategy allocated to each MS is performed before transmission of every downlink frame. The implications of reporting

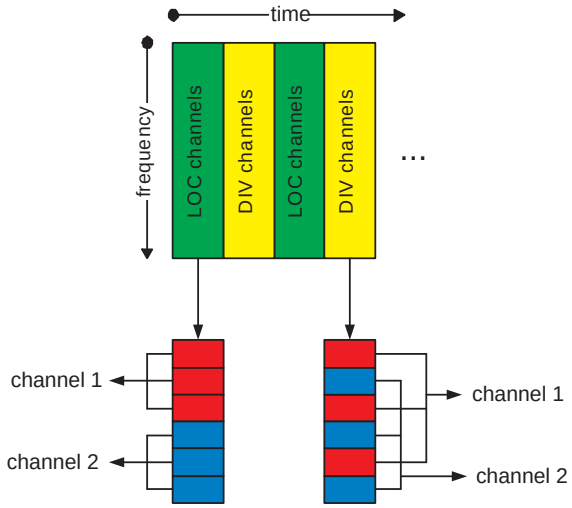

Figure 4.2: LOC and DIV subchannels within an OFDM frame

the CSI on a frame basis are analyzed in Section 4.3. The simulation results prior to Section 4.3 assume a rate adaptation on a symbol by symbol basis.

The OFDM data subcarriers are grouped to form subchannels that are allocated to the users in the system. One subchannel consists of a number of subcarriers that can be contiguous or not. In this context, the terms Localized (LOC) and Diversity (DIV) subchannels are employed to refer to the two types of aggregated subcarriers in the OFDMA system. LOC subchannels consist of contiguous subcarriers. DIV subchannels consist of non-contiguous subcarriers that are ideally separated (in frequency) by at least the coherence bandwidth to provide inherent diversity. Within a LOC subchannel, the SNR is assumed constant over the subcarriers; thus, it is suitable for rate adaptation across different LOC subchannels. The DIV subchannels are appropriate for application of frequency diversity coding. Figure 4.2 depicts the frame structure containing both LOC and DIV channels. The MS estimates the SNRs of each spatial link for both LOC and DIV channels.

4.1.1 Performance of MIMO Modes with Outdated Feedback

This section evaluates the performance of different MIMO techniques facing outdated feedback CSI. The results of this analysis are applied in the choice of the MIMO modes

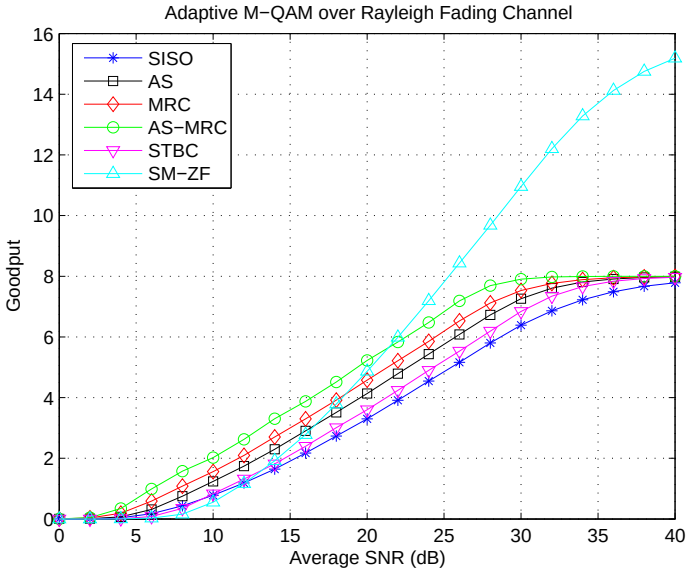

Figure 4.3: Spectral efficiency of system with no delay

considered in the transmit strategy proposed in Section 4.2. Additionally, the sensitivity of each MIMO scheme to the feedback delay is important when choosing the transmission mode in case of outdated CSI.

We consider a narrowband Rayleigh fading channel for a single-user, which is equivalent to regard one subcarrier in the system described above. An adaptive M-QAM selects the rate based on CSI received via feedback. Furthermore, six MIMO configurations are considered, SISO, AS and STBC at transmitter, MRC at receiver, and SM.

In the rate adaptive scheme with no feedback delay, both generic and updated thresholds deliver the same performance, as depicted in Figure 4.3. The dual stream SM exceeds in spectral efficiency all other MIMO modes at high SNR, whereas AS outperforms open-loop STBC. When the feedback experiences delay between the MS and BS, the CSI becomes outdated in time-variant channels, and updated thresholds are needed to compensate the uncertainty of the CSI.

The impact of low delays, e.g., $f_d\tau \leq 0.03$, is negligible. However, when the normalized feedback delay increases, SM and SISO modes suffer a considerable impact if generic thresholds are employed, as depicted in Figure 4.4 for $f_d\tau = 0.06$. As the theoretical

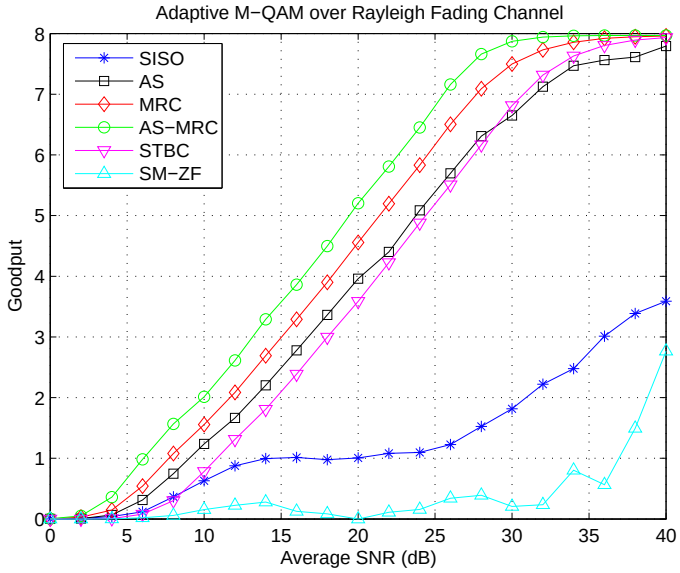

Figure 4.4: Spectral efficiency of system with $f_d\tau = 0.06$ and generic thresholds

analysis in Chapter 3 suggests, Figure 4.5 shows that the performance of the schemes more sensitive to feedback is greatly improved when the delay is taken into account by employing updated thresholds.

The use of multiple antennas to exploit diversity with STBC makes the system more robust to feedback delays when compared to multiplexing and AS. The results in Figure 4.5 also show that STBC scheme slightly outperforms AS at higher SNR after a threshold average SNR value. In fact, the loss in performance when the system commits an error in the rate selection increases at higher average SNR, and AS is more vulnerable to such errors in outdated feedback scenarios. The crossing point between STBC and AS depends on the normalized delay considered, and the results show that the SNR value of transition is lower in high delay scenarios. At very high normalized delay conditions, STBC outperforms AS in all the SNR range, thus proving to be more robust than AS in the presence of feedback delay.

Results show that SM with significant feedback delay still achieves high performance in good channel conditions. However, the threshold of SNR from which this technique outperforms single stream options increases from around 20 dB in no delay case to the

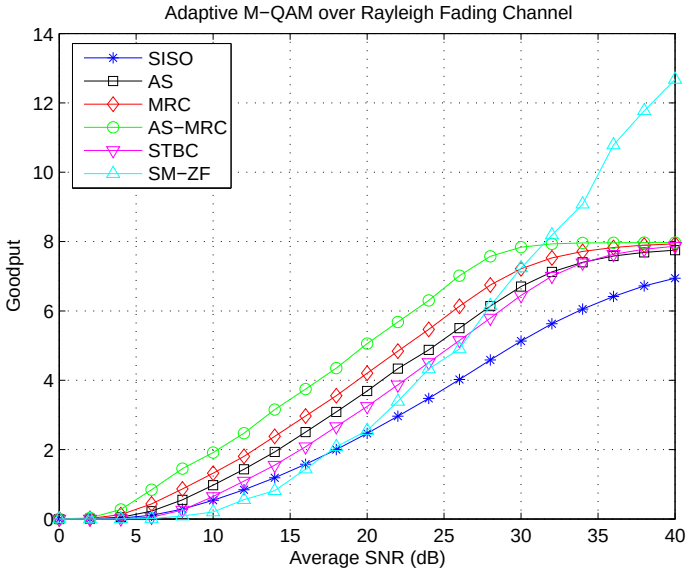

Figure 4.5: Spectral efficiency of system with $f_d\tau = 0.06$ and updated thresholds

vicinity of 30 dB with normalized delay of 0.06. Consequently, SM requires a higher SNR to be effective.

4.1.2 Histogram of Modulation Levels

In this section, we show the probability of selection of each modulation for transmission using the SNR thresholds proposed in Chapter 3. There are five regions of rate allocation, consisting of the no data transmitted region and the four modulations (QPSK, 16-QAM, 64-QAM, and 256-QAM).

In absence of delayed feedback, the rate adaptive scheme selects the constellation according to the SNR generic thresholds. Figure 4.6 presents the histogram of the modulations selected with generic thresholds. Since generic thresholds do not consider the feedback delay, distribution of selected modulations remains constant for any delay. However, the throughput incurs in losses when the feedback delay increases, as shown in the previous section.

The use of updated thresholds for the delayed feedback cases changes the distribution of the selected modulations. Figure 4.7 depicts the histogram for a normalized delay of

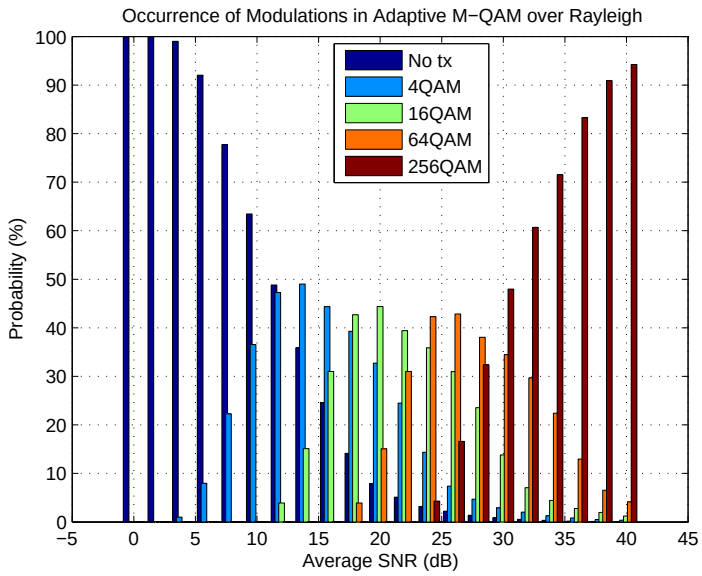

Figure 4.6: Modulation histogram of SISO with generic thresholds

0.10. The rate adaptive scheme shows a more conservative choice of the modulation level for each average SNR value, i.e., the probability of the lower order modulations increases. In other words, the system is more conservative when compared to generic thresholds in the sense that lower modulations or no transmission are preferred by the system for a longer range of SNR.

The more conservative choice of modulation in the presence of delay avoids the increase in the probability of error by delaying the transmission. In a similar fashion, the use of Hybrid Automatic Repeat Request (HARQ) allows the transmission in poor channel conditions, or higher feedback delays, by requesting retransmission in case of error. This procedure proves efficient when there is no information about the channel, or when the user experiences a high feedback delay for a short period. As such, the delay updated thresholds and HARQ are complimentary techniques, since one is preemptive and is based on channel knowledge, while the other adapts transmission upon failure.

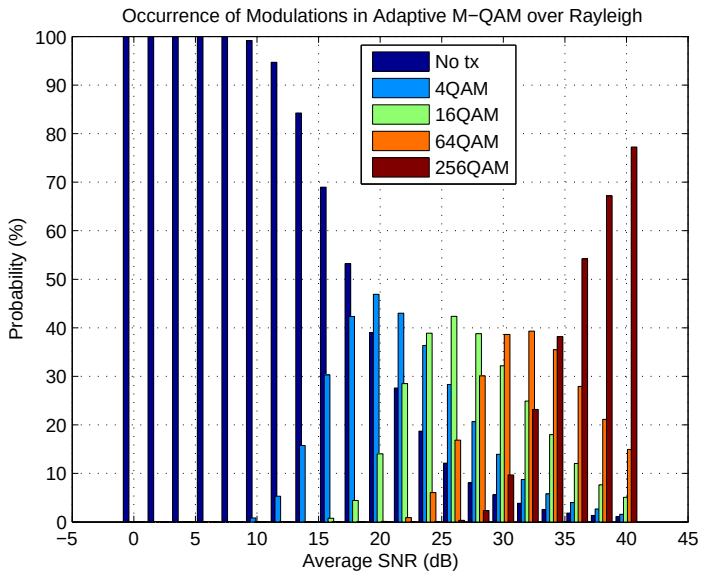

Figure 4.7: Modulation histogram of SISO with updated thresholds and normalized delay $f_d\tau = 0.1$

4.2 Transmit Strategy

This section proposes a procedure for switching among MIMO techniques in the downlink multiuser OFDMA system, described in Section 4.1. The switching decision is based on the CSI, feedback delay, and the time variability of the channel. The purpose of this work is to identify transmission strategies for the BS in a multimode MIMO configuration. We propose a mechanism to select the MIMO mode and apply the rate adaptation thresholds based on the SNR, feedback delay, and the time variability of the channel.

The BS is assumed to have two uncorrelated antennas for transmission. The MIMO modes considered are listed according to the number of antennas at the receiver and are presented in Table 4.1. If the MS has one antenna, the BS transmits the signal from any antenna (SISO), the best antenna (AS), or two antennas using diversity (STBC). If the MS has two antennas, an MRC receiver is used to combine the signals. In this case, the BS has the options of transmitting through one antenna (SIMO), the best antenna (AS-MRC), two antennas extracting diversity (STBC), or two antennas using multiplexing (SM).

Terminal	Transmitter	Receiver	Configuration
Single rx	single tx	single rx	SISO
(case 2×1)	AS	single rx	MISO
	STBC	single rx	MISO
Multi rx	single tx	MRC	SIMO
(case 2×2)	SM	ZF	MIMO
	AS	MRC	MIMO
	STBC	MRC	MIMO

Table 4.1: Available MIMO modes

In the presence of such a wide range of possible MIMO modes, it is necessary to define criteria for the selection of modes. The schemes that require CSI at the transmitter are more sensitive to delays in the feedback; thus, the main criterion is the reliability of the CSI. We define the reliability measure as the relative prediction error variance, $\upsilon_{\mathbf{h}\epsilon_\mathbf{h}}$, defined in Chapter 3. This measure is closely related with the normalized feedback delay. The second criterion is the range of the SNR received via feedback, i.e., the CSI. The SNR is used for rate adaptation in LOC subchannels, and for selection between dual stream, i.e., SM, and single stream MIMO.

The proposed transmit strategy for the MIMO switching system is divided into two parts, according to the number of antennas at the receiver. The selection criterion is then described based on the available MIMO modes. In scenarios with unreliable CSI, AS and SM are not considered due to the performance losses shown in Chapter 3. LOC channels are used only at high CSI reliability situations, otherwise DIV subchannels are more effective.

For a single antenna MS, one threshold for the reliability is needed, ψ_1. When the CSI is reliable, i.e., $\upsilon_{\mathbf{h}\epsilon_\mathbf{h}} < \psi_1$, the system chooses AS for transmission, and allocates the user in LOC subchannels. The rate is adapted according to the CSI received. For unreliable CSI, i.e., $\upsilon_{\mathbf{h}\epsilon_\mathbf{h}} \geq \psi_1$, the system selects STBC for transmission, and allocates the user DIV subchannels. In this case, the adaptive modulation uses the long term average CSI. Table 4.2 summarizes transmission strategies in the MISO 2×1 configuration.

When the MS has two antennas, two thresholds for the reliability are proposed, ψ_1 and ψ_2. For a very reliable CSI, $\upsilon_{\mathbf{h}\epsilon_\mathbf{h}} < \psi_1$, the system considers AS or SM for transmission

Feedback	MIMO mode	Allocation	CSI for AMC
Reliable CSI $\upsilon_{\mathbf{h}\epsilon_\mathbf{h}} < \psi_1$	AS	LOC subchannel	predicted SNR
Unreliable CSI $\upsilon_{\mathbf{h}\epsilon_\mathbf{h}} \geq \psi_1$	STBC	DIV subchannel	long term average SNR

Table 4.2: Selection criterion for the transmit strategy in MISO 2×1

Feedback	MIMO mode	Allocation	CSI for AMC
Reliable CSI $\upsilon_{\mathbf{h}\epsilon_\mathbf{h}} < \psi_1$	AS-MRC or SM	LOC subchannel	predicted SNR
Reliable CSI $\psi_1 \leq \upsilon_{\mathbf{h}\epsilon_\mathbf{h}} < \psi_2$	AS-MRC	LOC subchannel	predicted SNR
Unreliable CSI $\upsilon_{\mathbf{h}\epsilon_\mathbf{h}} \geq \psi_2$	STBC-MRC	DIV subchannel	long term average SNR

Table 4.3: Selection criterion for the transmit strategy in MIMO 2×2

in LOC subchannels. The transmit mode that delivers the highest throughput is selected on the basis of the predicted SNR. Typically, AS is better than SM at low SNR or in strong spatial correlation scenarios. A mid-range interval of reliability, $\psi_1 \leq \upsilon_{\mathbf{h}\epsilon_\mathbf{h}} < \psi_2$, is justified by the different sensitivity of dual and single stream modes to delay. In this interval, AS is selected for transmission, and the MS is allocated in LOC subchannels. The rate level is obtained based on the CSI received in the feedback message. When the feedback is unreliable, i.e., $\upsilon_{\mathbf{h}\epsilon_\mathbf{h}} \geq \psi_2$, the BS transmits over both antennas using STBC, allocates DIV channels, and selects rate based on long term average SNR. Table 4.3 summarizes transmission strategies in the MIMO 2×2 configuration.

We consider two separate blocks for the adaptive MIMO and adaptive rate schemes based on feedback, as represented in Figure 4.8. The BS selects the MIMO mode by analysis of long term average SNR and normalized feedback delay. The rate selection depends on the frame SNR estimation and on the updated SNR thresholds. Section 4.2.1 proposes the MIMO look-up tables with the values of the reliability thresholds found as a result of the analysis of throughput achieved with each scheme.

The description of the switching process is also presented in the form of flowcharts in Figures 4.9 and 4.10 to identify the actions described above for the cases of single or multiple antennas at the receiver, respectively.

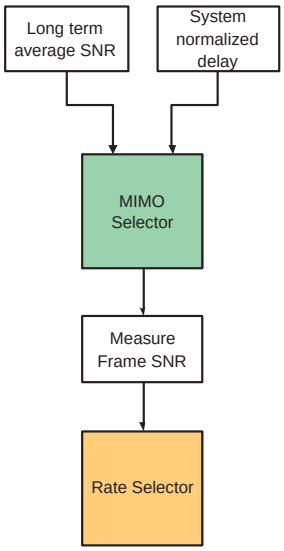

Figure 4.8: Flowchart of MIMO switching mechanism

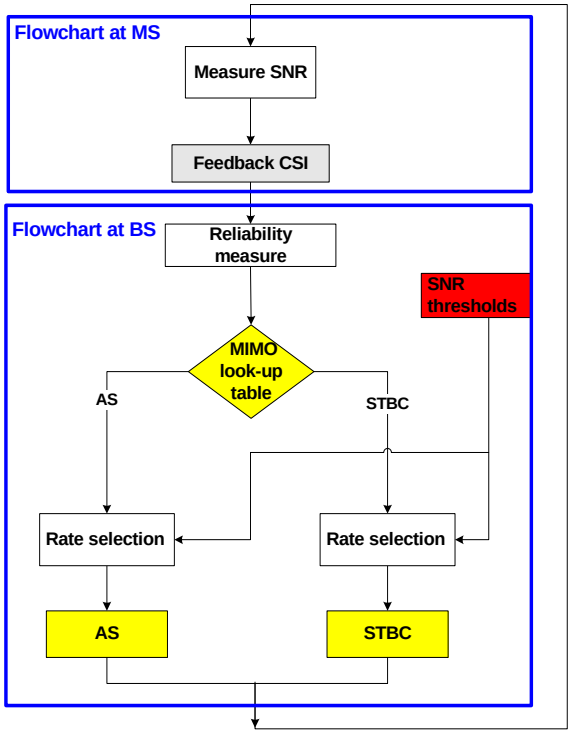

Figure 4.9: Flowchart for downlink MISO 2×1 configuration

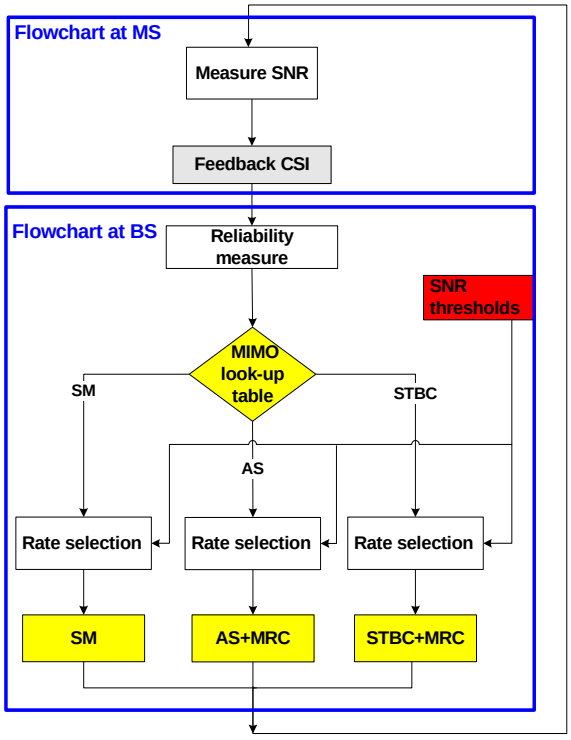

Figure 4.10: Flowchart for downlink MIMO 2×2 configuration

4.2.1 MIMO Look-up Tables

The proposed MIMO switching mechanism requires the a priori information on the intervals of channel and feedback conditions that favor each MIMO mode. Look-up tables are an efficient solution for feedback based adaptive techniques.

The MIMO mode selector checks from the look-up table the technique that delivers the highest performance for each pair of delay-SNR. Hence, the MIMO look-up table fits into a two-dimensional space, based on the channel quality and feedback delay. For a given scenario, we tune the system for each combination of SNR and delay, i.e., the mechanism selects the MIMO mode that delivers the highest spectral efficiency in a Rayleigh fading channel.

The look-up table is static for a given scenario and is saved at the BS. The proposed system measures the long term average SNR of the link and keeps track of the feedback delay and time variability of the channel, and uses the SNR and delay thresholds to switch MIMO scheme according to the look-up table.

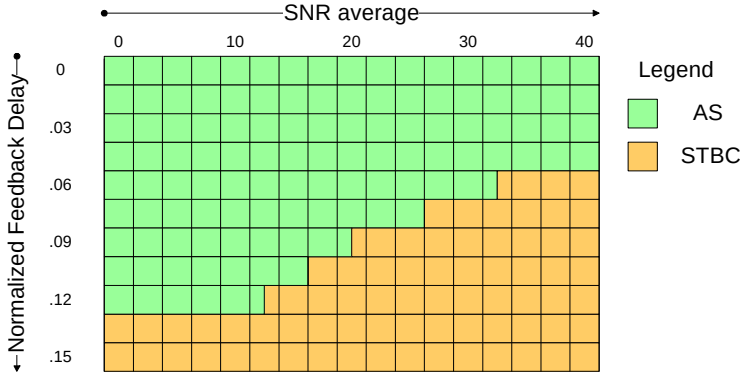

Figure 4.11: MISO 2×1 look-up table

Following the transmission strategy described above, two cases are considered: the single antenna MS, and the dual antenna MS. We select best performing MIMO configuration for a range of feedback delays. The MISO 2×1 look-up table, depicted in Figure 4.11, is obtained by choosing the scheme with the highest throughput for each combination of average SNR and delay. From the available single transmitter modes, only AS and STBC are selected, since the SISO is outperformed in all conditions. AS is preferred for lower delays, while STBC proves to be more robust for a high feedback delay.

Figure 4.12 shows the adaptation when there is no delay in the feedback. In this case, the system chooses AS for transmission over the full range of SNR conditions. Thus, the curve of the adaptive system overlaps the performance curve of AS. When a normalized delay of 0.10 is experienced by the feedback channel, the system uses AS for transmission at low SNR, and selects STBC at high SNR conditions, as shown in the look-up table. Figure 4.13 depicts the performance of the adaptive system that overlaps the performance with the highest throughput scheme at each SNR value.

Following the same procedure for the modes available with two receive antennas, we obtain the MIMO 2×2 look-up table depicted in Figure 4.14. In this case, SM delivers the highest throughput. However, it is more sensitive to the feedback delay; therefore, it is preferred in low delay scenarios and good channel conditions. The more robust STBC delivers higher performance at higher delays, while AS is preferred at poor channel conditions and low to mid-range delay scenarios.

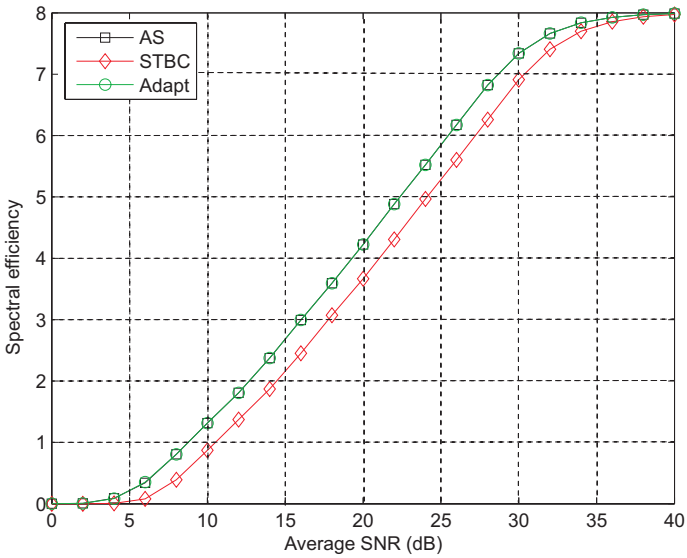

Figure 4.12: Spectral efficiency of MISO 2×1 look-up table with no delay

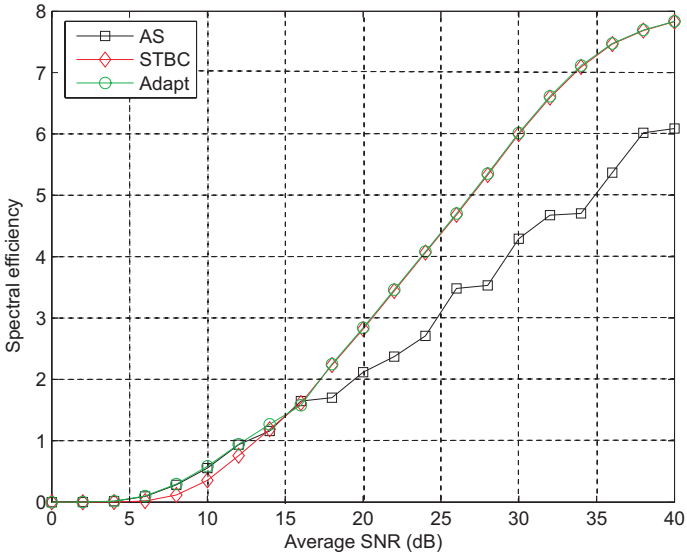

Figure 4.13: Spectral efficiency of MISO 2×1 look-up table with $f_d\tau = 0.10$

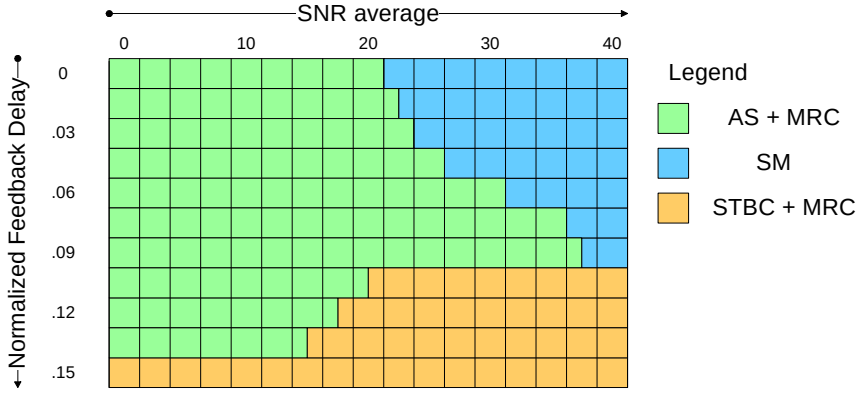

Figure 4.14: MIMO 2×2 look-up table

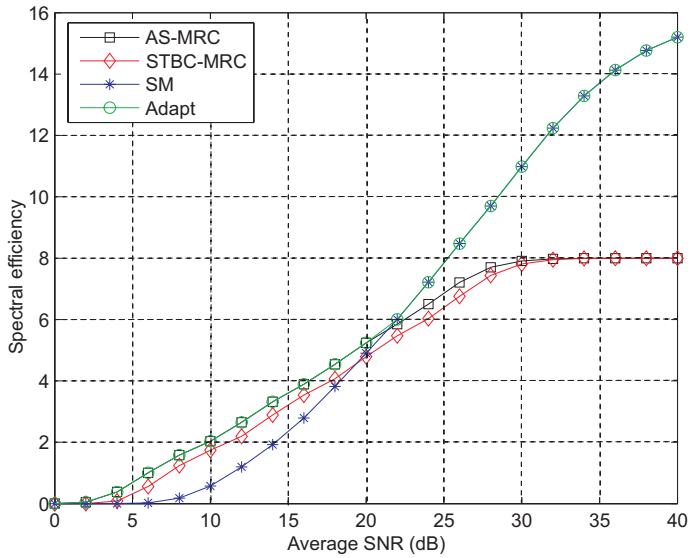

Figure 4.15: Spectral efficiency of MIMO 2×2 look-up table with no delay

Figures 4.15 and 4.16 show the results for the cases with no feedback delay and with a normalized delay of 0.09, respectively. In the case of no delay, the system selects AS at low SNR of up to 20 dB and switches to SM at higher values of SNR. In the presence of a normalized feedback delay lower than 0.09, the adaptation continues to switch between AS and SM, but with a threshold observed at higher SNR as seen in Figure 4.16. For delays higher than 0.1, STBC achieves higher throughput than SM in good channel conditions, and it is the preferred choice for all the SNR range for delays higher than 0.15.

For a single receive antenna terminal, the MIMO selection switches between AS and STBC, whereas for a multiple antenna terminal, the scheme includes the SM option, and

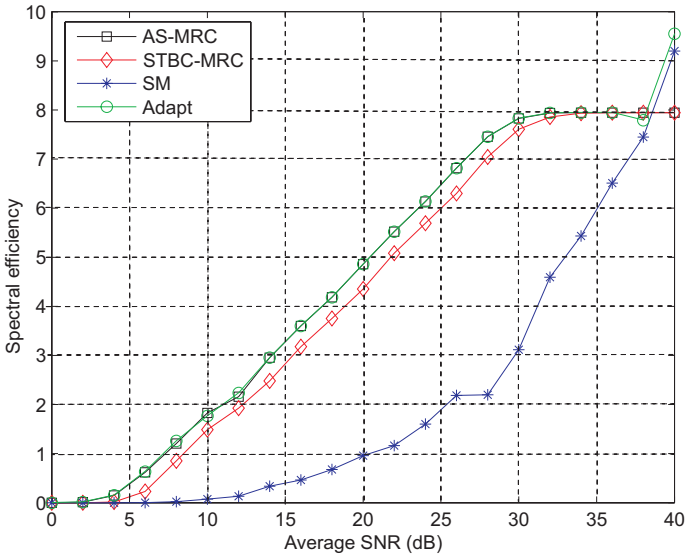

Figure 4.16: Spectral efficiency of MIMO 2×2 look-up table with $f_d\tau = 0.09$

more transition values are necessary.

The MIMO look-up table proves to be useful in a system that supports terminals with various speeds. For a wide range of mobility, the BS deals with stationary, as well as fast speed users. The MSs in the first category experience an almost constant channel, while the high velocity MSs have a time-variant channel, therefore, a high normalized feedback delay. In this heterogeneous scenario, the MIMO look-up table accommodates all users according to their channel time variability, which would not be possible with a fixed MIMO solution.

4.2.2 Summary

This section described the transmit strategies of a MIMO switching system combined with rate adaptation. We have detailed the actions and flowcharts of the proposed scheme, and the threshold values were presented in the form of a MIMO look-up table.

The system shows more advantages in scenarios with users at various levels of mobility, since supporting stationary users involves substantially different approach than fast speed MS.

4.3 Feedback Design Issues

In the simulation results shown so far, the modulation level is selected on a symbol by symbol basis, i.e., the MS measures and sends via feedback the SNR of every symbol. In a more practical approach, as presented in the system description of Section 4.1, the feedback reports the channel quality experienced in a frame received at the MS. On the basis of the feedback received, the BS chooses the rate to apply in the next downlink frame.

The analytical design of SNR thresholds updated with the feedback delay faces two important issues in such frame based feedback. First, the optimal SNR value to be reported in the feedback has to be defined. Second, the optimal length for the delay to be considered has to be chosen. A comparison of different solutions for these issues is tackled in Sections 4.3.1 and 4.3.2.

4.3.1 Reporting SNR of a Frame

In a mobility scenario, the SNR varies from symbol to symbol within the downlink frame. On the basis of the SNR estimated for all symbols, the feedback reports one value of SNR for the received frame. Although this parameter is bounded by the placement of the pilots in the frame, we assume a perfect channel estimation for all symbols in the frame.

It is usual to report the average SNR across all symbols within the frame. However, other solutions of using single symbols can also be advantageous. We consider the cases of selecting the SNR of the first symbol in the frame, the average across all symbols of the frame, and the last symbol in the frame. The last symbol has a higher time correlation with the frame where the information will be used, i.e., the delay is lower, but it captures only one symbol. Figure 4.17 depicts a representation of the three options to report the SNR value.

Results were obtained for a normalized frame duration of 0.05 and a normalized feedback delay of 0.1. These values occur for a scenario where a system with carrier frequency of 2 GHz and frame duration of 1 ms supports users at the speed of 27 km/h,

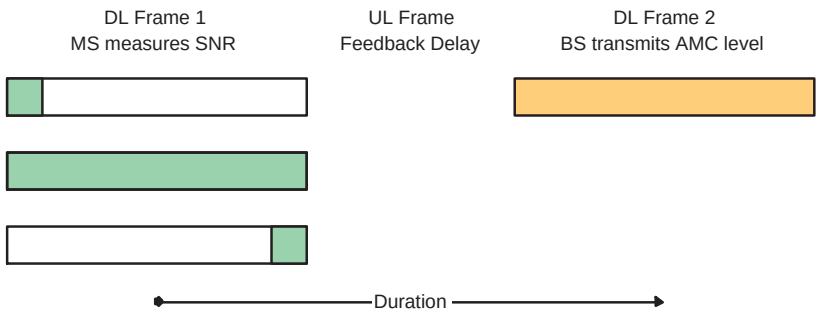

Figure 4.17: Reporting the SNR of a frame

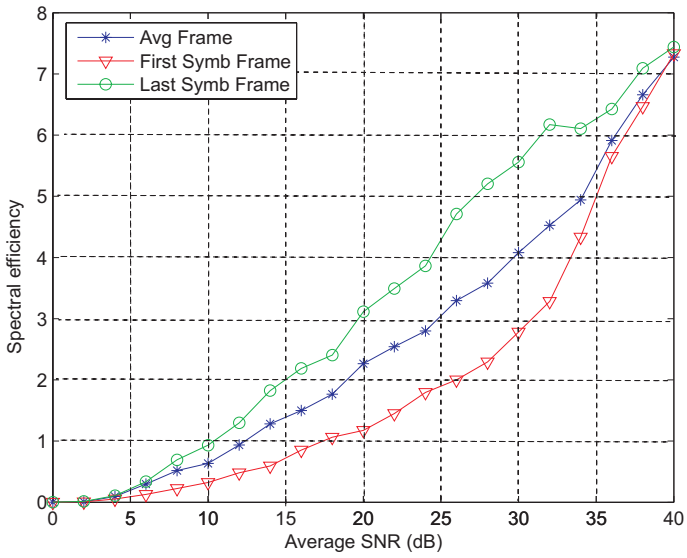

Figure 4.18: Spectral efficiency for different reported SNR with $f_d\tau = 0.1$

and the feedback delay corresponds to two frames. Figure 4.18 presents the results for the different options of selecting the CSI for feedback, based on the SNR of symbols of the frame. On account of a higher time correlation between the measure and the adaptation at the BS, reporting the SNR of the last symbol of the frame is shown to achieve the best performance. This solution provides the CSI with the lowest gap between received frame at MS and transmitted frame from the BS, and it reveals more gain at mid-range SNR.

4.3.2 Length of Delay between Frames

In the system proposed in this chapter, the BS receives the feedback from the terminal, and then it chooses the modulation level based on the updated thresholds, computed with the

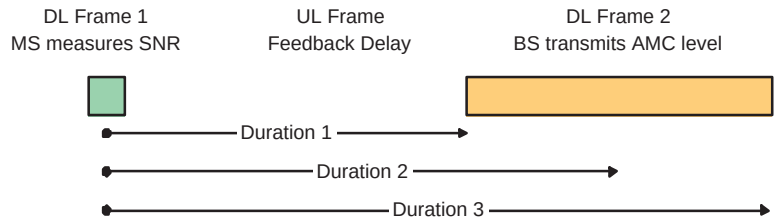

Figure 4.19: Different durations for designing AMC thresholds

knowledge of the feedback delay. The length of the delay between the symbol when the MS measures the SNR and the downlink frame at BS may have various interpretations. The duration of the delay can be calculated with respect to the first symbol, the middle, or the last symbol of the transmitted frame at the BS. Following the results from Section 4.3.1, the SNR of the last symbol of the received frame is reported via feedback. Figure 4.19 shows the different delays considered.

Figure 4.20 depicts the spectral effiency of the system when using updated SNR thresholds computed with the different delays. As in the previous section, the frame has a normalized length of 0.05, and a normalized feedback delay of 0.1. The *Duration* 1 corresponds to a normalized delay of 0.075 in the design of updated SNR thresholds, whereas *Duration* 2 and *Duration* 3 represent values of 0.1 and 0.125 of normalized delay, respectively.

The analysis of the results suggests that the three regions of average SNR should be considered separately. At poor channel conditions, with an SNR below 15 dB, the thresholds computed from the lowest delay, referred to as *Duration* 1, achieve better performance. As the updated thresholds are conservative in the rate adaptation, a higher delay considered implies a later start in the rise of the curve. In fact, considering a delay of 0.075, the system needs 10 dB to deliver 0.5 Mbit/s/Hz, while in a scenario with 0.125 delay, the system achieves the same throughput only at 17 dB of average SNR. In the range of 15 to 32 dB, the highest throughput is obtained with the normalized length 0.1. This delay considers the middle point of the frame and is more accurate for the symbols around the center of the frame when compared to the extremes, providing the highest

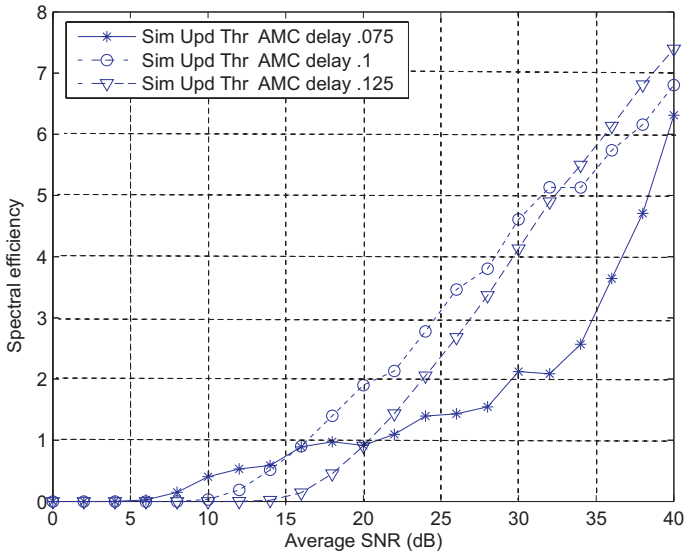

Figure 4.20: Spectral efficiency of different AMC thresholds with $f_d\tau = 0.1$

accuracy coverage of the frame. Above 32 dB, the SNR thresholds based on the duration with respect to the last symbol of the frame, *Duration* 3, deliver the highest performance. The high delay allows for a conservative and assured selection of rate, a preferable choice in very good SNR conditions.

On the basis of these findings, an adaptive approach to determine the best delay in the computation of thresholds for each region can be used. However, this adaptation is very sensitive to different scenarios. A more general approach consists of using the time delay between the last symbol of the frame at MS and the middle of the frame at BS, since it outperforms the other options in the mid-range SNR.

4.3.3 Summary

This section evaluated and proposed two features of the feedback design in the context of rate selection on a per frame basis. The analysis suggests that the MS measures the SNR of the last symbol of the received frame to send in feedback, and that the thresholds take into account the delay with respect to the center of the downlink frame.

4.4 Conclusions

This chapter proposed the general framework and specific mechanisms for a MIMO-OFDMA system. The focus was the design of a system that is aware of error in adapting to outdated channel information.

We proposed a MIMO switching mechanism based on the analysis of channel conditions and a measure of the channel information reliability delivered by the feedback. In accordance with this system, MIMO look-up tables were presented in a two-dimensional perspective to indicate the most favorable MIMO mode in a grid of average SNR and normalized feedback delay.

In terms of feedback design, the terminal should report to the BS the SNR of the last symbol of the received frame. Furthermore, the SNR thresholds should be computed based on a delay with respect to the center of the transmitted frame.

Having proposed a mechanism to select the MIMO mode on the basis of the performance and channel statistics of the link-level, in the next chapter, we assume a system-level perspective of cellular networks, and analyze the interference effects in MIMO and OFDM systems.

Chapter 5

Cochannel Interference and Asynchronous OFDM

The previous chapters described various MIMO techniques, link adaptation, and feedback issues at the link level. This chapter focuses on the system aspects of OFDM cellular networks, CCI, and asynchronous interference. Due to a high demand for spectrum use, CCI is one of the main sources of performance degradation in a cellular wireless system. Although transmit spatial diversity has been proposed in various standards as an effective mean to enhance wireless link reliability, the interaction of MIMO diversity techniques with CCI is still an open topic of research [B06]. In addition, the presence of cochannel signals in OFDM networks introduces additional interference that the system should cope with.

Cellular radio systems suffer from CCI in the downlink that arises from neighbor BSs transmissions. Such scenario is commonly encountered at the cell edge of urban macrocells, and the assumption of Rayleigh fading for both the desired and interfering signals is usually appropriate since both links experience deep fading from the terminal to the base station. Spatial diversity is an effective tool to provide robustness in the link at cell edge. Open-loop transmit diversity and receiver MRC are considered for the desired link. The analysis of the average probability of bit error of M-ary QAM considers the presence

of multiple independent interferers. The results are applicable to systems employing open-loop transmit diversity and MRC with coherent demodulation. The study analyzes the interaction between the number of equal power interferers and the spatial diversity order.

Asynchronous signals in OFDM system introduce additional interference in the performance of both broadcast and unicast scenarios. Even with synchronized transmissions at all BSs in the cellular scenario, the delay between cochannel signals arriving at the terminal increases the interference level creating ISI into the OFDM system [And05]. A larger cell radius of a hexagonal cellular layout increases the delays of the signals from neighbor BSs. In the unicast scenario, we consider linear receivers for interference cancelation, MRC and MMSE, to cope with CCI signals arriving from different BSs. Furthermore, we compare the performance of a suboptimal receiver based on the received signal covariance matrix.

The chapter is outlined as follows. Section 5.1 investigates the performance of spatial diversity systems in a scenario limited by CCI. Section 5.2 focuses on the effect of asynchronous received signals in the downlink of OFDM cellular scenarios for broadcast and unicast transmissions using spatial diversity. Section 5.3 concludes the chapter.

5.1 Effect of Cochannel Interference on Spatial Diversity

This section investigates the average probability of bit error performance of spatial diversity in the presence of independent equal power interferers. The performance of receive diversity in a fading environment with AWGN and CCI is traditionally measured in terms of outage probability, i.e., the probability of a user to be deprived of the service. Nevertheless, the average BER is also used to describe the performance of such systems as an important measure to determine the robustness of the link [CS99]. The average bit error rate in an MRC system that has independent interferers with identical or distinct mean powers was derived in [CA03]. In addition, the authors in [BZR05] present a comparison, in terms of statistical gain differences, of optimal combining and MRC algorithms in presence of interference. The interaction between the number of interferers and the

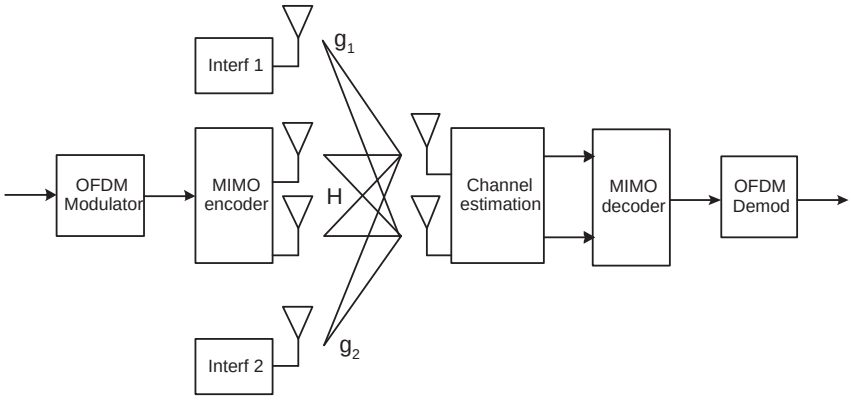

Figure 5.1: System model of MIMO desired link with multiple single antenna cochannel interferers

spatial diversity order studied here helps to understand the impact of using multiantennas in interference limited scenarios.

5.1.1 System Model

This section considers the downlink MIMO diversity channel, where both the BS and terminal have multiple antennas to exploit diversity. Moreover, we consider a number of single antenna interfering signals present at all diversity branches, as represented in Figure 5.1.

At the receiver end, the signals at the N_r antennas are weighted using MRC to maximize the output SNR. Although it is known that MRC is suboptimal in the presence of non-spectrally white interference, it is a practical blind technique for most communication standards that include MIMO diversity. The channel estimation of the desired link is assumed perfect at the receiver. The N_t antennas at the transmitter encode the signal using an orthogonal open-loop transmit diversity scheme, STBC.

Considering L interferers with one transmit antenna each, the interference channel fading model may be written as

$$\mathbf{y} = \sqrt{\frac{E_s}{N_t}}\mathbf{H}\mathbf{s} + \sum_{i=1}^{L}\sqrt{E_i}\mathbf{g}_i\mathbf{s}_i + \mathbf{w} \ ,$$

where $\mathbf{H}_{[N_r \times N_t]}$ is the channel matrix, $\mathbf{y}$ is the signal at the receiver array, $\mathbf{s}$ is the desired transmitted signal, $\mathbf{s}_i$ is the interferer i transmitted signal, and $\mathbf{g}_i$ is the channel of the single-antenna interferer i. Here, E_s and E_i are the powers of the desired and interfering users, respectively, while $\mathbf{w}$ is the complex AWGN with zero mean and variance N_0.

When employing orthogonal open-loop transmit diversity, and MRC at the receiver using the knowledge of the desired signal channel, the detected signal is calculated from

$$\mathbf{H}^H\mathbf{y} = \sqrt{\frac{E_s}{N_t}}\mathbf{H}^H\mathbf{H}\mathbf{s} + \sum_{i=1}^{L}\sqrt{E_i}\mathbf{H}^H\mathbf{g}_i\mathbf{s}_i + \mathbf{H}^H\mathbf{w} \ ,$$

where $(.)^H$ denotes the Hermitian transpose. In this case, the Signal to Interference and Noise Ratio (SINR), γ, can be written as

$$\gamma = \frac{\frac{1}{N_t}\|\mathbf{H}\|_F^2\frac{E_s}{N_0}}{\sum_{i=1}^{L}\frac{|\mathbf{H}^H\mathbf{g}_i|^2}{\|\mathbf{H}\|_F^2}\frac{E_i}{N_0}+1} \ , \tag{5.1}$$

where $\frac{E_s}{N_0}$ and $\frac{E_i}{N_0}$ are the average pre-processing SNR of desired link and Interference to Noise Ratio (INR) of user i. We define $\rho^a = \frac{E_s}{N_0}$ as the average pre-processing SNR per spatial link, and $\rho^I = \frac{E_s}{N_0}$ as the average pre-processing INR contribution of each interferer at the receive antenna. $\|\mathbf{H}\|_F^2 \equiv \mathrm{tr}(\mathbf{H}\mathbf{H}^H) = \sum_{p=1}^{N_r}\sum_{q=1}^{N_t}|h_{p,q}|^2$ is the squared Frobenius norm, i.e., the total power gain of the channel. We use (5.1) in the following section to characterize statistically the detected SINR.

5.1.2 Channel Statistics for Diversity and Interference

The wireless channel is a flat fading channel varying in time according to the classical Doppler. We assume the channel to be slowly time-varying, so that it is approximately constant for two consecutive symbols. The multipath fading environment is characterized by the Rayleigh fading channel for both the desired and interfering links. This scenario can be found in cellular radio systems, where neighbor cells introduce CCI in the desired link. Moreover, all the diversity branches of the desired link and the interfering signals are assumed to fade independently.

Under these assumptions, the SNR of the desired signal follows a chi-square distribution with $2N_tN_r$ degrees of freedom, as presented in Appendix D.3, and its PDF is given by

$$A = \frac{1}{N_t}\|\mathbf{H}\|_F^2\rho^a \ ,$$
$$f_A(a) = \frac{a^{N_tN_r-1}}{\Gamma(N_tN_r)\left(\frac{\rho^a}{N_t}\right)^{N_tN_r}}\exp\left(-\frac{a}{\frac{\rho^a}{N_t}}\right) \ .$$

Considering L equal power interferers, the total INR was proved in [CS99] to follow a chi-square distribution with $2L$ degrees of freedom:

$$B = \sum_{i=1}^{L}\frac{|\mathbf{H}^H\mathbf{g}_i|^2}{\|\mathbf{H}\|_F^2}\rho^I \ ,$$
$$f_B(b) = \frac{b^{L-1}}{\Gamma(L)\left(\rho^I\right)^L}\exp\left(-\frac{b}{\rho^I}\right) \ .$$

By taking the interpretation of the SINR as $SINR = \frac{SNR}{INR+1}$, i.e., $\gamma = \frac{A}{B+1}$, its PDF can be obtained from the distributions of SNR and INR employing the integration property for independent variables,

$$f_\gamma(\gamma) = \int_0^\infty (w+1)f_A\left((w+1)\gamma\right)f_B(w)\,dw \ . \tag{5.2}$$

Using the distributions of the random variables described above, it has been proved in [CA03, AR01] that the density function of the SINR is derived with the modified canonical distribution, thus obtaining a closed-form:

$$f_\gamma(\gamma) = \frac{\gamma^{N_tN_r-1}}{\Gamma(N_tN_r)\Gamma(L)\left(\frac{\rho^a}{N_t}\right)^{N_tN_r}}\exp\left(-\frac{\gamma N_t}{\rho^a}\right)\sum_{n=0}^{N_tN_r}C_n^{N_tN_r}\frac{(\rho^I)^n\Gamma(L+n)}{\left(\frac{\rho^I N_t}{\rho^a}\gamma+1\right)^{L+n}} \ . \tag{5.3}$$

The expression of the distribution of the SINR (5.3) is used below to derive the average probability of bit error.

5.1.3 Average Probability of Bit Error

This section presents the analytical study of the average probability of bit error. The mean BER, $\overline{P_b}$, is obtained by averaging over the PDF of the SINR given in (5.3),

$$\overline{P_b}(M) = \int_0^\infty P_b(M,\gamma) f_\gamma(\gamma) d\gamma \ , \tag{5.4}$$

where M is the order of the modulation employed, and $P_b(M,\gamma)$ is the BER in AWGN. Several approaches can be followed in order to obtain a closed-form approximation of (5.4), and to study the performance of each technique with respect to the average probability of bit error.

As shown in Appendix E.1, the approximation for the probability of bit error valid for M-QAM is

$$P_b(M,\gamma) \approx 0.2 \exp\left(-\gamma \frac{1.6}{M-1}\right) \ . \tag{5.5}$$

Note that the approximation of this formula is tight for lower order modulations; thus, in order to ensure an accuracy of up to 1 dB, we target modulations lower than or equal to 64-QAM.

By applying (5.5) and (5.3) to (5.4), we derive the average probability of error:

$$\begin{aligned}\overline{P_b}(M) \approx & \frac{0.2}{\Gamma(N_t N_r)\left(\frac{\rho^a}{N_t}\right)^{N_t N_r}} \sum_{n=0}^{N_t N_r} C_n^{N_t N_r} (\rho^I)^n \frac{\Gamma(L+n)}{\Gamma(L)} \\ & \times \int_0^\infty \frac{\gamma^{N_t N_r-(L+n+1)}}{\left(\frac{1}{\gamma}+\frac{N_t \rho^I}{\rho^a}\right)^{L+n}} \exp\left[-\gamma\left(\frac{N_t}{\rho^a}+\frac{1.6}{M-1}\right)\right] d\gamma \ ,\end{aligned}$$

where the integral in this expression still has no known closed-form expression. However, in a high Signal to Interference Ratio (SIR) scenario, e.g., when the user is close to the cell center with a strong desired signal, but some interference from neighbor BSs still exists,

the expression can be simplified, using a hign-SNR approximation $\frac{\rho^I}{\rho^a} \to 0$, to

$$\overline{P_b}(M) \approx \frac{0.2}{\Gamma(N_t N_r)\left(\frac{\rho^a}{N_t}\right)^{N_t N_r}} \sum_{n=0}^{N_t N_r} C_n^{N_t N_r} (\rho^I)^n \frac{\Gamma(L+n)}{\Gamma(L)} \times \int_0^\infty \gamma^{N_t N_r - 1} \exp\left[-\gamma\left(\frac{N_t}{\rho^a} + \frac{1.6}{M-1}\right)\right] d\gamma \ .$$

The average BER can then be approximated in closed-form as

$$\overline{P_b}(M)|_{SIR \gg 1} \approx \frac{0.2}{\left(1 + \frac{1.6}{M-1}\frac{\rho^a}{N_t}\right)^{N_t N_r}} \sum_{n=0}^{N_t N_r} C_n^{N_t N_r} (\rho^I)^n \frac{\Gamma(L+n)}{\Gamma(L)} \ . \tag{5.6}$$

The next section argues that a closed-form expression of the average bit error probability allows a better understanding of the interactions between spatial diversity and interference.

5.1.4 Results and Discussion

This section presents analytical results of a system with multiple equal power interferers in a Rayleigh fading scenario, and with QPSK transmission.

As mentioned in the previous section, the exact closed-form for the average BER (5.4) is unknown; thus, this expression can be approximated with a numerical integration method. Using a trapezoidal numerical integration, we evaluate the performance of a MIMO diversity system in the presence of interferers. Figure 5.2 depicts the mean BER, $\overline{P_b}(M)$, versus the number of interferers for a system employing QPSK modulation and coherent detection. The result is based on the standard formula for P_b under AWGN that is shown in Appendix B in (B.1). The analysis assumes that all the interferers have the same power-to-noise ratio, $\rho^I = 0$ dB, and the number of interferers present in the system varies. Figure 5.2 represents the degradation of a MIMO diversity system when increasing the number of interferers, i.e., raising the total interference power.

It is worthwhile noting that the performance gain obtained with transmit antennas disappears faster than the gain obtained with receive antennas, see Figure 5.2. Even in

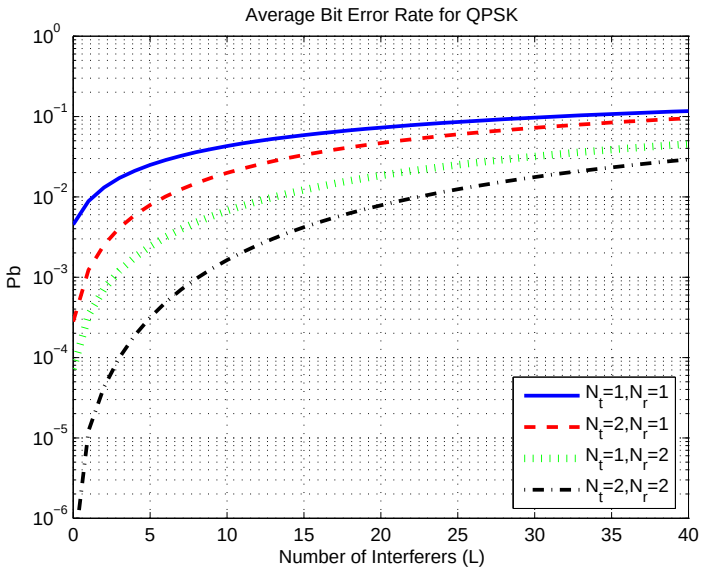

Figure 5.2: Average BER versus the number of interferers with high power. SNR $\rho^a =$ 20 dB, and INR per interferer $\rho^I = 0$ dB

a high interference scenario, there is a gain when using MRC compared to SISO, while a higher number of transmit antennas does not improve the performance significantly. For instance, at a BER of 10^{-2}, receive diversity can cope with up to thirteen interferers, while transmit diversity can cope with only five interferers. This effect can be explained by the presence of array gain in MRC scheme that makes the scheme more robust to interference, compared to open loop transmit diversity.

In Section 5.1.3, we propose a closed-form expression (5.6) for the asymptotic analysis of the average probability of bit error. In order to assess the accuracy of this expression, we consider a scenario with a desired signal SNR of 20 dB and multiple interferers, each having an INR of -10 dB, thus satisfying high SIR condition. Figure 5.3 illustrates the average BER for both methods of approximation, i.e., the numerical integration and the asymptotic closed-form. As the SIR increases, the curves tend to overlap, then validating the approach in the asymptotic analysis.

An important factor in the analysis of the interference in MIMO diversity systems is the effect of the number of interference sources to the average probability of bit error. Therefore, we consider a constant total interference power, ρ^I_{total}, and vary the number of

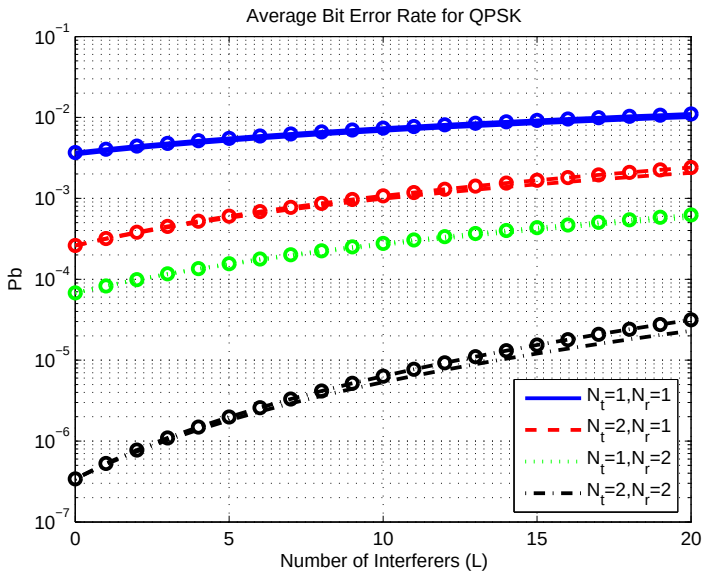

Figure 5.3: Average BER versus the number of interferers with low power. SNR is $\rho^a = 20$ dB and INR per interferer is $\rho^I = -10$ dB. The lines with '$\circ$' represent the approximation of the closed form expression (5.6)

interferers. Moreover, we consider that each interferer has the same power, i.e., the total interference power is shared among the interferers with INR of $\rho^I = \frac{\rho^I_{total}}{L}$. Figure 5.4 shows the closed-form expression of $\overline{P_b}(M)$ versus the number of interferers for different MIMO configurations. Assuming the same total interference power, we see that the performance of a SISO link is independent of the number of active interferers in the system. However, when spatial diversity is higher than one, the impact of the number of interferers appears. In fact, when exploiting diversity at mid SINR range, the average BER turns out to be lower with a larger number of weak interferers than with fewer strong interference sources.

In order to understand the relation between the number of interferers and the spatial diversity, we analyze the closed-form expression in the asymptotic behavior of $\overline{P_b}(M)|_{SIR \gg 1}$. From (5.6), we can separate the sum in n and use the property of the

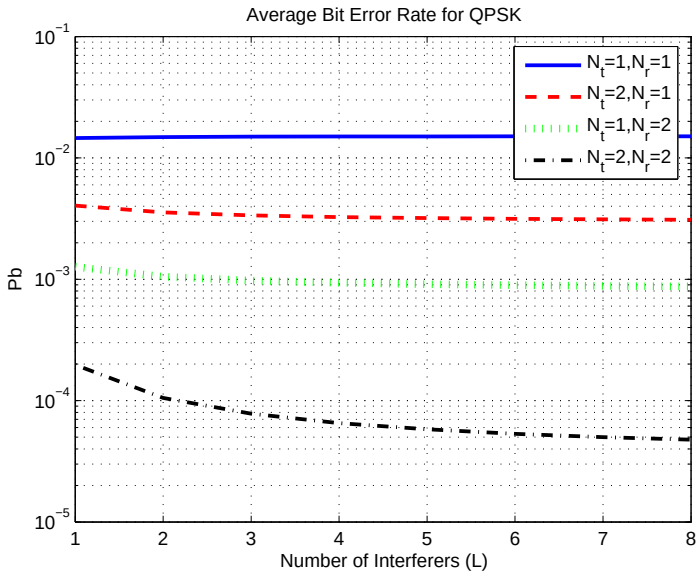

Figure 5.4: Average bit error rate versus the number of interferers when the SINR remains constant. SNR is $\rho^a = 25$ dB and total INR is $L\rho^I = 10$ dB, i.e., a constant SINR of $\gamma \approx 14.6$ dB

complete gamma function, $\Gamma(a) = (a-1)!$, to obtain the following expression:

$$\overline{P_b}(M)|_{SIR\gg 1} \approx \frac{0.2}{\left(1+\frac{1.6}{M-1}\frac{\rho^a}{N_t}\right)^{N_tN_r}} \times \left[1 + N_tN_r\rho^I_{total} + \sum_{n=2}^{N_tN_r} C_n^{N_tN_r}(\rho^I_{total})^n \prod_{k=1}^{n-1}\left(1+\frac{k}{L}\right)\right] . \quad (5.7)$$

Note that for $N_tN_r = 1$, the value of $\overline{P_b}(M)|_{SIR\gg 1}$ does not depend on the number of active interferers L, but it only depends on the total power of interference. Moreover, as observed in numerical evaluation, when the spatial diversity of the desired signal increases, i.e., $N_tN_r \geq 2$, the number of equal power interferers affects the average probability of bit error. In fact, for a given diversity order, a lower value of L will increase the probability of bit error. The last product term of (5.7) also shows that a higher diversity order system is more sensitive to the value of L. However, this effect is only valid for low number of interferers. Figure 5.4 shows that $\overline{P_b}$ tends to be constant for $L > 6$.

5.1.5 Summary

In this section, we studied the impact of CCI on the performance of a spatial diversity link. The average probability of bit error is evaluated considering that both the interfering and desired signals experience Rayleigh fading channels. Transmit diversity proved to be less robust to an increase in the number of interferers, compared to receive diversity. We derived a closed-form expression for the asymptotic performance of average probability of bit error, and used it to explain the relation between the number of interferers and the diversity order of the system.

In the case of a constant total interference power, the number of active interferers was shown to have impact on the performance of a system with spatial diversity. More specifically, we showed that it is preferable to have multiple weak interferers when compared to one single strong interferer, and this effect tends to be more marked with the increase of the diversity order at mid-range SINR conditions.

5.2 Asynchronous Cochannel Signals in Cellular OFDM Systems

This section focuses on the impact of time-delayed signals in OFDM cellular scenarios. Due to its relevance in intercell interference, two configurations are considered for transmission in the downlink, broadcast and unicast.

In the OFDM downlink of both unicast and broadcast schemes, the asynchronous signals at the terminal, originated at different BSs, create an additional source of interference, i.e., ISI. This issue has a greater effect in the uplink, due to the asynchronism among users [THJ05, And05]. However, in the downlink problem, even with synchronized BSs, the differences in propagation delay create interference that is difficult to avoid with simple receivers at the terminal side. Several algorithms have been proposed for downlink intercell time synchronization at the receiver [KMAH02, JSC+07], and it is generally accepted that synchronized transmission from BSs is a practical assumption [And05, SH03].

This section assumes a downlink channel with synchronized BSs and linear receivers at the MS.

In broadcast transmission, the users at cell edge benefit from diversity gain by combining the signals from different BSs, leading to increased performance. Nevertheless, the long delays experienced by the terminal in the channel impulse response affect the performance, and new channel models need to be defined [Col07].

In single-frequency cellular networks, the unicast transmission to the users at cell edge experiences high levels of CCI. Although adaptive antenna arrays can be used to minimize the CCI in single-frequency networks [LS99], this technique requires the channel matrix coefficients to be available at the transmitter. Therefore, the effect of asynchronous signals in the OFDM performance, as well as the robustness of MIMO diversity techniques against CCI, still remains open to research [B̈06].

5.2.1 System Model

We consider the downlink of an OFDM system with L cochannel signals, as represented in Figure 5.1 in Section 5.1. Additionally, this section focuses on system level aspects, including a realistic number of interferers, and assuming that the received signals experience different propagation delays and pathloss from the BSs to the terminal. The OFDM system uses a bandwidth of 10 MHz with 1024 subcarriers, and a CP length of 72 samples that correspond to 4.67 µs, equivalent to the 3GPP LTE specifications [3GP06a]. The 600 available data subcarriers are allocated to one user. The implementation of the system in the link-level simulator is described in Appendix G. Furthermore, two transmission types are considered for the simulation of cochannel signals, broadcast and unicast.

5.2.1.1 Linear model for Unicast and Broadcast

A narrowband linear model describes the received signal at one OFDM subcarrier, and it is used to decode the signal.

Broadcast All the BSs transmit the same data, while the receiver is considered to perfectly estimate the combined channel. The narrowband linear model can be written as

$$\mathbf{y} = \left(\sqrt{E_s}\mathbf{H} + \sum_{i=1}^{L} \sqrt{E_i}\mathbf{G}_i \right) \mathbf{s} + \mathbf{w} + \delta \ ,$$

where E_s and $\mathbf{H}$ are the power and the channel matrix of the strongest signal, respectively. The symbol $\mathbf{s}$ represents the data source transmitted in broadcast, $\mathbf{G}_i$ is the channel matrix of the signal i, and E_i represents its power. Here, $\mathbf{w}$ is the AWGN, and δ corresponds to the error introduced by the asynchronous nature of the other received signals in the OFDM demodulation process.

Unicast The desired BS transmits the data at the same time as the interferers send independent streams of information, i.e., CCI. When MRC receiver is considered, we assume ideal channel knowledge of the desired link, and no information about interferers. On the other hand, for the MMSE receiver, the system employs channel knowledge of the desired and interfering links. The narrowband linear model is written as

$$\mathbf{y} = \sqrt{E_s}\mathbf{H}\mathbf{s} + \sum_{i=1}^{L} \sqrt{E_i}\mathbf{G}_i\mathbf{s}_i + \mathbf{w} + \delta \ ,$$

where $\mathbf{s}_i$ are the independently generated interfering data streams. As in the broadcast case, E_s and $\mathbf{H}$ are the power and the channel matrix of the desired signal, while E_i and $\mathbf{G}_i$ are the power and the channel matrix of the interfering signal i, respectively.

5.2.1.2 Cellular Scenario

The scenario layout is represented in Figure 5.5, and it consists of a hexagonal grid cellular scenario of two tiers with nineteen BSs and three sectors each, similar to the 3GPP evaluation method [3GP06a]. The letters in the figure identify the positions of the terminal in the cell. Four positions correspond to the cell-edge users, A, B, C, and F. In addition, two locations are considered in the mid-range of the cell, D and E.

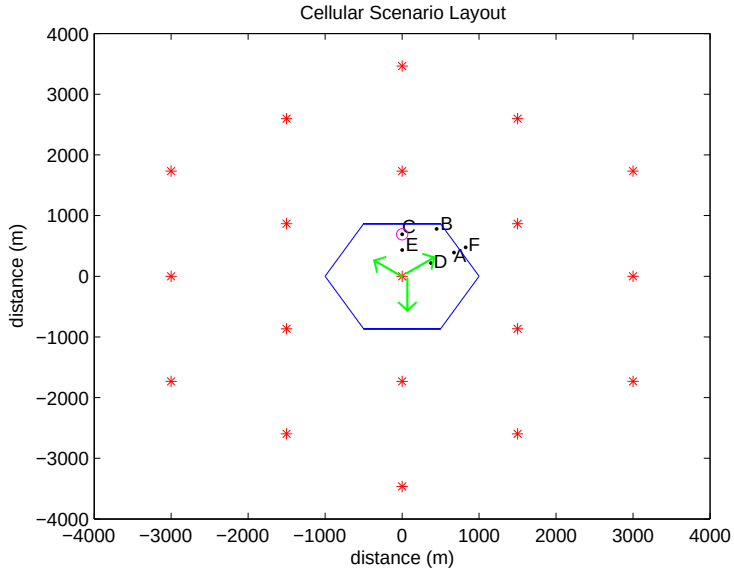

Figure 5.5: Cellular scenario for a cell radius of 1000 m

As specified by [3GP07], the antenna pattern of a three sector BS has the directional gain given by

$$A(\theta) = -\min\left[12\left(\frac{\theta}{\theta_{-3\text{dB}}}\right)^2, A_m\right] \quad , \tag{5.8}$$

where $-180^\circ \leq \theta \leq 180^\circ$ is the angle between the direction of departure and the boresight of the antenna, $\theta_{-3\text{dB}} = 70^\circ$ is the 3 dB beamwidth, and $A_m = 20$ dBi. The boresight points at the middle of the hexagonal cell side, as shown by the arrows in Figure 5.5, and the antenna gain at the BS is 14 dBi. The serving BS, i.e., the closest BS to the terminal, may have either one single transmit antenna in SIMO configuration, or two spatially uncorrelated transmit antennas in MIMO configuration for the desired link. The other BSs are assumed to have a single transmit antenna.

5.2.1.3 Channel Power Delay Profile

The multipath channel model used in this work is the Vehicular A model with 6 taps [3GP07]. The average power and delay of the paths is depicted in Figure 5.6(a). We assume that the links from all BSs to the terminal follow the same PDP.

In the cellular scenario described above, the user assigned to the central BS receives

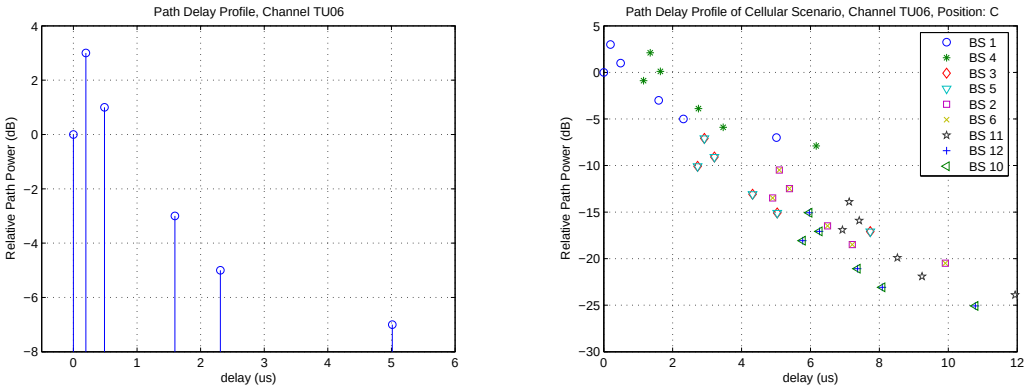

(a) power delay profile of TU 6 paths channel

(b) power delay profile of the received signal

Figure 5.6: Average power of the channel paths of a terminal in position C of the cellular layout with cell radius 1000 m

the signal from all BSs with a certain attenuation and delay that depends on its position in the cell. The pathloss model considered is the macrocell scenario specified in [3GP07]. We assume that all the BSs are synchronized at transmission in the downlink, and focus on the propagation time delay between the signal received from its own BS, and the signal received from neighboring BSs. The channel PDP takes into account the delay between that signal, in addition to the attenuation due to pathloss and antenna patterns. The PDP experienced by a terminal in the position C of the cell is depicted in Figure 5.6(b). The eight strongest neighboring BSs are considered for simulation of interference.

5.2.2 Effect of Cochannel Signals in Broadcast

The results for broadcast are obtained with a SIMO configuration between the closest BS and the terminal, i.e., the BS has one transmit antenna, and the receiver has two antennas. The system uses a 16-QAM modulation and 2/3 rate turbo code. The signals received are properly weighted using MRC to maximize the output SNR.

In order to assess the effect of the delay between cochannel transmissions, we consider the effect of two broadcast signals that arrive at the terminal separated by a certain time delay. Although a stronger cochannel signal boosts the performance by providing diversity for the link, when this delay is larger than the CP, it causes interference. In the OFDM

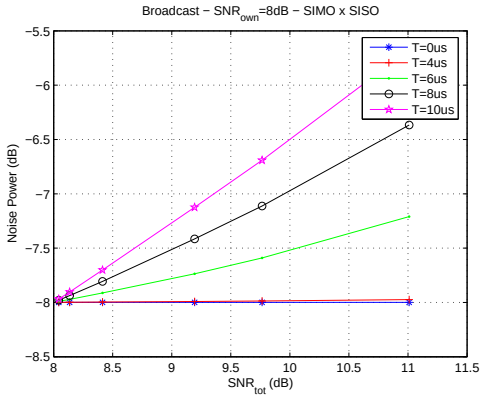

(a) noise and interference to desired signal power ratios

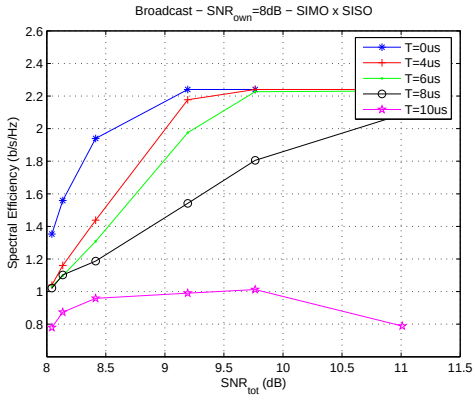

(b) spectral efficiency

Figure 5.7: Effect of single interferer delays in broadcast

system, additional interference arises when the delay is such that part of the channel taps arrive outside the CP. For this simulation, the power of the first signal is fixed to an SNR of 8 dB, while one delayed cochannel signal is considered with increasing power, i.e., the total SNR increases. The graph in Figure 5.7(a) shows, for various delays of the cochannel signal, the noise power arising from the combined effect of white gaussian noise and ISI due to channel taps arriving after the CP based on the combined PDP. The abscissa of the graph shows the total SNR of the combined signals. At higher SNR, i.e., with stronger cochannel signal arriving at a certain delay, the noise and ISI power increases. As expected, this effect is only significant when the delay is greater than the length CP, which is 4.67 µs.

Figure 5.7(b) shows the spectral efficiency at different delays. It is worthwhile noting that when a long delay is experienced, there is a peak of performance in the balance of powers of the first signal to arrive, and of the delayed cochannel signal. The stronger power of the delayed signal degrades the performance, since it introduces ISI into the system. The diversity benefit of broadcast is achieved only for delays up to 6 µs.

After studying the effect of a single delayed cochannel signal, we analyze the impact of cellular configurations in broadcast transmissions. In the cellular scenario described in Section 5.2.1.2, we analyze the performance of a terminal positioned at the cell edge,

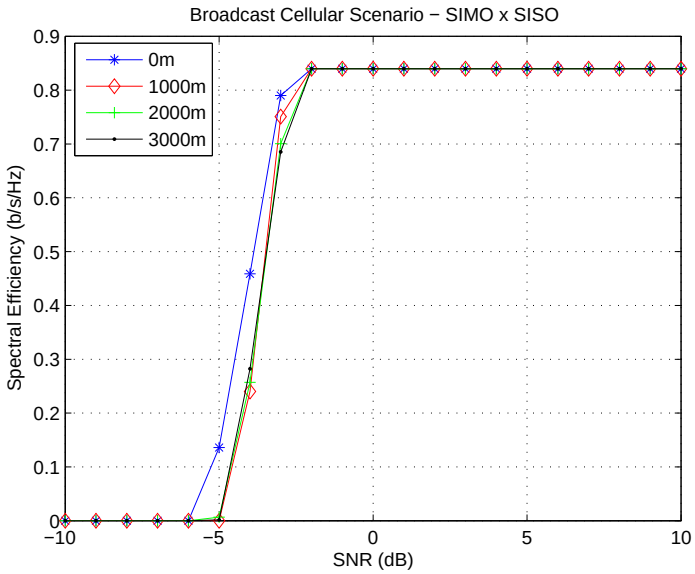

Figure 5.8: Spectral efficiency of downlink cellular broadcast system for different cell radius. The modulation employed is QPSK and the coding rate is 1/2

position *B*. For simulation purposes, we consider the eight strongest signals arriving from the neighboring BSs. In order to study the effect of the asynchronous signals on the OFDM demodulation, we consider different radiuses for the cellular layout. A radius of 1000 m corresponds to an Inter-Site Distance (ISD) of 1732 m. As the distance in-between the BSs increases, the delay in-between the received signals at the terminal increases due to larger propagation time differences. Therefore, a higher ISD of the scenario implies an inherently looser time synchronization of the received signals. When strong signals arrive out of the cyclic prefix duration, the OFDM symbol suffers ISI. In the following results, the curve with legend "0 m" corresponds to a reference case, when both signals arrive at the same time instant, i.e., no time delay.

The graph in Figure 5.8 depicts the spectral efficiency of the system with QPSK modulation and 1/2 code rate in the position B in the cell. Only a slight degradation in the throughput can be observed. The effect of asynchronous signals at the receiver can be shown more clearly at higher modulation orders, since these are more sensitive. The spectral efficiency of a user at cell edge employing 16-QAM with 2/3 coding rate is given in Figure 5.9 for the same three cell radius. The results evidence a spectral efficiency loss

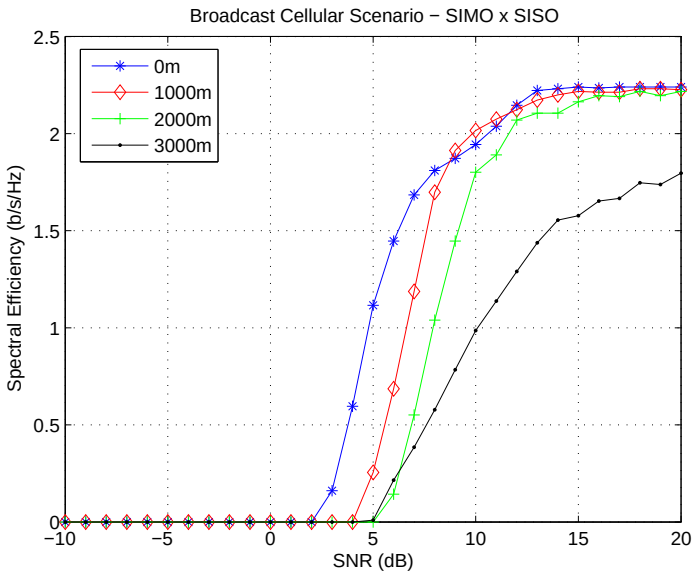

Figure 5.9: Spectral efficiency of downlink cellular broadcast system for different cell radius. The modulation employed is 16-QAM and the coding rate is 2/3

with increasing cell size, especially noticeable for the 3000 m radius. For micro cells with cell radius lower than 1000 m, the degradation in performance does not exceed 1 dB.

5.2.3 Effect of Cochannel Signals in Unicast

Similarly to the previous section, a SIMO setup with two antennas at the receiver is considered with MRC, i.e., no knowledge of the interferers' channels is assumed.

We analyze the effect of a unicast system with two signals arriving at the terminal, where the first signal is the desired link, and the second signal accounts for CCI with time delay. The graph in Figure 5.10(a) shows the noise power arising from the combined effect of white gaussian noise and ISI due to signal energy arriving after the CP length. The power of the closest BS, E_s, is fixed, while one delayed interferer is considered with decreasing power, i.e., the total SINR increases. It can be seen that at a lower SINR, i.e., with stronger cochannel signal arriving at a certain delay, the noise power increases. One observes that this effect is only significant when the delay is greater than the CP of 4.67 µs. Furthermore, the Interference to Signal Ratio (ISR) is plotted in the same graph to show the relation with the noise power. A strong interferer power degrades the system

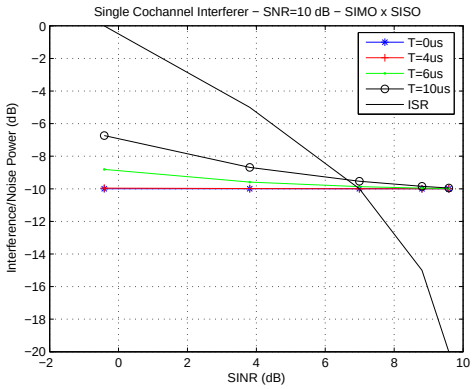

(a) noise and interference to desired signal power ratios

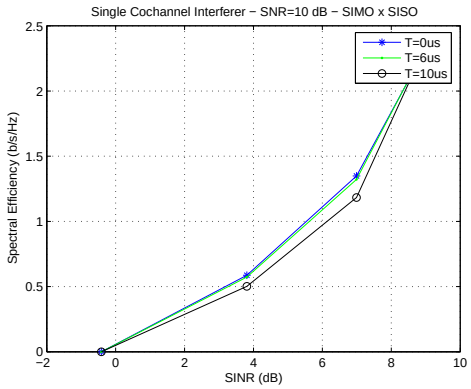

(b) spectral efficiency

Figure 5.10: Effect of single interferer delays in unicast

performance proportionally to the ISR. For low SINR, the ISR effect is greater than the interference due to the delay between signals, thus making the effects of interference and time delay difficult to separate.

For the same simulation configuration, Figure 5.10(b) illustrates the spectral efficiency at different delays. All the curves include the interference signal with power defined by ISR, shown in previous graph. The performance degradation due to asynchronous interference is not as noticeable as in the broadcast case, since in this situation the performance is limited by the interference power directly. Moreover, we note that the spectral efficiency is also lower than in broadcast case.

After studying the effect of a single delayed cochannel interferer, we analyze the impact of unicast transmissions in cellular configurations. Using the cellular scenario described in Section 5.2.1.2, the simulations are run for a terminal situated in different positions at the cell in a unicast system. The hexagonal cells have a radius of 1000 m, i.e., ISD of 1732 m. The receiver has two antennas, and the signals are combined using MRC, assuming perfect channel estimation of the link with the serving BS. The channel gains of the interfering BSs are unknown at the receiver. The spectral efficiency versus the desired signal SNR is given in Figure 5.11.

Figure 5.12 depicts the performance of a terminal at the cell edge for various cell

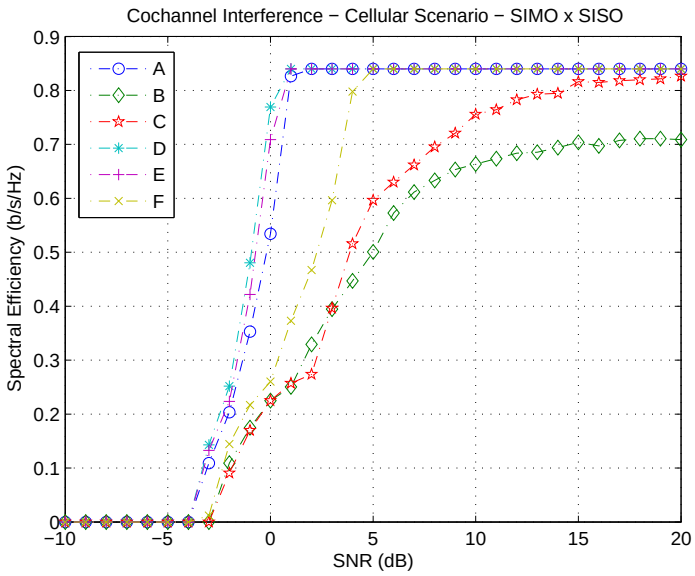

Figure 5.11: Spectral efficiency for different positions in the cell. Unicast signal with QPSK and MRC receiver

radiuses. A higher order of modulation is used in this simulation, since it is more sensitive to the interference arising due to signal delays. Although with large cells the OFDM system suffers degradation from the increased delays of asynchronous signals, the interference power plays a more important role than the ISI effects. This can be seen by the ISR level in Figure 5.10(b) and the moderate effect of delays in Figure 5.12.

5.2.4 Known Interference with MMSE Detection

MRC is a suboptimal approach for multiple antennas in the presence of cochannel interferers [CFS97]. Optimal combining is achieved at the cost of estimating the channel of all interferers [SH98]. Figure 5.13 shows that the performance is increased when MMSE receiver is used with the knowledge of the interfering channels. Higher gains in spectral efficiency are obtained at cell edge, i.e., positions B, C, and F, where interference is high. In the following, we study an MMSE-like receiver that does not require the knowledge of the interfering signal channels.

This section investigates the gain in performance available by using interfering channel information at the receiver. In the presence of CCI, the optimal combining is achieved

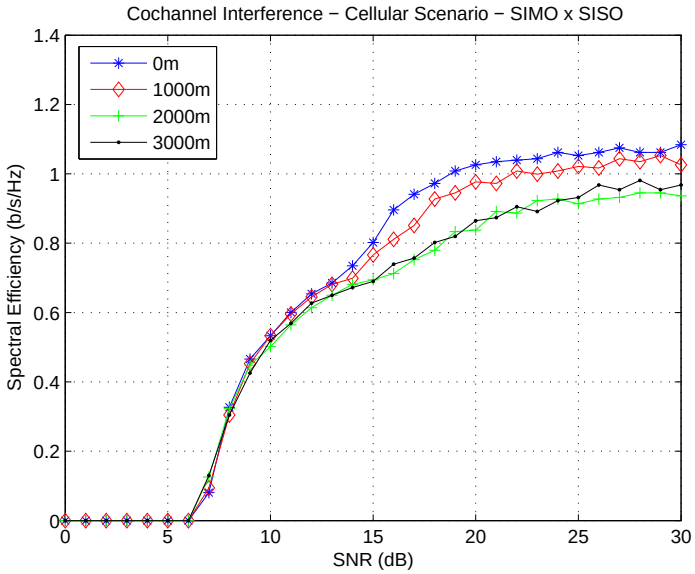

Figure 5.12: Spectral efficiency for different positions in the cell. Unicast signal and 16-QAM

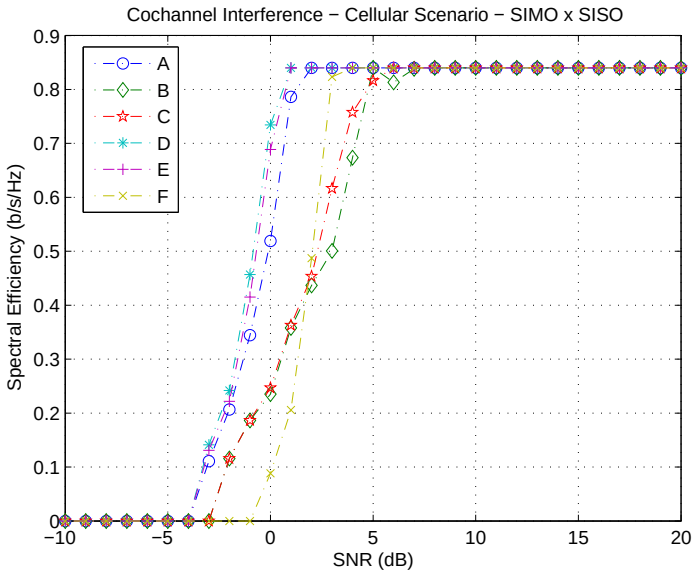

Figure 5.13: Spectral efficiency for different positions in the cell. Unicast signal with QPSK and MMSE receiver

using an MMSE receiver with the knowledge of the interfering link channels. We consider a more practical case where the channel information is estimated from the received signal without knowledge of the individual interferer channels. This is achieved by using an estimate of the covariance matrix of the received signal as follows:

$$R_{yy} = E[yy^H] \ ,$$
$$\widehat{y} = yR_{yy}^{-1} \ .$$

In order to obtain a robust estimate of the covariance matrix, a large number of symbols is needed for statistics. In a slow variation channel, the required period of analysis increases, since we need to observe the channel for a longer period to obtain a closer estimate of the real average.

The OFDM system has a Fast Fourier Transform (FFT) size of 1024 for a bandwidth of 10 MHz, and we consider the speed of 3 km/h. At this speed, the coherence time of the channel is 32.2 ms. Similarly, based on the RMS delay spread of the Vehicular A channel profile, i.e., 370 ns [ITU97], the 50% coherence bandwidth is 430 kHz. We use an averaging window to obtain an estimate of the covariance matrix of the received signal. The window has 80 symbols, corresponding to 5.3 ms, and 6 subcarriers, corresponding to 58.6 kHz, i.e., it is within the coherence time and coherence bandwidth, respectively. The averaging window choice is based on preliminary studies to maximize performance for the time and frequency selectivity. We refer this scheme as Windowing-MMSE.

In a SIMO configuration of the desired channel, the performance at the cell edge of a cellular scenario with ISD of 1732 m is shown in Figure 5.14. The performance of MMSE with full channel knowledge is clearly superior to the MRC receiver with unknown interfering channels. However, it is also shown that the performance of the Windowing-MMSE scheme described above achieves a performance very close to MMSE. In the following, we study the performance of the receiver with transmit spatial diversity.

As introduced in Chapter 2, space-time coding is an open-loop transmit diversity scheme where diversity is achieved, e.g., STBC [TJC99]. The same concept can also be

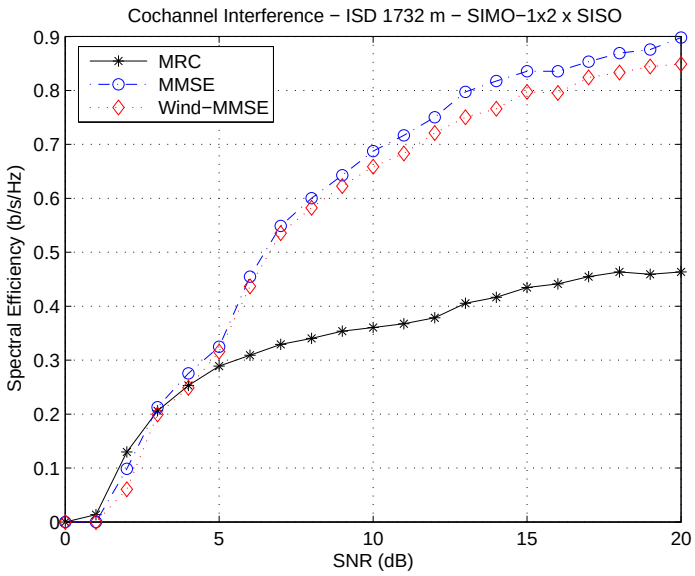

Figure 5.14: Spectral efficiency for receivers MRC, MMSE, and Window-MMSE for SIMO configuration. Unicast signal and 16-QAM

implemented in the frequency domain, applied on consecutive OFDM subcarriers, i.e., SFBC. We consider a system that employs SFBC in the presence of CCI. Figure 5.15 shows the results for a 2×2 configuration for the desired link and single transmit antenna interferers.

Although the gain compared to the use of MRC is still considerable, the degradation due to the use of an estimate of the covariance matrix of the received signal is greater than the observed in the previous SIMO case, i.e., the degradation is up to 40% of spectral efficiency.

5.2.5 Summary

This section analyzed the impact of time-delayed signals in the downlink of an OFDM cellular system and showed a very different effect in broadcast and unicast scenarios.

The results revealed that in a broadcast transmission a tradeoff exists between the strength of other than own BS signals and their relative time delay. This fact strengthens the conclusion that the ISD of the scenario has to be taken into account in the choice of the CP length. In unicast, the delay between received signals at the terminal has a lower

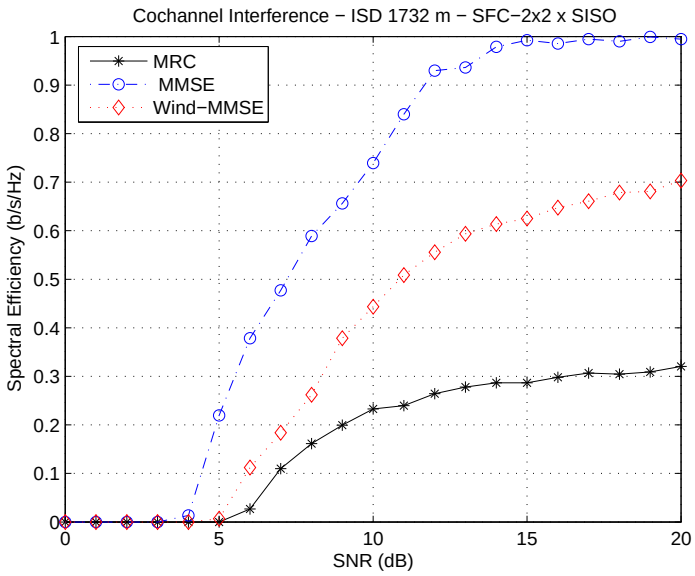

Figure 5.15: Spectral efficiency for receivers MRC, MMSE, and Window-MMSE for MIMO diversity. Unicast signal with 16-QAM

impact on performance, since the interference power introduced by the CCI links accounts for a larger part of the loss. The loss in performance due to a larger distance in-between BSs appeared to affect cellular scenarios with radius beyond 2000 m.

In the presence of interferers, the optimal combining of multiple receive antennas is achieved only if full channel knowledge of the interfering links is used. A more practical blind receiver strategy that approaches the performance of the MMSE receiver, Windowing-MMSE, was implemented in the system. This technique is based on the estimate of the covariance matrix of the received signal, averaged over time and frequency. Although the results of Windowing-MMSE for SIMO present a significant gain over MRC, achieving a performance very close to MMSE, this technique becomes more sensitive channel estimation errors when transmit diversity is employed. When using SFC, the loss with respect to the MMSE receiver is about 40%, showing that the covariance matrix estimation is more sensitive in this case. Nevertheless, the proposed scheme still outperforms the MRC receiver.

5.3 Conclusions

This chapter studied the effect of CCI in the performance of spatial diversity links and OFDM systems.

For a MIMO diversity link that is affected by interference, transmit diversity loses its performance gain in the presence of multiple interferers faster than receive diversity. Therefore, in stronger interference scenarios, it is more reliable to have a higher number of receive antennas, rather than transmit antennas. We derived a closed-form expression of the asymptotic behavior of the average probability of bit error. This expression was then used to analytically explain the relation between the number of interferers and diversity. When applying spatial diversity, a lower number of interferers resulted in an increase in BER performance.

The impact of time delay between cochannel signals was shown to have a very different effect in each transmission mode. In fact, while in broadcast transmission the time synchronization plays a crucial role in spectral efficiency performance, in unicast transmission this issue has a lower impact. These results suggested that cellular scenarios with radius beyond 2000 m experienced the degradation of performance if a longer CP was not applied in broadcast transmission.

In the presence of interferers, we compared the use of optimal combining with channel knowledge and a suboptimal receiver to increase performance with respect to MRC. Simulating the link level impact on a coded system, the performance of SIMO configuration showed that the gap between the suboptimal and optimal MMSE receivers was very small. However, when SFBC was employed, the technique became more sensitive to estimation errors, due to the larger covariance matrix.

Chapter 6

Conclusions and Future Work

This thesis addressed the integration of spatial processing with multicarrier and channel-aware techniques. The thesis attempted to answer the question: "What is the effect of the interaction between multiantenna OFDM and channel-aware adaptation in interference and time-varying scenarios?" As a result, the main contributions were: the development of an analytical framework of rate adaptation for selected MIMO schemes in a time-varying channel, the design of a MIMO switching mechanism and subchannel allocation of a MIMO-OFDM system, and the analytical evaluation of the effect of Cochannel Interference (CCI) on spatial diversity.

Multiple antenna processing increases spectral efficiency through array, diversity, and/or multiplexing gains. The comparison and discussion of the integration of OFDM with different MIMO processing schemes in Chapter 2 has confirmed that antenna arrays are well-suited to outdoor low angular spread scenarios when compared with spatial diversity.

A recent framework of spatial processing introduced the linear dispersion concept in MIMO, and codes that exploit both high spatial rate and diversity. We demonstrated that the use of trace orthogonal design space-frequency LDC with linear receivers combined with AMC provides a tradeoff between spatial diversity and multiplexing in a practical system. However, we need to avoid a BER floor if the number of receive antennas is no

larger than the number of transmit antennas. In fact, the LDC shows poor results at a high modulation order and a low number of receive antennas, but it does reveal a superior performance at low SNR with smaller constellations.

In the subsequent part of the study, Chapter 3 focused on problems inherent in the use of CSI for fast adaptation via feedback in mobile scenarios. An analytical framework of rate adaptation for selected MIMO schemes in a time-varying channel was developed, and the results suggest that a careful design must be made when aiming at fast adaptation of transmission parameters when using MIMO techniques. More specifically, we focused on the reliability of the CSI transmitted via feedback, and the effect of outdated channel knowledge on different MIMO modes: spatial diversity, multiplexing, and antenna selection. New closed-form expressions for BER performance were obtained for the selected MIMO techniques. On the strength of these expressions, we derived analytical SNR thresholds to adapt modulation based on outdated channel information. These thresholds are thus dependent on the MIMO configuration and on a measure of reliability that integrates the time correlation and feedback delay.

The previous work and results suggest that a measure of the feedback delay and time variability of the channel is required in choosing the MIMO scheme that delivers the highest throughput. In Chapter 4, we took into consideration the design of a selection of transmission parameters in a MIMO-OFDM system, and proposed a two stage modulation and MIMO mode selection. In the first stage, the system uses a look-up table to switch between MIMO modes based on the average channel strength and the feedback delay. In the second stage, the analytical thresholds, specific to the MIMO scheme selected, are applied to choose the modulation for transmission based on the CSI. Therefore, instead of merely using the CSI in the fast adaptation of modulation, we proposed a mechanism for modulation and MIMO selection based on feedback delay and terminal mobility.

The presence of CCI creates additional challenges to the performance of spatial diversity systems. In Chapter 5, we developed an analytical framework to evaluate the performance of spatial diversity in the presence of CCI. The outcome suggests that there

is an effect of varying the number of interfering sources affecting a spatial link with a diversity order above two. In fact, with a linear MRC receiver, a single strong interferer degrades the BER performance to a greater extent than multiple weak interferers.

In cellular systems, the asynchronous received signals that arrive in the downlink from multiple BSs have a different effect in broadcast and unicast modes of OFDM. We showed that a cellular scenario with cell radius beyond 2 km degrades significantly the broadcast transmission in macrocells, and has a lower impact in unicast. Furthermore, we showed the performance obtained with an optimal combining receiver based on full channel knowledge in the presence of interferers, and compared with suboptimal and MRC receivers. Although suboptimal schemes have significant performance gains for single transmit antenna, the use of spatial transmit diversity increases the sensitivity of such schemes to the estimation errors, leading to poorer results.

6.1 Future Work

Research into the areas addressed in this thesis calls for continued efforts. This section discusses directions for further developments and studies.

The implementation of non-linear receivers for LDC requires a tradeoff between diversity and multiplexing versus a higher complexity. The latter option is more suitable in the uplink, since the BS may handle higher complexity. Thus, more advanced receivers deserve special interest focused on the increase in performance and the synchronization of multiple signals.

In cellular scenarios, the study of cochannel signals, either as interference or broadcast, calls for the development of MIMO specific interference cancelation algorithms, or interference avoidance spectrum management strategies that take into account the sensitivity of the channel matrix.

Given the insight into the design of modulation thresholds for the feedback CSI, the downlink MIMO selection of a practical system must be based on BS measurements of the link performance. Thus, the design of a transmission mode selection that includes a

measure of the reliability of the feedback must be followed by a study of the hardware constraints. Moreover, higher layer issues, such as multiuser scheduling, HARQ, and packet prioritization, also require a cross-layer approach.

The increasing variety of online services available for mobile terminals and the aim at an extended coverage favors the use of multiantenna processing. As a result, the integration of MIMO algorithms in wireless networks raises a large number of challenges, and is expected to drive research in years to come.

Appendix A

Wireless Channel

A.1 Propagation Path Loss and Shadowing

The propagation loss is the attenuation suffered by a signal while propagating through a medium, such as the air. The propagation loss is proportional to the distance between transmitter and receiver, and can be represented in logarithmic units, dB, by

$$L_P = L_{\text{ref}} + 10n \log d_{[\text{km}]} \ .$$

Several models estimate the propagation loss depending on the environment. Most often the values considered for n vary between 2 (Free Space Model) and 4, but can be superior in some scenarios.

The choice of which path loss model to use is related to the target environment. Since most mobile communication systems operate over irregular terrain, many models, based in measurements, have been developed to achieve a better accuracy on these environments. Some of the most cited models that predict signal attenuation in urban areas include the Okumura's model, later on extended with an empirical formulation developed by Hata, and the Walfish-Ikegami model [Rap96].

In some wireless environments, signals suffer significant attenuation caused by large obstacles in the line of communication. In addition, the obstacles cause reflections that add

interference to the connection. Thus, some areas with high path loss may become shadow areas, i.e., the connection can not be established within that region. Therefore, these phenomena are referred to as shadowing. Shadowing causes a loss in network performance that varies slowly both with time and position, hence it is usually referred to as slow fading. It is common to describe the shadowing by a log-normal statistical model with PDF [Rap96]:

$$f(x) = \frac{1}{\sqrt{2\pi}\sigma_l}\frac{1}{x}\exp\left[-\left(\frac{\ln x - \overline{x_l}}{\sqrt{2\pi}\sigma_l}\right)^2\right] \quad .$$

A.2 Mobility and Multipath

In a mobile environment, several objects reflect or diffract radio signals. Reflection occurs when a wave hits an obstacle that is very large compared to its wave length. On the other hand, if the obstacle hit by the wave has smaller dimensions than the wave length, the signal is scattered in many directions. When there is an object obstructing the path between the transmitter and the receiver, diffraction occurs from the edges. Therefore, the transmitted signal arrives over different paths to the receiver. Owing to differences in the distances of the paths, the signals have various phases and arrive at distinct time instants. Consequently, the receiver gets a combination of these signals.

In a Line of Sight (LOS) environment, the first signal arrives directly through the shortest path (inline) with higher power than all the others. Since multipath signals arrive with different phase offsets, they will interfere with the LOS component, resulting in random fades alternating between destructive and constructive reflections. Multipath induces fast fading in the channel, and in NLOS all the multipath signals arrive from diffractions with reduced power, resulting in a weak connection [Kim02]. In NLOS environment, the fading amplitude is characterized by Rayleigh distribution,

$$f(x) = \frac{2x}{\overline{x^2}}\exp\left[\frac{-x^2}{\overline{x^2}}\right] \quad . \tag{A.1}$$

Scenarios where a LOS component is present are modeled as Rician channels with the

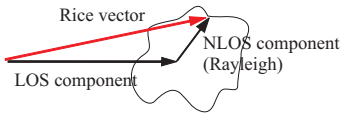

Figure A.1: Rice distribution vector

fading described by

$$f(x) = \frac{2x}{x_R^2} \exp\left[-\frac{x^2 + x_0^2}{x_R^2}\right] I_0\left(\frac{x x_0}{\frac{x_R^2}{2}}\right) \ .$$

Rice's statistical model describes the arriving signals through the multipath channel as the sum of a fixed vector x_0 (LOS component) with a Rayleigh distribution vector x_R (NLOS component), as represented in Figure A.1.

The multipath signal model is characterized by the time domain baseband Channel Impulse Response (CIR), defined as

$$\mathbf{g}(\tau, t) = \sum_{l=1}^{L} \mathbf{g}_l(t)\delta(\tau - \tau_l) \ ,$$

where $\mathbf{g}_l(t)$ is the complex channel coefficient of the multipath l at time t, and τ_l its the delay. Delay spread is the duration of the period between the first and the last multipath signals received. A common measure of characterization of wireless channels is the RMS delay spread, defined as

$$\sigma_\tau = \sqrt{\frac{1}{P_r}\int_0^\infty \tau^2 P(\tau) d\tau - \overline{\tau}^2} \ ,$$

where P_r is the total received power, $P(\tau)$ is the distribution of power over the delay of the multipath signals, and $\overline{\tau}$ is the average delay. Table A.1 presents typical values of RMS delay spread for different environments.

Time dispersion occurs when the multipath signals arrive after the symbol duration, i.e., the delay spread is longer than the symbol period leading to ISI and is common in broadband communications [Fla03]. The delay spread causes ISI if it is longer than the symbol period. As the bandwidth of the system increases, the symbol period reduces, and ISI appears in high delay spread scenarios. The time-dispersive CIR generates a frequency-

Scenario	RMS delay spread
Typical office environment, NLOS	50 ns
Typical large open space and office environment, NLOS	100 ns
Typical large open space, NLOS	150 ns
Typical large open space, LOS	140 ns
Typical large open space, NLOS	250 ns
Urban microcell	2 μs

Table A.1: Channel RMS delay spread

selective channel in the frequency domain. To combat this effect, complex equalizers are needed at the receiver in single carrier systems. On the other hand, when the delay spread is smaller than the symbol duration, there is no time dispersion, and the fading is flat. Multicarrier systems such as OFDM use multiple low rate streams with longer symbol period (narrowband subcarriers) to avoid ISI.

A.2.1 Doppler Effect

The speed of the terminal moving relative to the BS causes the Doppler effect and affects the performance of the system. The Doppler effect leads to a shift on the received frequency, either higher when mobile terminal is moving toward the base station, or lower when it is moving away from the base station. Equation (A.2) shows the deviation of the frequency at the receiver when the transmitted signal has a wavelength of λ, the relative speed to the transmitter is v, and the angle between the velocity and the wave is α:

$$f_d = \frac{v}{\lambda \cos \alpha} \ . \tag{A.2}$$

The maximum Doppler frequency is $\frac{v}{c} f_c$, and it is hereafter referred to as f_d. Here, c is the speed of light, and f_c is the carrier frequency.

The Doppler spectrum is classically characterized by a uniform circle distribution as in [Par00]:

$$S(f) = \frac{3}{2\pi f_d \left(1 - (\frac{f}{f_d})^2\right)^{-\frac{1}{2}}} \ , \quad -f_d \leq f \leq f_d \ . \tag{A.3}$$

To introduce the time variability of the channel, Jakes Model is adopted [JC94]. This model considers a scattering environment close to the MS, where the multipath signals arrive with a uniform distribution from $[0, 2\pi]$. The relative velocity between the transmitter and the receiver defines the maximum Doppler frequency that is used to correlate the samples of the channel in time domain. The correlation between two channel coefficients separated by a delay of τ follows

$$\rho = J_0(2\pi f_d \tau) \ . \tag{A.4}$$

A.2.2 Coherence Bandwidth and Coherence Time

Multipath is a critical way to establish a connection when there is no LOS path between the transmitter and the receiver. The possibility of maintaining a connection while the user is moving around is now a feature that can not be dissociated from a wireless environment. Nevertheless, both multipath and mobility lead to a distortion and dispersion of the wireless signal.

Multipath leads to a situation where two signals with different frequencies need to have a separation between frequencies larger than the frequency band, B_c, to be statistically independent. On the other hand, two signals in different time instants need to have a separation between instants larger than the coherence time, T_c, to be statistically independent.

Adopting a definition of coherence time as the time over which the time correlation function is 0.5 over a Rayleigh fading channel and an exponential delay profile, the B_c and T_c are approximated as [Rap96]

$$B_c \approx \frac{1}{2\pi\sigma_\tau} \tag{A.5}$$

$$T_c \approx \sqrt{\frac{9}{16\pi f_d^2}} \approx \frac{0.423}{f_d} \ , \tag{A.6}$$

where f_d is the maximum Doppler shift, and σ_τ is the delay spread. Table A.2 shows the

v [km/h]	f_d [Hz]	T_c [ms]
3	54	7.83
10	180	2.35
20	360	1.175
50	900	0.47
100	1800	0.235
250	4500	0.094

Table A.2: Channel coherence time at 5 GHz

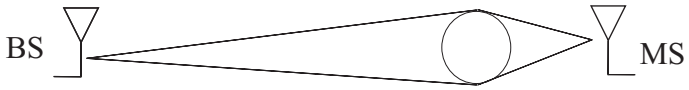

Figure A.2: Angular spread at the BS and the MS

values of coherence time for different terminal speeds at a carrier frequency of 5 GHz.

A.2.3 Angular Spread

In a multipath channel, each signal at the receiver has a specific angle of incidence of the plane wave called Direction of Arrival (DoA). The angular spread is the standard deviation of the different DoAs weighted with the path energies and is given by [LR99]

$$\Phi = \sqrt{\frac{\sum_{l=1}^{L} \left(\phi_l - E[\phi]\right)^2 |\mathbf{h}_l|^2}{\sum_{l=1}^{L} |\mathbf{h}_l|^2}} \ ,$$

where ϕ_l and $\mathbf{h}_l$ are the DoA and the channel coefficient of the multipath signal l, respectively.

In indoor environments, the angular spread of the signals received by the mobile station is much higher than in outdoor scenarios. Owing to the longer distance that separates the transmitter and the receiver in an outdoor situation, the angles of the received signals from multipath are narrower. Since in outdoor environments the scatterers are usually closer to the MS when compared to the BS, the angular spread at the MS is broader than the one experienced by the BS, as shown in Figure A.2.

Appendix B

OFDM

OFDM is a modulation technique that is very effective in mitigating adverse multipath effects of a broadband wireless channel [NP00]. The robustness against frequency selective fading, as well as narrowband interference, combined with an efficiently use of spectrum, have pushed OFDM to be the primary physical layer adopted in several standards. Moreover, affordable implementation complexity of OFDM became a reality following the latest developments in integration technology that made the FFT chips economic to apply in receivers and transmitters.

This technology is already in use in systems like Digital Audio Broadcasting (DAB), Digital Video Broadcasting (DVB), and Digital Subscriber Line (DSL). Moreover, OFDM has been successfully used in omnipresent WLANs, where high data rate is achieved for local area coverage. In recent years, significant interest arose in using OFDM for Wide Area Network (WAN), where higher data rate, higher Quality of Service (QoS), and wider coverage area are envisioned along with vehicular user mobility.

B.1 OFDM Overview

OFDM is a special case of multicarrier transmission, in which a single wideband carrier, carrying a data stream, is divided into multiple lower rate streams and transmitted over orthogonal subcarriers. This is a modulation applied to the data-modulated signal before

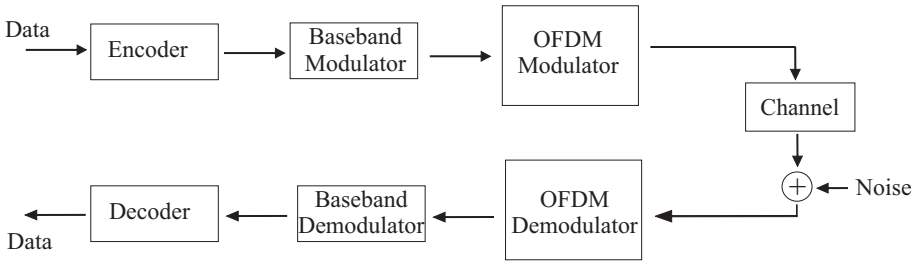

Figure B.1: OFDM transceiver model

transmitting the signal through the channel, as presented in Figure B.1.

In Frequency Division Multiplexing (FDM) systems, the frequency carriers operate on bands that are separated with a guard band to avoid interference. Unlike conventional FDM, the efficient use of spectrum in OFDM is achieved by overlapping the subcarriers exploiting their orthogonality. The channels are modulated with mathematical orthogonal basic functions that are linearly independent using an IDFT.

Figure B.2 shows the spectrum of an OFDM carrier after IDFT operation, i.e., sinc function, as well as the combined OFDM signal with multiple carriers. The carriers spacing must be a multiple of $\frac{1}{T_u}$, so that the integration of the signal of one carrier over the OFDM symbol period T_u nulls the contributions of all other carriers, as represented in

$$\frac{1}{T_u}\int_0^{T_u} e^{j2\pi(f_i-f_k)t}dt = \begin{cases} 1 & \text{if } i = k \ , \\ 0 & \text{if } i \neq k \ . \end{cases}$$

In Figure B.2, one may observe that the peak of each subcarrier coincides with the zero crossing of all the others [HT01].

OFDM deals with ISI by adding a guard time larger than the expected delay spread to each symbol. The bandwidth of the system is not severely affected, since the duration is considerably larger owing to the low bandwidth subcarriers that transmit the signal. As a result, no complex equalizers are required at high data rate connections, reducing the complexity and cost of receivers.

In order to maintain the orthogonal properties of the transmitted signals, a cyclic extension of the OFDM symbol, referred to as CP, is used as the guard time. A CP is

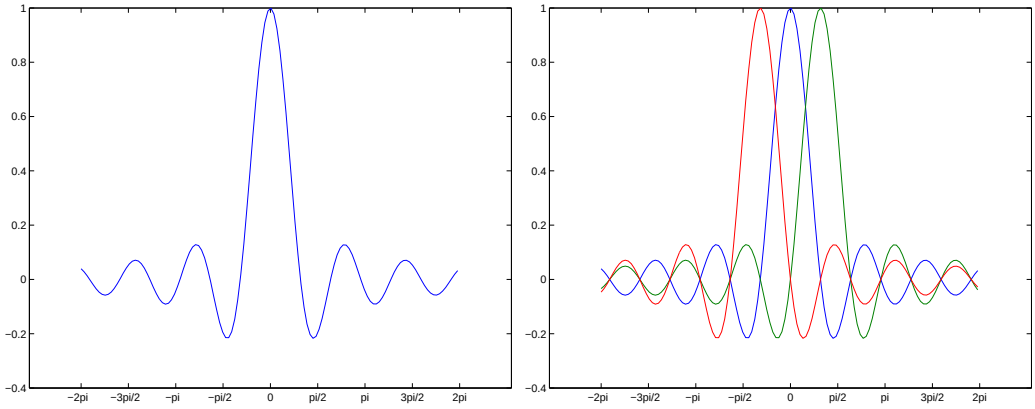

Figure B.2: Spectrum of an OFDM subcarrier (left) and a combined OFDM signal with three subcarriers overlapped (right)

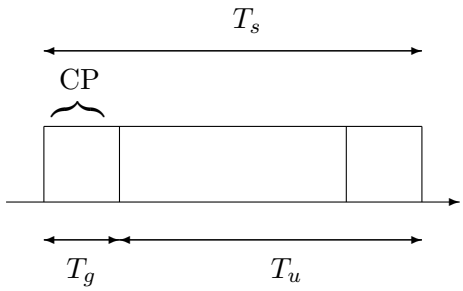

Figure B.3: OFDM symbol in time domain

simply a copy of the last part of the OFDM symbol, as shown in Figure B.3. The ICI is avoided if the multipath delays are shorter than the CP, since an integer number of cycles within the Discrete Fourier Transform (DFT) integration time is guaranteed [RDF04]. Although the CP introduces a loss in efficiency, the benefit it brings pays off [HT01].

The out-of-band spectrum of an OFDM symbol decreases rather slowly, according to a sinc function. Raised cosine windowing is a technique commonly used in OFDM systems to force the spectrum decrease steeper at symbol boundaries [NP00].

The design of OFDM systems requires a tradeoff among network's demands. After selecting the environment and frequency band to deploy the system, it is necessary to characterize the wireless channel so that the common delay spread is known. One can assume that a CP length of two to four times the RMS delay spread avoids ISI and ICI. The symbol duration is chosen according to the bit rate desired for the connection, the

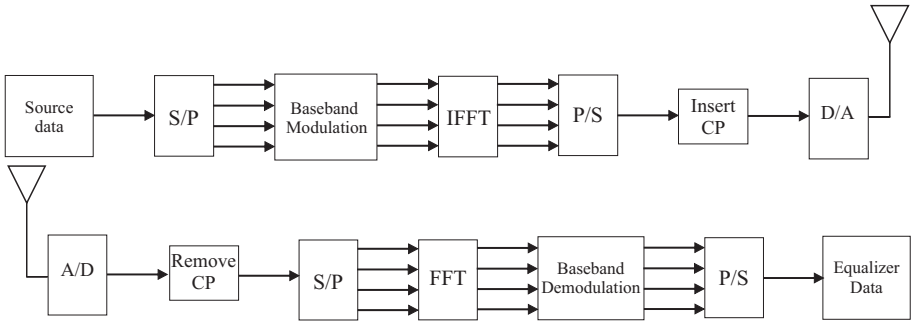

Figure B.4: Model of an OFDM transmitter (above) and receiver (under)

modulation used, and the number of subcarriers of the system. It is a common practice to assign a guard time of about 20% the duration of the symbol [NP00].

B.1.1 OFDM Statistical Model

Considering an OFDM system with N orthogonal subcarriers, the transmitter splits the source data in parallel streams carried by the subcarriers. A generic model for an OFDM transmitter and receiver is presented in Figure B.4.

The s^{th} OFDM symbol has a duration of T_u and is obtained using the data sequence for the s^{th} subcarrier block $\mathbf{d}_s[k]$, where $k = 0, \ldots, N-1$. Defining the subcarrier spacing as Δf, the time domain signal is written as

$$x_s(t) = \frac{1}{\sqrt{T_u}} \sum_{k=0}^{N-1} \mathbf{d}_s[k] \exp\left[j2\pi\Delta f k t\right], \quad 0 \leq t < T_u \ .$$

The discrete time representation of the signal using the IDFT and a subcarrier spacing of $\Delta f = \frac{1}{T_u}$ follows:

$$x_s[n] = \frac{1}{\sqrt{N}} \sum_{k=0}^{N-1} \mathbf{d}_s[k] \exp\left[j2\pi \frac{kn}{N}\right], \quad 0 \leq n < (N-1) \ .$$

After the conversion to time domain, the signal is extended by adding the CP of time T_g, so the total OFDM symbol duration is $T_s = T_u + T_g$. The OFDM signals are concatenated in time domain and up-converted to the carrier frequency of the system.

At the receiver, first the signal is down-converted, then the CP is removed, and DFT is applied. Assuming the CIR to be shorter than the CP duration, T_g, and perfect synchronization, the received symbols can be written in terms of the source symbols as

$$u_s[k] = \mathbf{d}_s[k]\mathbf{h}_s[k] + \mathbf{w}_s[k] \ ,$$

where $\mathbf{w}_s[k]$ is the AWGN sample with zero mean and variance N_0, and $\mathbf{h}_s[k]$ is the channel, response in frequency for subcarrier k and symbol s.

The SNR, γ, for the received signal at subcarrier k is given by

$$\gamma_k = \frac{E_s}{N_0} E\left[|\mathbf{h}[k]|^2\right] \ ,$$

where E_s is the transmitted signal power, and $E[.]$ is the statistical mean of the observations. The probability of bit error of a system depends on the modulation and the SNR. For Binary Phase Shift Keying (BPSK) over AWGN channel, the BER is governed by

$$P_b^{\text{BPSK}} = \frac{1}{2} \operatorname{erfc}\left(\sqrt{\frac{1}{\log_2 M}\frac{E_s}{N_0}}\right) \ ,$$

where $\operatorname{erfc}(z) = \frac{2}{\sqrt{\pi}} \int_z^\infty e^{-t^2} dt$. For higher order Phase Shift Keying (PSK) modulations, when Gray bit mapping is used, the BER is approximated by [Car86]

$$P_b^{M-\text{PSK}} \approx \frac{1}{\log_2 M} \operatorname{erfc}\left(\sqrt{\frac{E_s}{N_0}} \sin\frac{\pi}{M}\right) \ .$$

Another modulation of interest that is widely used in OFDM systems is the QAM. In this case, the BER of rectangular M-QAM with Gray bit mapping over AWGN channel is approximated by

$$P_b^{M-\text{QAM}} \approx \frac{2}{\log_2 M}\left[1 - \frac{1}{\sqrt{M}}\right] \operatorname{erfc}\left(\sqrt{\frac{3}{2(M-1)}\frac{E_s}{N_0}}\right) \ . \tag{B.1}$$

Appendix C

Antenna Arrays

An antenna array is a set of antenna elements used to produce a highly directive radiation beam. This beam can be realized by an array of elemental radiators, as dipoles. This technique is referred to as beamforming, and it operates on the array of antennas to shape its radiation pattern. By assigning different weights to each element of the array, the beams are shaped to maximize the signal in the direction of the wavefront of the desired signal. This method has an important impact both on increasing SNR for the established connection, and on reducing interference for the neighbor connections.

Beamforming can be applied at the receiver or at the transmitter of the radio link. Here, we introduce the linear arrays as a receiver technique with the weights calculated based on the channel estimates.

C.1 Uniform Linear Arrays

Figure C.1 shows a uniform linear array formed by N_r elements with fixed distance, d, between them. The array receives the signal from direction θ relative to the array broadside, the DoA. The corresponding delay in time for the signal to propagate relative to neighbor antenna elements is $\frac{d \sin \theta}{c}$, where c is the speed of light.

The received signal at p element can be written relative to the first element with a

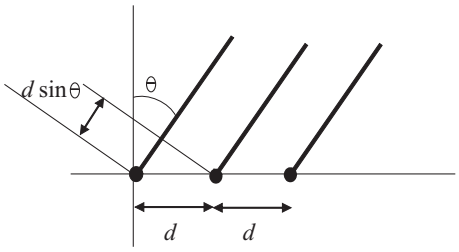

Figure C.1: Uniformly spaced linear array

phase shift due to time delay as [Ven03]

$$u_p(t) = u_1(t) \exp\left[-j\frac{2\pi}{\lambda}(p-1)d\sin\theta\right] \quad , \quad p = 1, \ldots, N_r \ .$$

The $[N_r \times 1]$ vector of the received signal, $\mathbf{y}$, is represented by

$$\mathbf{y}(t) = \mathbf{a}(\theta)u_1(t) \ ,$$

where $\mathbf{a}$ is the array response defined by

$$\begin{aligned} \mathbf{a}(\theta_l) &= [1, \exp(j\alpha_l), ..., \exp(j(N_r-1)\alpha_l)] \ , \\ \alpha_l &= \frac{2\pi}{\lambda}d\sin\theta_l \ . \end{aligned} \tag{C.1}$$

Consider L signals arriving at the array with different angles θ_l. The resulting received vector is the superposition of the signals and noise given by

$$\mathbf{y} = \sum_{l=1}^{L} \mathbf{a}(\theta_l)u_l \ .$$

C.2 Beamforming

The beamforming process combines the signal from each antenna element multiplied by a complex weight vector $\mathbf{w}$. The output of a narrowband beamformer is obtained by

summing up the antenna outputs

$$z(n) = \sum_{p=1}^{N_r} w_p^* y_i(n) = \mathbf{w}^H \mathbf{y}(n) \ .$$

Therefore, the beamformer response, or array factor, results as

$$F(\theta) = \sum_{p=1}^{N_r} w_p^* \exp\left[-j\frac{2\pi}{\lambda}(p-1)d\sin\theta\right] \ .$$

The complex weights are computed by an optimization algorithm that maximizes a certain cost function, not necessarily the direction of the signal. A beamformer that directs the beam toward the signal needs to estimate the DoA by applying the weights $w_p = |w| \exp[-j(p-1)\frac{2\pi}{\lambda} d \sin\theta]$.

There exist beamformers that optimize other cost functions, such as the maximum SNR proposed in [App76], the MMSE, or the Least-Square (LS). These are referred to as optimal beamforming. Instead of trying to solve directly the equation for the optimal solution, iterative approaches have been proposed, referred to as adaptive algorithms. These techniques are especially suited when the mobile environment is time-variable, and the weight vector needs to be updated periodically.

Considering the problem of minimizing the MSE between the received and transmitted signals, the cost function is [LR99]

$$J(\mathbf{w}) = E\left[|\mathbf{w}^H \mathbf{y}(n) - \mathbf{d}(n)|^2\right] \ .$$

The optimal weights for MMSE are expressed as

$$\mathbf{w}_{opt} = \mathbf{R}_{\mathbf{yy}}^{-1} r_{\mathbf{yd}} \ ,$$

where $\mathbf{R}_{\mathbf{yy}}$ is the correlation matrix $[N_r \times N_r]$ of the received signal, and $r_{\mathbf{yd}}$ is the cross-correlation vector between the transmitted data and the received signal.

Appendix D

Antenna Diversity

Multiple uncorrelated antennas at the receiver or transmitter can be used to improve link robustness or increase data throughput.

The idea behind diversity is to transmit the same data symbols over independent channels. The more independent channels are combined, the less likely it is that all of them fall into deep fading simultaneously. There are three main types of diversity:

- Time (temporal) Diversity
- Frequency (spectral) Diversity
- Space (spatial) Diversity

Time diversity is effective in time-variant channels, when the data is repeated on different symbols to increase the probability of correct decoding. In a slow fading channel, a temporal diversity technique, like time interleaving, produces large delays. Equivalently, spectral diversity is effective only over frequency-selective fading channels, as in the case of broadband systems. Spatial diversity uses the antenna domain and can be employed to reduce fading impact when the channel is neither time nor frequency-selective. The antennas are placed with several wavelengths of distance between each other, such that the signals are uncorrelated.

There are two types of gain related to the use of receiver or transmit diversity,

array gain and diversity gain. While array gain results from coherently combining multiple signals, diversity gain is associated with a more favorable distribution of the output SNR [Gol05].

Traditionally, spatial diversity is exploited by involving multiple antennas in transmitter and/or receiver. When multiple antennas are used at the receiver (or transmitter), then the spatial diversity scheme is labelled as receive (or transmit) diversity.

D.1 Receive Diversity

Receive diversity combines independent fading signals so that the resultant SNR is increased. Most available techniques are linear, i.e., the processing consists of a weighted sum of the different branches. A general combining system for a receiver with N_r antennas is represented by

$$y(t) = \sum_{p=1}^{N_r} \alpha_p u_p(t) = \sum_{p=1}^{N_r} \alpha_p \big[h_p(t) s(t) + w_p(t) \big] \ ,$$

where α_p and u_p are the weight and received signal for antenna p, respectively. The transmitted signal is represented by $s(t)$, while $h_p(t)$ and w_p are the fading channel coefficient and noise for antenna p.

Selection Combining This technique selects the branch with higher SNR, γ, from the N_r independent signals. If k corresponds to the channel that satisfies $\gamma_k \geq \gamma_p$ for $p = 1, \ldots, N_r$, the weights mentioned above for the general combining case is defined by

$$\alpha_p = \begin{cases} 1 & p = k \ , \\ 0 & p \neq k \ . \end{cases}$$

Maximal Ratio Combining In MRC, the signals of N_r branches are linearly combined in order to maximize the SNR. Unlike selection combining, the weights in MRC are in this case all nonzero and co-phase the received signals, i.e., $\alpha_p = h_p^*$.

Equal Gain Combining Although MRC is optimal in terms of SNR, equal gain combining is a simpler technique that co-phases the signals and combines with the same weight. Therefore, it does not need the knowledge of the SNR. The weights are then $\alpha_p = \exp[-j\theta_p]$, where θ_p is the phase of the signal at antenna p.

D.2 Transmit Diversity

Transmit diversity is a reasonable choice for the downlink of a cellular system to increase the robustness of the link. If channel knowledge is available at the receiver, closed-loop schemes can extract array gain. However, in the following we assume no channel information at the transmitter. Only open-loop schemes that exploit diversity gain are considered.

Combining STBC with OFDM provides spatial diversity gain over frequency selective fading channels. In effect, space-time coding is applied on blocks of data symbols instead of processing individual symbols.

D.2.1 Space-Time Coding

STC is a hybrid technique that applies both space and time diversity in a combined way [PNG03]. The most common form of STC used for diversity is STBC. STC was first introduced by Alamouti [Ala98] when presenting a two branch transmitter diversity scheme that achieves full diversity.

The STBC proposed in [Ala98] transmits two symbols over two antennas and two symbol durations according to the transmit matrix:

$$\mathbf{S} = \begin{pmatrix} \mathbf{s}_n & \mathbf{s}_{n+1} \\ \mathbf{s}_{n+1}^* & \mathbf{s}_n^* \end{pmatrix} \quad .$$

Under the assumption of constant fading over two consecutive symbols, the scheme achieves diversity order of two.

Extending the concept of STBC, Tarokh [TJC99] proposed transmission blocks for more than two transmit antennas that achieve full diversity, such as the code for four

antennas and spatial rate 3/4, i.e., three symbols are transmitted over a block of four symbol periods:

$$\mathbf{S} = \begin{pmatrix} \mathbf{s}_n & \mathbf{s}_{n+1} & \frac{\mathbf{s}_{n+2}}{\sqrt{(2)}} & \frac{\mathbf{s}_{n+2}}{\sqrt{(2)}} \\ \mathbf{s}_{n+1}^* & \mathbf{s}_n^* & \frac{\mathbf{s}_{n+2}}{\sqrt{(2)}} & -\frac{\mathbf{s}_{n+2}}{\sqrt{(2)}} \\ \frac{\mathbf{s}_{n+2}^*}{\sqrt{(2)}} & \frac{\mathbf{s}_{n+2}^*}{\sqrt{(2)}} & \frac{-\mathbf{s}_n - \mathbf{s}_n^* + \mathbf{s}_{n+1} - \mathbf{s}_{n+1}^*}{2} & \frac{-\mathbf{s}_{n+1} - \mathbf{s}_{n+1}^* + \mathbf{s}_n - \mathbf{s}_n^*}{2} \\ \frac{\mathbf{s}_{n+2}^*}{\sqrt{(2)}} & -\frac{\mathbf{s}_{n+2}^*}{\sqrt{(2)}} & \frac{\mathbf{s}_{n+1} + \mathbf{s}_{n+1}^* + \mathbf{s}_n - \mathbf{s}_n^*}{2} & -\frac{\mathbf{s}_n + \mathbf{s}_n^* + \mathbf{s}_{n+1} - \mathbf{s}_{n+1}^*}{2} \end{pmatrix}.$$

D.2.2 Space-Frequency Coding

Although STBC provides diversity in time-varying channels, it is not effective in scenarios with fading constant over long periods. Another disadvantage of STBC is the inherent latency, since the decoding process requires the system to wait until the full block is received before decoding. This issue becomes more important as the encoding block size increases.

In the frequency domain, the problems above mentioned are avoided. The same concept of STBC codes can be implemented in space and frequency domain. In frequency selective channels, combined with OFDM, SFBC maps the symbols into subcarriers instead of time symbols. In one OFDM symbol, the scheme decodes the full block avoiding the latency problem [LW00]. SFBC also performs better at higher speeds due to encoding within one single OFDM symbol. Nevertheless, it suffers degradation if the channel response is nearly constant in frequency, since there is no frequency diversity.

D.3 SNR Statistics

This section presents the statistics of the output SNR, or post-processing SNR, for various MIMO schemes under Rayleigh fading.

The wireless channel is a flat fading channel varying in time according to Jakes model. The channel is slowly time-varying, and it is assumed constant for the number of consecutive symbols corresponding to the transmit diversity block size under analysis,

e.g., two symbols for Alamouti scheme. The channel consists of a single tap flat fading characterized by Rayleigh statistics.

In NLOS scenarios, it is common to use Rayleigh fading model to describe the wireless channel behavior. The channel coefficients, $\mathbf{h}$, follow a complex Gaussian distribution of zero mean and variance $\sigma^2_{\mathbf{h}}$. Then, the channel amplitude, $|\mathbf{h}|$, is Rayleigh distributed as in (A.1). The power of the channel is given by $p = |\mathbf{h}|^2$, and follows an exponential distribution [Pro01],

$$f(p) = \frac{1}{\sigma^2_{\mathbf{h}}} \exp\left[-\frac{p}{\sigma^2_{\mathbf{h}}}\right] \ .$$

The SNR of the link relates to the transmit power and noise as $\gamma = \frac{E_s}{N_0}|\mathbf{h}|^2$. For a simpler representation of the SNR statistics, we consider the noise and transmit signal to have unitary powers, such that $\gamma = |\mathbf{h}|^2$. Consequently, the PDF of the SNR of a SISO link follows an exponential distribution:

$$f(\gamma) = \frac{1}{\sigma^2_{\mathbf{h}}} \exp\left[-\frac{\gamma}{\sigma^2_{\mathbf{h}}}\right] \ .$$

D.3.1 Spatial Diversity

This section presents the analytical distributions for the post-processing SNR when orthogonal spatial diversity schemes are considered. We assume N_t transmitters and N_r receivers where appropriate, and the fading links are i.i.d. following Rayleigh statistics.

D.3.1.1 Maximal Ratio Combining

MRC is a diversity technique that maximizes SNR from the utilization of independent fading channels. This method needs channel knowledge, since it consists in weighting the symbols at each antenna by the conjugate of the channel coefficient. As the channel knowledge is commonly assumed to be available at the receiver, this technique is usually regarded as a receive diversity scheme. In a SIMO configuration, the post-processing SNR

and the corresponding distribution are given by [Pro01]

$$\gamma = \sum_{p=1}^{N_r} |\mathbf{h}_p|^2 \ ,$$
$$f(\gamma) = \frac{1}{(N_r-1)!\left(\sigma_{\mathbf{h}}^2\right)^{N_r}} \gamma^{N_r-1} \exp\left[\frac{-\gamma}{\sigma_{\mathbf{h}}^2}\right] \ . \tag{D.1}$$

D.3.1.2 Space Time Coding

Orthogonal STBC is an open-loop transmit diversity schemes that achieve full diversity gain [Ala98, TJC99]. Since it assumes no knowledge of the channel, unlike MRC, it does not bring array gain. Therefore, the average SNR keeps constant when increasing the number of antennas. The post-processing SNR and its PDF are given by [BH01]

$$\gamma = \frac{1}{N_t} \sum_{q=1}^{N_t} |\mathbf{h}_q|^2 \ ,$$
$$f(\gamma) = \frac{1}{(N_t-1)!\left(\frac{\sigma_{\mathbf{h}}^2}{N_t}\right)^{N_t}} \gamma^{N_t-1} \exp\left[\frac{-\gamma}{\frac{\sigma_{\mathbf{h}}^2}{N_t}}\right] \ . \tag{D.2}$$

D.3.1.3 MIMO Spatial Diversity

When a MIMO link is used to extract diversity from the system, both STBC and MRC diversity schemes are employed. The N_t antennas at the transmitter encode the signal using STBC, without channel knowledge. The available power at the transmitter is equally divided among the transmission antennas when implementing STBC. Furthermore, the N_r received signals are combined with MRC, using channel knowledge ideally estimated at the receiver. In this situation, the SNR of the signal is chi-square distributed with $2N_tN_r$ degrees of freedom. The resulting γ and its PDF are then given by

$$\gamma = \frac{1}{N_t} \sum_{p=1}^{N_r} \sum_{q=1}^{N_t} |\mathbf{h}_{p,q}|^2 \ ,$$
$$f(\gamma) = \left(\frac{N_t}{\sigma_{\mathbf{h}}^2}\right)^{N_tN_r} \frac{\gamma^{N_tN_r-1}}{(N_tN_r-1)!} \exp\left[-\frac{N_t\gamma}{\sigma_{\mathbf{h}}^2}\right] \ . \tag{D.3}$$

D.3.2 Spatial Multiplexing

A MIMO wireless link can also be used to create parallel data streams between the transmitter and the receiver, i.e., SM. A simple MIMO spatial multiplexing scheme can be achieved with the ZF receiver. This scheme forms $\min(N_t, N_r)$ parallel data streams [PNG03] without channel knowledge at the transmitter, i.e., the available power is equally divided among the transmitter antennas. Although there are more advanced techniques to perform SM that achieve better performances, only ZF has a known expression for the PDF of the post-processing SNR of each stream. In a MIMO channel that applies SM-ZF, the SNR of i^{th} stream is as follows:

$$\gamma_i = \frac{1}{N_t} \frac{1}{[(\mathbf{H}^H\mathbf{H})^{-1}]_{i,i}} \ ,$$

where $[.]_{i,i}$ is the i^{th} diagonal value of a matrix, and $(.)^H$ represents the hermitian of the matrix. The SNR of each stream has a chi-square distribution with $2(N_r - N_t + 1)$ degrees of freedom [PNG03]:

$$f(\gamma) = \frac{1}{\left(\frac{\sigma^2_{\mathbf{h}}}{N_t}\right)^{N_r - N_t + 1} (N_r - N_t)!} \gamma^{N_r - N_t} \exp\left[-\frac{\gamma}{\frac{\sigma^2_{\mathbf{h}}}{N_t}}\right] \ . \tag{D.4}$$

D.3.3 Antenna Selection

AS is a spatial diversity scheme usually considered at the transmitter side due to its low feedback requirement. It uses partial CSI, i.e., an indication of the antenna with highest channel gain. The post-processing SNR for AS with N_t antennas follows:

$$\gamma = \max(\gamma_1, ..., \gamma_{N_t}) \ .$$

In perfect channel estimation and no delay conditions, the PDF of the resulting SNR is obtained from second order statistics, i.e., through the derivative of the Cumulative Distribution Function (CDF). Assuming that the channel at each branch is i.i.d., with

PDF, $f_{\text{siso}}(\gamma)$, and CDF, $F_{\text{siso}}(\gamma)$, the PDF of the resulting SNR is [Pro01]

$$\begin{aligned} F_{\text{as}}(\gamma) &= \left(F_{\text{siso}}\right)^{N_t} \quad , \\ f_{\text{as}}(\gamma) &= \frac{\partial F_{as}}{\partial \gamma} = N_t f_{\text{siso}}(\gamma)(F_{\text{siso}}(\gamma))^{N_t-1} \\ &= \frac{N_t}{\sigma_{\mathbf{h}}^2}\left(1-\exp\left[-\frac{\gamma}{\sigma_{\mathbf{h}}^2}\right]\right)^{N_t-1}\exp\left[-\frac{\gamma}{\sigma_{\mathbf{h}}^2}\right] \quad . \end{aligned}$$

Note that the expression for the SNR distribution can be written in a different form,

$$f_{\text{as}}(\gamma) = N_t \sum_{q=0}^{N_t-1}(-1)^q C_q^{N_t-1}\frac{1}{\sigma_{\mathbf{h}}^2}\exp\left[-\frac{\gamma}{\frac{\sigma_{\mathbf{h}}^2}{q+1}}\right] \quad .$$

Appendix E

Adaptation and Scheduling

This appendix introduces the concepts of two techniques to adapt the transmission on the basis of the channel conditions. In adaptive modulation, the transmitter selects the constellation size to modulate the symbols. In multiuser scheduling, the transmitter chooses the user that should be use the channel.

E.1 Adaptive Modulation

The adaptation of the transmission parameters to the fading conditions can lead to an increase in throughput, to the optimization of the transmit power, or to the reduction of the probability of bit error. These results are achieved by using favorable channel conditions to send higher data rates or to use lower power [Gol05].

Practical adaptive schemes select the modulation and coding applied to maximize spectral efficiency, while maintaining a certain QoS measured over the probability of error. It was shown in [CG01] that the adaptation of both rate and power does not bring significant advantage over the adaptation of only rate. Therefore, we describe an adaptive modulation technique that has a constant transmit power and aims at not exceeding the maximum instantaneous BER.

The adaptation of the rate can easily be done by changing the constellation size of the modulation, while maintaining the same symbol rate of the system. In this study, we

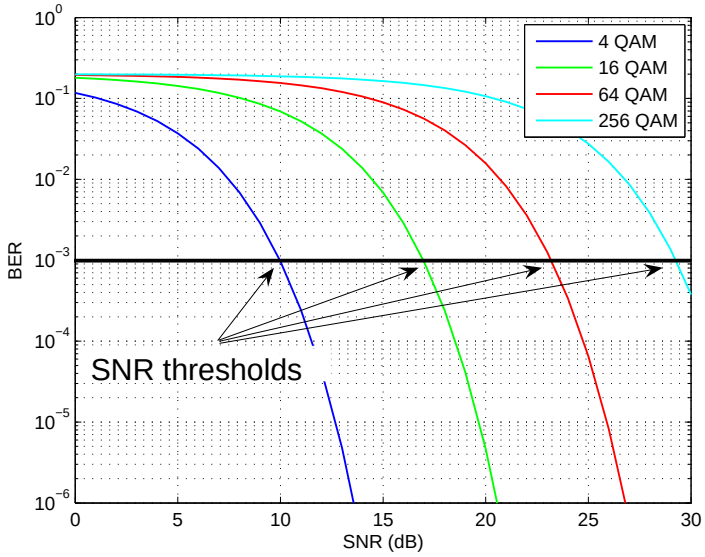

Figure E.1: BER of M-ary QAM over flat fading channel and thresholds for instantaneous BER constraint

restrict the adaptation to a discrete set of M-QAM orders. Owing to an easier practical implementation, we limit the selection to the group of square constellations.

The target of the adaptation is to maintain the instantaneous BER lower than a defined value, $BER(\gamma) \leq BER_t$. Thus, the system needs to estimate the BER performance with respect to the SNR of the link. The discrete rate adaptation divides the SNR range into R+1 regions to select one of the R constellation sizes available. Each modulation order M_i is chosen when the SNR falls into region i delimited by SNR thresholds (or switching thresholds), γ_i. Each region corresponds to the interval $[\gamma_i, \gamma_{i+1}[$. The thresholds are the values of SNR that indicate the transition to a higher modulation available while keeping the BER under the constraint, as shown in Figure E.1.

The switching thresholds can be obtained following a theoretical or a simulation approach. The latter requires a numerical inspection of simulation results to identify the threshold values for each modulation size individually. A theoretical approach that can be generalized to any size of modulation is thus more appealing.

To find an expression of the SNR thresholds with respect to the BER_t, we need to invert the expression of BER performance. As mentioned in Appendix A, the BER for

M-QAM with Gray bit mapping is approximated as [Pro01]

$$P_b^{M-\mathrm{QAM}} \approx \frac{2}{\log_2 M}\left[1-\frac{1}{\sqrt{M}}\right]\mathrm{erfc}\left(\sqrt{\frac{3}{2(M-1)}\frac{E_s}{N_0}}\right) \ .$$

This expression is not easily invertible; therefore, the thresholds can not be described in a closed-form solution. Thus, we use the approximation proposed in [CG01] for M-QAM, $M = 2^{k_i} \geq 4$ with Gray bit mapping and constant transmit power

$$BER(\gamma_i) \approx c_1 \exp\left[\frac{-c_2\gamma_i \frac{1}{\int_{\gamma_0}^{\infty} f(\gamma)d\gamma}}{2^{c_3 k_i}-c_4}\right], \quad 0 \leq i \leq R-1 \ ,$$

where $c_{1,2,3,4}$ are constants specific for the modulations employed. In the case of M-QAM, $M = 2^{k_i} \geq 4$, the constants are $c_1 = 0.2$, $c_2 = 1.6$, $c_3 = 1$, and $c_4 = 1$. Here, $f(\gamma)$ is the SNR distribution of the link. Considering a cut-off threshold of zero, i.e., $\gamma_0 = 0$, the system still transmits the lowest rate at the very low SNR. Then the BER approximation reduces to

$$BER(\gamma_i) \approx 0.2 \exp\left[\frac{-1.6\gamma_i}{2^{k_i}-1}\right], \quad 0 \leq i \leq R-1 \ .$$

Note that this approximation of BER is invertible and allows to present the thresholds in a closed-form.

E.2 Multiuser Scheduling

In multiuser scenarios, the fact that each user has a different fading state at each moment can be used by scheduling to increase the capacity of the system. Through opportunistic scheduling, the BS selects the user that has the best channel at each time. A large number of users combined with a large dynamic range of the fading channel variability boost the gain obtained by MUD.

The two basic scheduling algorithms that deliver fairness or maximum throughput are round-robin and maximum SNR schedulers. While these algorithms serve two contrary goals, tradeoff schemes were proposed to achieve a balanced solution, from which we

selected proportional fair scheduler and opportunistic beamforming.

Round-robin Scheduler Also known as fair scheduler, the round-robin scheduler serves all users in a sequential fashion, i.e., the user u to be allocated in slot n is found from

$$u = 1 + (n-1) \mod U \ ,$$

where U is the number of users in the system. This algorithm is independent of the channel conditions and does not exploit MUD. On the other hand, it provides fairness among users and achieves the best overall delay performance.

Maximum SNR Scheduler This scheme selects the user with the best SNR, γ, at each slot, and attains the highest efficiency. The user u is scheduled in slot n if it satisfies the condition

$$u = \arg\max_i \gamma_i(n) \ .$$

This scheduler achieves maximum MUD, i.e., the diversity order equals the number of users in the system. However, it becomes impractical due to unfairness characteristic among users experiencing different average SNR. In fact, users at low average SNR are not allocated resources due to the poor channel conditions experienced, hence increasing outage probability of the system.

Proportional Fair Scheduler This technique provides a tradeoff between maximum MUD and fairness. The selection of the user to be served is based on the ratio of the short-term SNR over the long term averaged SNR. This algorithm selects the user u to be scheduled in slot n if

$$u = \arg\max_i \frac{\gamma_i(n)}{\bar{\gamma}_i(n)} \ ,$$

where $\bar{\gamma}_i(n)$ is the average SNR measured over a sliding window T_w

$$\bar{\gamma}_i(n+1) = \begin{cases} (1-\frac{1}{T_w})\bar{\gamma}_i(n) + \frac{1}{T_w}\gamma_i(n) \ , & \text{if user } i \text{ is scheduled,} \\ (1-\frac{1}{T_w})\bar{\gamma}_i(n) \ , & \text{if user } i \text{ is not scheduled.} \end{cases}$$

Opportunistic Beamforming If the channel experiences flat or slow fading, the maximum MUD scheduler transmits primarily to the users with better SNR condition. Instead of using the proportional fair scheduler, fairness can be introduced with an antenna array that produces random channel fluctuations. This artificial increase of channel variability was proposed by [VTL02] and is referred to as Opportunistic Beamforming. This technique sees fast fading not as a source of unreliability, but as a randomization tool that allows users to receive transmission slots when experiencing high SNR.

Appendix F

Statistics of SNR and Analytical BER Using Prediction

This appendix describes the process followed to obtain the closed-form expressions of the BER and SNR thresholds presented in Chapter 3. After proposing an unbiased predictor for adaptive modulation, the author in [Ekm02] derives analytical expressions for the BER performance of SISO flat fading channels. In this appendix, we extend the analytical formulations to other MIMO schemes, spatial diversity, multiplexing, and AS.

The remainder of the appendix is organized as follows. Section F.1 introduces the unbiased predictor. Section F.2 derives the conditional distributions of the true and predicted SNR based on known Rayleigh channel statistics of Section D.3. Then, the conditional distributions are used in Section F.3 to derive the expressions of BER performance.

F.1 Unbiased Power Predictor

The power predictor proposed in [Ekm02] is based on a prediction of the channel coefficients at instant $n - L$, to be applied at instant n, i.e., $\hat{\mathbf{h}}_{n|n-L}$. The true power of the

channel and the SNR at instant n are defined as

$$p_n = |\mathbf{h}_n|^2 \ ,$$
$$\gamma_n = |\mathbf{h}_n|^2 \frac{E_s}{N_0} \ .$$

The average channel power is defined as $\sigma^2_{\mathbf{h}} = E[|\mathbf{h}_n|^2]$, while the average SNR is given by

$$\bar{\gamma} = E[|\mathbf{h}_n|^2] \frac{E_s}{N_0} \ .$$

The predictor is based on past observations of the channel coefficients. The instantaneous predicted SNR at time n with horizon L, $\hat{\gamma}_{n|n-L}$, and the predicted complex channel gain, $\hat{\mathbf{h}}_{n|n-L}$, are given by

$$\hat{\gamma}_{n|n-L} = \hat{p}_{n|n-L} \frac{E_s}{\sigma^2_{\mathbf{h}}} \ ,$$
$$\hat{\mathbf{h}}_{n|n-L} = \mathbf{H}^{\text{pilot}}_{n-L} \theta \ ,$$

where θ is the predictor vector and $\mathbf{H}^{pilot}_{n-L}$ is the regressor vector with m observations of the channel, $\mathbf{H}^{\text{pilot}}_{n-L} = \left[\mathbf{h}^{\text{pilot}}_{n-L}, \mathbf{h}^{\text{pilot}}_{n-L-m}, ..., \mathbf{h}^{\text{pilot}}_{n-L-(k-1)m}\right]$. The observations are affected by an additive estimation error, $\mathbf{h}^{\text{pilot}}_n = \mathbf{h}_n + e_n$.

In an adaptive modulation scheme, the transmission is adjusted through the value of SNR at the time of transmission, and not through the channel gain, $\hat{\mathbf{h}}$. The use of the squared amplitude of the predictor as a predictor for the channel power, $\hat{p}_b = |\hat{\mathbf{h}}|^2$, results in a biased estimate [Ekm02].

The unbiased quadratic power predictor described in [Ekm02, ESA02] is obtained as follows:

$$\hat{p} = \left|\mathbf{H}^{\text{pilot}}_{n-L}\theta\right|^2 + \sigma^2_{\mathbf{h}} - E\left[|\hat{\mathbf{h}}_{n|n-L}|^2\right] \ . \tag{F.1}$$

The criterion to choose the predictor vector θ was a Wiener adjustment. This method ensures the optimal linear predictor in the MSE sense. It is shown in [Ekm02], that the θ optimal in MSE sense for the channel predictor, also ensures an MSE optimal

power predictor. Thus, the optimal adjustment for both cases reads

$$\begin{aligned}\theta &= R^{-1}_{\mathbf{H}^{\text{pilot}}_{n-L}} r_{\mathbf{h}\mathbf{H}^{\text{pilot}}_{n-L}} \ , \\ r_{\mathbf{h}\mathbf{H}^{\text{pilot}}_{n-L}} &= E\left[\mathbf{h}_n \mathbf{H}^{\text{pilot}}_{n-L}\right] \ , \\ R_{\mathbf{H}^{\text{pilot}}_{n-L}} &= E\left[\mathbf{H}^{\text{pilot}}_{n-L}\left(\mathbf{H}^{\text{pilot}}_{n-L}\right)^H\right] \ .\end{aligned}$$

When the predictor vector is optimally adjusted, the channel gain prediction error, $\epsilon_{\mathbf{h}} = \mathbf{h}_n - \hat{\mathbf{h}}_n$, and the power prediction error, $\epsilon_p = p_n - \hat{p}_n$, have variances:

$$\begin{aligned}\sigma^2_{\epsilon_{\mathbf{h}}} &= \sigma^2_{\mathbf{h}} + (r_{\mathbf{h}\mathbf{H}^{\text{pilot}}})^H R^{-1}_{\mathbf{H}^{\text{pilot}}_{n-L}} r_{\mathbf{h}\mathbf{H}^{\text{pilot}}} \ , \\ \sigma^2_{\epsilon_p} &= (\epsilon_{\mathbf{h}})^2 + \left|(r_{\mathbf{h}\mathbf{H}^{\text{pilot}}})^H R^{-1}_{\mathbf{H}^{\text{pilot}}_{n-L}} r_{\mathbf{h}\mathbf{H}^{\text{pilot}}}\right|^2 \ .\end{aligned}$$

From (F.1), the optimal unbiased quadratic power predictor can be expressed in terms of MSE-optimal linear channel predictor as

$$\hat{p}_{n|n-L} = \left|\hat{\mathbf{h}}_{n|n-L}\right|^2 + \sigma^2_{\mathbf{h}} - \sigma^2_{\hat{\mathbf{h}}} = \left|\hat{\mathbf{h}}_{n|n-L}\right|^2 + \sigma^2_{\epsilon_{\mathbf{h}}} \ .$$

Therefore, the unbiased power predictor reduces to

$$\hat{p}_{n|n-L} = |\hat{\mathbf{h}}_{n|n-L}|^2 + \sigma^2_{\epsilon_{\mathbf{h}}} \ . \tag{F.2}$$

In the derivations obtained for the predictor, an important variable to introduce is the relative variance of the prediction error,

$$\upsilon_{\mathbf{h}\epsilon_{\mathbf{h}}} = \frac{\sigma^2_{\epsilon_{\mathbf{h}}}}{\sigma^2_{\mathbf{h}}} \ . \tag{F.3}$$

F.2 Distribution of Predicted SNR for MIMO

The statistical distribution of the channel power is known for each MIMO scheme and is shown in Section D.3. However, when using a predictor, an error between the predicted

value of the power and the true power of the channel changes the PDF of the SNR. Therefore, here we derive the conditional probability of the true SNR given the predicted SNR.

F.2.1 SISO

A Rayleigh channel is assumed, and an unbiased quadratic power predictor is applied with optimized parameters, as described in Appendix F.1. The true SNR experienced by the channel, and the prediction with horizon L, are represented by γ_n and $\hat{\gamma}_{n|n-L}$, respectively. The time subscripts of the variables are dropped to simplify the expressions.

The derivation of the following expressions for SISO case are detailed in [ESA02]. Although only the main results are presented for SISO, the intermediate steps can be obtained substituting the number of antennas to one in the derivations of the SM or MIMO diversity.

Using the distribution of SNR in Appendix D.3, and the power prediction mechanism, the PDF of the predicted SNR, $\hat{\gamma}$, is given by [Ekm02]

$$f(\hat{\gamma}) = \frac{U\left(\hat{\gamma} - \bar{\gamma}\upsilon_{\mathbf{h}\epsilon_\mathbf{h}}\right)}{\bar{\gamma}\left(1 - \upsilon_{\mathbf{h}\epsilon_\mathbf{h}}\right)} \exp\left[-\frac{\hat{\gamma} - \bar{\gamma}\upsilon_{\mathbf{h}\epsilon_\mathbf{h}}}{\bar{\gamma}\left(1 - \upsilon_{\mathbf{h}\epsilon_\mathbf{h}}\right)}\right] \quad , \tag{F.4}$$

where $U(.)$ is the Heaviside function, and $\upsilon_{\mathbf{h}\epsilon_\mathbf{h}}$ is the relative variance of the prediction error.

F.2.1.1 Conditional PDF for True and Predicted SNR

The PDF of the true SNR, γ, conditioned on the predicted SNR, $\hat{\gamma}$, is

$$f(\gamma|\hat{\gamma}) = \frac{U(\gamma)U\left(\hat{\gamma} - \bar{\gamma}\upsilon_{\mathbf{h}\epsilon_\mathbf{h}}\right)}{\bar{\gamma}\upsilon_{\mathbf{h}\epsilon_\mathbf{h}}} \exp\left[-\frac{\gamma + \hat{\gamma} - \bar{\gamma}\upsilon_{\mathbf{h}\epsilon_\mathbf{h}}}{\bar{\gamma}\upsilon_{\mathbf{h}\epsilon_\mathbf{h}}}\right] I_0\left(\frac{2}{\bar{\gamma}\upsilon_{\mathbf{h}\epsilon_\mathbf{h}}}\sqrt{\gamma\left(\hat{\gamma} - \bar{\gamma}\upsilon_{\mathbf{h}\epsilon_\mathbf{h}}\right)}\right) \quad , \tag{F.5}$$

where I_0 is the zero order modified Bessel function of first kind, defined as

$$I_0(z) = \sum_{k=0}^{\infty} \frac{\left(\frac{1}{4}z^2\right)^k}{(k!)^2} \quad .$$

F.2.2 Spatial Multiplexing

A similar approach as described in [Ekm02] was followed to determine the expressions for links using multiple antennas both at transmitter and receiver and employing SM with ZF receiver.

Consider a Rayleigh fading channel, an SM system, with N_t transmit antennas, N_r receive antennas and a ZF receiver. As shown in Appendix D.3.2, the true power of each of the streams is a random variable with a PDF given by a chi-square distribution with $2(N_r - N_t + 1)$ degrees of freedom and the power shared by all transmit antennas:

$$f(p) = \frac{U(p)}{\left(\frac{\sigma^2_{\mathbf{h}}}{N_t}\right)^{N_r - N_t + 1} (N_r - N_t)!} p^{N_r - N_t} \exp\left[-\frac{p}{\frac{\sigma^2_{\mathbf{h}}}{N_t}}\right] \quad .$$

Consider the configurations with the same number of antennas at receiver and transmitter, i.e., $N_r = N_t = N_a$. In this case, if the links are independent, the spatial rate is N_a. Thus, the PDF of true power of each stream follows a chi-square distribution with two degrees of freedom:

$$f(p) = \frac{U(p)}{\frac{\sigma^2_{\mathbf{h}}}{N_a}} \exp\left[-\frac{p}{\frac{\sigma^2_{\mathbf{h}}}{N_a}}\right] \quad .$$

Since the predicted channel coefficients are weighted sums of zero-mean complex Gaussian random variables, they also follow a zero-mean complex Gaussian distribution [TAG99]. Thus, the predicted power is also chi-square distributed. Using the definition of the biased predicted power, $\hat{p}_b$, in terms of the unbiased predictor, i.e., $\hat{p}_b = \hat{p} - \sigma^2_{\epsilon_{\mathbf{h}}}$, one obtains the distribution of the unbiased predictor,

$$f(\hat{p}) = \frac{U(\hat{p} - \sigma^2_{\epsilon_{\mathbf{h}}})}{\frac{\sigma^2_{\mathbf{h}} - \sigma^2_{\epsilon_{\mathbf{h}}}}{N_a}} \exp\left[-\frac{\hat{p} - \sigma^2_{\epsilon_{\mathbf{h}}}}{\frac{\sigma^2_{\mathbf{h}} - \sigma^2_{\epsilon_{\mathbf{h}}}}{N_a}}\right] \quad .$$

Applying the transformation of variables $\hat{\gamma} = \bar{\gamma}\frac{\hat{p}}{\sigma^2_{\mathbf{h}}}$, $\frac{d\hat{\gamma}}{dp} = \frac{\hat{\gamma}}{\sigma^2_{\mathbf{h}}}$, the PDF of the pre-

dicted SNR, $\hat{\gamma}$, reads

$$f(\hat{\gamma}) = \frac{f_{\hat{p}}(\bar{\gamma}\frac{\hat{p}}{\sigma^2_{\mathbf{h}}})}{\frac{d\hat{\gamma}}{d\hat{p}}} = \frac{U(\hat{\gamma} - \bar{\gamma}\upsilon_{\mathbf{h}\epsilon_{\mathbf{h}}})}{\bar{\gamma}\left(\frac{1-\upsilon_{\mathbf{h}\epsilon_{\mathbf{h}}}}{N_a}\right)} \exp\left[-\frac{\hat{\gamma} - \bar{\gamma}\upsilon_{\mathbf{h}\epsilon_{\mathbf{h}}}}{\frac{\bar{\gamma}}{N_a}(1-\upsilon_{\mathbf{h}\epsilon_{\mathbf{h}}})}\right] \ .$$

F.2.2.1 Conditional PDF for True and Predicted SNR

Since both true and predicted power of the channel are exponentially distributed, their joint PDF is given by the bivariate of the chi-square distribution with two degrees of freedom [Ekm02, TAG99]. The bivariate distribution is written as

$$f(y_1, y_2) = \alpha_1 \exp\left[-\alpha_2\left(\frac{y_1}{\sigma_1^2} + \frac{y_2}{\sigma_2^2}\right)\right] I_0\left(\alpha_3\sqrt{y_1 y_2}\right) \ , \tag{F.6}$$

where I_0 is the modified Bessel function of zero order and the constants α_i are given, for $y_1 = \mathbf{h}$ and $y_2 = \hat{\mathbf{h}}$, as follows:

$$\alpha_1 = \frac{1}{\sigma^2_{\mathbf{h}}\sigma^2_{\hat{\mathbf{h}}} - |r_{\mathbf{h}\hat{\mathbf{h}}}|^2} \ , \tag{F.7a}$$

$$\alpha_2 = \frac{\sigma^2_{\mathbf{h}}\sigma^2_{\hat{\mathbf{h}}}}{\sigma^2_{\mathbf{h}}\sigma^2_{\hat{\mathbf{h}}} - |r_{\mathbf{h}\hat{\mathbf{h}}}|^2} \ , \tag{F.7b}$$

$$\alpha_3 = \frac{2|r_{\mathbf{h}\hat{\mathbf{h}}}|}{\sigma^2_{\mathbf{h}}\sigma^2_{\hat{\mathbf{h}}} - |r_{\mathbf{h}\hat{\mathbf{h}}}|^2} \ . \tag{F.7c}$$

If the predictor coefficients are MSE optimal, as described in Appendix F.1, then $r_{\mathbf{h}\hat{\mathbf{h}}} = \sigma^2_{\hat{\mathbf{h}}} = \sigma^2_{\mathbf{h}} - \sigma^2_{\epsilon_{\mathbf{h}}}$, and the constants in (F.7) simplify to

$$\alpha_1 = \frac{1}{\sigma^2_{\epsilon_{\mathbf{h}}}(\sigma^2_{\mathbf{h}} - \sigma^2_{\epsilon_{\mathbf{h}}})} \ , \tag{F.8a}$$

$$\alpha_2 = \frac{\sigma^2_{\mathbf{h}}}{\sigma^2_{\epsilon_{\mathbf{h}}}} \ , \tag{F.8b}$$

$$\alpha_3 = \frac{2}{\sigma^2_{\epsilon_{\mathbf{h}}}} \ . \tag{F.8c}$$

Using (F.8) in (F.6), the joint distribution of the true and predicted power with an SM system can be expressed as

$$f(p,\hat{p}) = \frac{U(p)U(\hat{p}-\sigma^2_{\epsilon_\mathbf{h}})}{\sigma^2_{\epsilon_\mathbf{h}}(\sigma^2_\mathbf{h}-\sigma^2_{\epsilon_\mathbf{h}})} \exp\left[-\frac{\sigma^2_\mathbf{h}}{\sigma^2_{\epsilon_\mathbf{h}}}\left(\frac{p}{\frac{\sigma^2_\mathbf{h}}{N_a}} - \frac{\hat{p}-\sigma^2_{\epsilon_\mathbf{h}}}{\frac{\sigma^2_\mathbf{h}-\sigma^2_{\epsilon_\mathbf{h}}}{N_a}}\right)\right] I_0\left(\frac{2N_a}{\sigma^2_{\epsilon_\mathbf{h}}}\sqrt{p(\hat{p}-\sigma^2_{\epsilon_\mathbf{h}})}\right) \quad .$$

Then, the conditional PDF of the true power conditioned to the predicted power value is

$$\begin{aligned} f(p|\hat{p}) &= \frac{f(p,\hat{p})}{f(\hat{p})} \\ &= \frac{U(p)U(\hat{p}-\sigma^2_{\epsilon_\mathbf{h}})}{\frac{\sigma^2_{\epsilon_\mathbf{h}}}{N_a}} \exp\left[-\frac{p+\hat{p}-\sigma^2_{\epsilon_\mathbf{h}}}{\frac{\sigma^2_{\epsilon_\mathbf{h}}}{N_a}}\right] I_0\left(\frac{2N_a}{\sigma^2_{\epsilon_\mathbf{h}}}\sqrt{p(\hat{p}-\sigma^2_{\epsilon_\mathbf{h}})}\right) \quad . \end{aligned}$$

Applying the transformation of variables $\hat{\gamma} = \bar{\gamma}\frac{\hat{p}}{\sigma^2_\mathbf{h}}$, the PDF of the SNR conditioned on the predicted SNR, is given by

$$\begin{aligned} f(\gamma|\hat{\gamma}) &= \frac{f_{p\hat{p}}\left(\bar{\gamma}\frac{p}{\sigma^2_\mathbf{h}}|\bar{\gamma}\frac{\hat{p}}{\sigma^2_\mathbf{h}}\right)}{\frac{d\hat{\gamma}}{d\hat{p}}} \\ &= \frac{U(\gamma)U(\hat{\gamma}-\bar{\gamma}\upsilon_{\mathbf{h}\epsilon_\mathbf{h}})}{\frac{\bar{\gamma}}{N_a}\upsilon_{\mathbf{h}\epsilon_\mathbf{h}}} \exp\left[-\frac{\gamma+\hat{\gamma}-\bar{\gamma}\upsilon_{\mathbf{h}\epsilon_\mathbf{h}}}{\frac{\bar{\gamma}}{N_a}\upsilon_{\mathbf{h}\epsilon_\mathbf{h}}}\right] I_0\left(\frac{2N_a}{\bar{\gamma}\upsilon_{\mathbf{h}\epsilon_\mathbf{h}}}\sqrt{\gamma(\hat{\gamma}-\bar{\gamma}\upsilon_{\mathbf{h}\epsilon_\mathbf{h}})}\right) \quad . \end{aligned} \tag{F.9}$$

F.2.3 MIMO Diversity

In this section, the analysis of SNR statistics using a predictor is extended to the MIMO diversity technique. We consider a configuration of multiple antennas at the transmitter, where the signal is encoded via STBC, and multiple antennas at the receiver, where the signal is combined through MRC.

As shown in Appendix D.3.1, in a Rayleigh fading channel, the true power of the signal at the receiver is distributed according to a chi-square distribution with $2N_tN_r$ degrees of freedom:

$$f(p) = \frac{U(p)}{\left(\frac{\sigma^2_\mathbf{h}}{N_t}\right)^{N_tN_r}(N_tN_r-1)!} p^{N_tN_r-1}\exp\left[-\frac{p}{\frac{\sigma^2_\mathbf{h}}{N_t}}\right] \quad . \tag{F.10}$$

The definition of biased predicted power applied to the MIMO diversity case is written as

$$\hat{p}_b = \frac{\sum_{q=1}^{N_t}\sum_{p=1}^{N_r}|\hat{\mathbf{h}}_{q,p}|^2}{N_t} \ ,$$

thus, the biased predicted power given in terms of the unbiased predictor is represented as follows:

$$\hat{p}_b = \hat{p} - \frac{\sum_{q=1}^{N_t}\sum_{p=1}^{N_r}\sigma^2_{\epsilon_{\mathbf{h}}q,p}}{N_t} \ .$$

Assuming the channel gain prediction error to be the same for all the links involved, the predictor reduces to $\hat{p}_b = \hat{p} - N_r\sigma^2_{\epsilon_{\mathbf{h}}}$. Substituting this expression in (F.10), the PDF of the unbiased predictor is

$$f(\hat{p}) = \frac{U(\hat{p} - N_r\sigma^2_{\epsilon_{\mathbf{h}}})}{\left(\frac{\sigma^2_{\mathbf{h}}-\sigma^2_{\epsilon_{\mathbf{h}}}}{N_t}\right)^{N_tN_r}(N_tN_r-1)!}(\hat{p} - N_r\sigma^2_{\epsilon_{\mathbf{h}}})^{N_tN_r-1}\exp\left[-\frac{\hat{p} - N_r\sigma^2_{\epsilon_{\mathbf{h}}}}{\frac{\sigma^2_{\mathbf{h}}-\sigma^2_{\epsilon_{\mathbf{h}}}}{N_t}}\right] \ .$$

Now, applying a transformation of variables $\hat{\gamma} = \bar{\gamma}\frac{\hat{p}}{\sigma^2_{\mathbf{h}}}$,

$$\begin{aligned} f(\hat{\gamma}) &= \frac{f_{\hat{p}}(\bar{\gamma}\frac{\hat{p}}{\sigma^2_{\mathbf{h}}})}{\frac{d\hat{\gamma}}{d\hat{p}}} \\ &= \frac{U(\hat{\gamma} - N_r\bar{\gamma}\upsilon_{\mathbf{h}\epsilon_{\mathbf{h}}})}{\bar{\gamma}\left(\frac{1-\upsilon_{\mathbf{h}\epsilon_{\mathbf{h}}}}{N_t}\right)^{N_tN_r}(N_tN_r-1)!}\left(\hat{\gamma}\frac{\sigma^2_{\mathbf{h}}}{\bar{\gamma}} - N_r\sigma^2_{\epsilon_{\mathbf{h}}}\right)^{N_tN_r-1}\exp\left[-\frac{\hat{\gamma} - N_r\bar{\gamma}\upsilon_{\mathbf{h}\epsilon_{\mathbf{h}}}}{\frac{\bar{\gamma}}{N_t}(1-\upsilon_{\mathbf{h}\epsilon_{\mathbf{h}}})}\right] \\ &= \frac{U(\hat{\gamma} - N_r\bar{\gamma}\upsilon_{\mathbf{h}\epsilon_{\mathbf{h}}})}{\left(\frac{\bar{\gamma}}{N_t}(1-\upsilon_{\mathbf{h}\epsilon_{\mathbf{h}}})\right)^{N_tN_r}(N_tN_r-1)!}(\hat{\gamma} - N_r\bar{\gamma}\upsilon_{\mathbf{h}\epsilon_{\mathbf{h}}})^{N_tN_r-1}\exp\left[-\frac{\hat{\gamma} - N_r\bar{\gamma}\upsilon_{\mathbf{h}\epsilon_{\mathbf{h}}}}{\frac{\bar{\gamma}}{N_t}(1-\upsilon_{\mathbf{h}\epsilon_{\mathbf{h}}})}\right] \ . \end{aligned}$$

F.2.3.1 Conditional PDF for True and Predicted SNR

In MIMO diversity channel model, to obtain the joint PDF of the true power and predicted power, one needs to apply the bivariate of the chi-square distribution with $2N_tN_r$ degrees of freedom. Since the chi-square distribution is a particular case of the gamma distribution, a bivariate gamma distribution can be used. However, the two-dimensional gamma distribution does not have a unique solution. The authors in [SAT82] proposed a solution for the bivariate of the gamma distribution, known as SAT (Smith, Adelfang and

Tubb) bivariate. This expression is also used in the context of channel prediction by the authors in [Hol02, OHH04].

As the chi-square distribution is a particular case of the gamma distribution, the bivariate of the chi-square distribution with $2N_tN_r$ degrees of freedom is

$$f(x_1,x_2)=\alpha_1(x_1x_2)^{\frac{N_tN_r-1}{2}}\exp\left[-\alpha_2\left(\frac{x_1}{\sigma_1^2}+\frac{x_2}{\sigma_2^2}\right)\right]I_{N_tN_r-1}(\alpha_3\sqrt{x_1x_2}) \ , \tag{F.11}$$

where $I_\beta(z)$ is the modified Bessel function of order β. The constants α_i are defined as follows:

$$\alpha_1=\frac{1}{(\sigma_1^2\sigma_2^2)^{\frac{N_tN_r-1}{2}}(1-\rho)\rho^{\frac{N_tN_r-1}{2}}(N_tN_r-1)!} \ , \tag{F.12a}$$

$$\alpha_2=\frac{1}{1-\rho} \ , \tag{F.12b}$$

$$\alpha_3=\frac{2\sqrt{\rho}}{1-\rho}\frac{1}{\sqrt{\sigma_1^2\sigma_2^2}} \ , \tag{F.12c}$$

where $\rho=\frac{|r_{x_1x_2}|^2}{\sigma_1^2\sigma_2^2}$, and $r_{x_1x_2}$ is the coefficient of correlation between the two random variables. Inserting ρ in (F.12), and assuming the variables x_1 and x_2 to be replaced by the true channel, $\mathbf{h}$, and the predicted channel, $\hat{\mathbf{h}}$, the constants can be written as

$$\alpha_1=\frac{1}{(\sigma_{\mathbf{h}}^2\sigma_{\hat{\mathbf{h}}}^2)^{\frac{N_tN_r-1}{2}}(1-\frac{|r_{\mathbf{h}\hat{\mathbf{h}}}|^2}{\sigma_{\mathbf{h}}^2\sigma_{\hat{\mathbf{h}}}^2})\left(\frac{|r_{\mathbf{h}\hat{\mathbf{h}}}|^2}{\sigma_{\mathbf{h}}^2\sigma_{\hat{\mathbf{h}}}^2}\right)^{\frac{N_tN_r-1}{2}}(N_tN_r-1)!} \ , \tag{F.13a}$$

$$\alpha_2=\frac{\sigma_{\mathbf{h}}^2\sigma_{\hat{\mathbf{h}}}^2}{\sigma_{\mathbf{h}}^2\sigma_{\hat{\mathbf{h}}}^2-|r_{\mathbf{h}\hat{\mathbf{h}}}|^2} \ , \tag{F.13b}$$

$$\alpha_3=\frac{2|r_{\mathbf{h}\hat{\mathbf{h}}}|}{\sigma_{\mathbf{h}}^2\sigma_{\hat{\mathbf{h}}}^2-|r_{\mathbf{h}\hat{\mathbf{h}}}|^2} \ . \tag{F.13c}$$

If the predictor coefficients are MSE optimal, as described in Appendix F.1, then

$r_{\mathbf{h}\hat{\mathbf{h}}} = \sigma^2_{\hat{\mathbf{h}}} = \sigma^2_{\mathbf{h}} - \sigma^2_{\epsilon_\mathbf{h}}$, and the constants in (F.13) simplify to

$$\alpha_1 = \frac{1}{\left(\sigma^2_{\mathbf{h}}(\sigma^2_{\mathbf{h}} - \sigma^2_{\epsilon_\mathbf{h}})\right)^{\frac{N_t N_r + 1}{2}} \upsilon_{\mathbf{h}\epsilon_\mathbf{h}} (1 - \upsilon_{\mathbf{h}\epsilon_\mathbf{h}})^{\frac{N_t N_r - 1}{2}} (N_t N_r - 1)!} \ , \tag{F.14a}$$

$$\alpha_2 = \frac{\sigma^2_{\mathbf{h}}}{\sigma^2_{\epsilon_\mathbf{h}}} \ , \tag{F.14b}$$

$$\alpha_3 = \frac{2}{\sigma^2_{\epsilon_\mathbf{h}}} \ . \tag{F.14c}$$

Inserting (F.14) into (F.11), the joint distribution of the true and predicted power with a STBC-MRC system results

$$\begin{aligned} f(p, \hat{p}) =& \alpha_1 \left(p(\hat{p} - N_r \sigma^2_{\epsilon_\mathbf{h}})\right)^{\frac{N_t N_r - 1}{2}} \exp\left[-\frac{p}{\frac{\sigma^2_{\epsilon_\mathbf{h}}}{N_t}} - \frac{\sigma^2_{\mathbf{h}}}{\sigma^2_{\epsilon_\mathbf{h}}} \frac{\hat{p} - N_r \sigma^2_{\epsilon_\mathbf{h}}}{\frac{\sigma^2_{\mathbf{h}} - \sigma^2_{\epsilon_\mathbf{h}}}{N_t}} \right] \\ & \times I_{N_t N_r - 1} \left(\frac{2}{\sigma^2_{\epsilon_\mathbf{h}}} \sqrt{p(\hat{p} - N_r \sigma^2_{\epsilon_\mathbf{h}})} \right) U(p) U(\hat{p} - N_r \sigma^2_{\epsilon_\mathbf{h}}) \ . \end{aligned}$$

Therefore, the distribution of the true power of the channel conditioned to the predicted power value is

$$\begin{aligned} f(p|\hat{p}) =& \frac{f(p, \hat{p})}{f(\hat{p})} \\ =& \frac{U(p) U(\hat{p} - N_r \sigma^2_{\epsilon_\mathbf{h}})}{\upsilon_{\mathbf{h}\epsilon_\mathbf{h}} (\sigma^2_{\mathbf{h}})^{\frac{N_t N_r + 1}{2}} (\sigma^2_{\mathbf{h}} - \sigma^2_{\epsilon_\mathbf{h}})^{-\frac{N_t N_r - 1}{2}} (1 - \upsilon_{\mathbf{h}\epsilon_\mathbf{h}})^{\frac{N_t N_r - 1}{2}}} \\ & \times p^{\frac{N_t N_r - 1}{2}} (\hat{p} - N_r \sigma^2_{\epsilon_\mathbf{h}})^{\frac{N_t N_r - 1}{2}} \exp\left[-\frac{p + \hat{p} - N_r \sigma^2_{\epsilon_\mathbf{h}}}{\frac{\sigma^2_{\epsilon_\mathbf{h}}}{N_t}} \right] I_{N_t N_r - 1} \left(\frac{2}{\sigma^2_{\epsilon_\mathbf{h}}} \sqrt{p(\hat{p} - N_r \sigma^2_{\epsilon_\mathbf{h}})} \right) \ . \end{aligned} \tag{F.15}$$

Applying the transformation of variables $\hat{\gamma} = \bar{\gamma} \frac{\hat{p}}{\sigma^2_{\mathbf{h}}}$ to (F.15), the PDF of the SNR γ

conditioned on the predicted SNR, $\hat{\gamma}$, is written as

$$\begin{aligned} f(\gamma|\hat{\gamma}) =& \frac{f_{p\hat{p}}\left(\bar{\gamma}\frac{p}{\sigma^2_{\mathbf{h}}}|\bar{\gamma}\frac{\hat{p}}{\sigma^2_{\mathbf{h}}}\right)}{\frac{d\hat{\gamma}}{d\hat{p}}} \\ =& U(\gamma)U(\hat{\gamma}-N_r\bar{\gamma}\upsilon_{\mathbf{h}\epsilon_{\mathbf{h}}})\frac{N_t}{\bar{\gamma}\upsilon_{\mathbf{h}\epsilon_{\mathbf{h}}}}\gamma^{\frac{N_tN_r-1}{2}}(\hat{\gamma}-N_r\bar{\gamma}\upsilon_{\mathbf{h}\epsilon_{\mathbf{h}}})^{-\frac{N_tN_r-1}{2}} \\ &\times\exp\left[-\frac{\gamma+\hat{\gamma}-N_r\bar{\gamma}\upsilon_{\mathbf{h}\epsilon_{\mathbf{h}}}}{\frac{\bar{\gamma}}{N_t}\upsilon_{\mathbf{h}\epsilon_{\mathbf{h}}}}\right]I_{N_tN_r-1}\left(\frac{2N_t}{\bar{\gamma}\upsilon_{\mathbf{h}\epsilon_{\mathbf{h}}}}\sqrt{\gamma(\hat{\gamma}-N_r\bar{\gamma}\upsilon_{\mathbf{h}\epsilon_{\mathbf{h}}})}\right) \quad . \end{aligned} \tag{F.16}$$

F.2.4 Antenna Selection

In this section, the analysis of SNR statistics using a predictor is extended to the AS technique. We consider a configuration of two antennas at the transmitter, and a selector that chooses the highest SNR link at each instant based on feedback.

Appendix D.3.3 shows that the PDF of the post-processing SNR for AS can be obtained from the SISO case by higher order statistics. Based on the results for SISO in Appendix F.2.1, one obtains the distributions for the AS with two antennas as follows:

$$\begin{aligned} f_{\text{as}}(\hat{\gamma}) =& 2f_{\text{siso}}(\hat{\gamma})F_{\text{siso}}(\hat{\gamma}) \\ =& U(\hat{\gamma}-\bar{\gamma}\upsilon_{\mathbf{h}\epsilon_{\mathbf{h}}})\frac{2}{\bar{\gamma}(1-\upsilon_{\mathbf{h}\epsilon_{\mathbf{h}}})}\exp\left[-\frac{\hat{\gamma}-\bar{\gamma}\upsilon_{\mathbf{h}\epsilon_{\mathbf{h}}}}{\bar{\gamma}(1-\upsilon_{\mathbf{h}\epsilon_{\mathbf{h}}})}\right]\left(1-\exp\left[-\frac{\hat{\gamma}-\bar{\gamma}\upsilon_{\mathbf{h}\epsilon_{\mathbf{h}}}}{\bar{\gamma}(1-\upsilon_{\mathbf{h}\epsilon_{\mathbf{h}}})}\right]\right) \quad . \end{aligned}$$

Now, with the results of the SISO case for joint distribution of SNR, we derive the

conditional PDF for AS:

$$\begin{aligned} f_{\text{as}}(\gamma|\hat{\gamma}) =& \frac{2f_{\text{siso}}(\gamma,\hat{\gamma})F_{\text{siso}}(\gamma,\hat{\gamma})}{2f_{\text{siso}}(\hat{\gamma})F_{\text{siso}}(\hat{\gamma})} = f_{\text{siso}}(\gamma|\hat{\gamma})F_{\text{siso}}(\gamma|\hat{\gamma}) \\ =& U(\gamma)U(\hat{\gamma}-\bar{\gamma}\upsilon_{\mathbf{h}\epsilon_{\mathbf{h}}})\frac{1}{\bar{\gamma}}\exp\left[-\frac{\gamma+\hat{\gamma}-\bar{\gamma}\upsilon_{\mathbf{h}\epsilon_{\mathbf{h}}}}{\bar{\gamma}\upsilon_{\mathbf{h}\epsilon_{\mathbf{h}}}}\right] I_0\left(\frac{2}{\bar{\gamma}\upsilon_{\mathbf{h}\epsilon_{\mathbf{h}}}}\sqrt{\gamma(\hat{\gamma}-\bar{\gamma}\upsilon_{\mathbf{h}\epsilon_{\mathbf{h}}})}\right) \\ &\times\left(1-\exp\left[-\frac{\hat{\gamma}-\bar{\gamma}\upsilon_{\mathbf{h}\epsilon_{\mathbf{h}}}}{\bar{\gamma}(1-\upsilon_{\mathbf{h}\epsilon_{\mathbf{h}}})}\right]\right)^{-1}\sum_{k=0}^{\infty}(1-\upsilon_{\mathbf{h}\epsilon_{\mathbf{h}}})^k \\ &\times\left(1-\exp\left[-\frac{\gamma}{\bar{\gamma}\upsilon_{\mathbf{h}\epsilon_{\mathbf{h}}}}\right]\sum_{n_1}^{k}\frac{1}{n_1!}\left(\frac{\gamma}{\bar{\gamma}\upsilon_{\mathbf{h}\epsilon_{\mathbf{h}}}}\right)^{n_1}\right) \\ &\times\left(1-\exp\left[-\frac{\hat{\gamma}-\bar{\gamma}\upsilon_{\mathbf{h}\epsilon_{\mathbf{h}}}}{\bar{\gamma}(1-\upsilon_{\mathbf{h}\epsilon_{\mathbf{h}}})}\right]\sum_{n_2=0}^{k}\frac{1}{n_2!}\left(\frac{\hat{\gamma}-\bar{\gamma}\upsilon_{\mathbf{h}\epsilon_{\mathbf{h}}}}{\bar{\gamma}\upsilon_{\mathbf{h}\epsilon_{\mathbf{h}}}(1-\upsilon_{\mathbf{h}\epsilon_{\mathbf{h}}})}\right)^{n_2}\right) \quad . \end{aligned} \tag{F.17}$$

F.3 M-QAM Performance

Using the distribution functions of the previous section, we show here the derivation of the BER performance of M-QAM for the different MIMO cases considered, SISO, multiplexing, diversity, and AS. Here, we aply the approximation of the BER given in Appendix E.1, i.e.,

$$BER(\gamma,\hat{\gamma}) \approx 0.2\exp\left[\frac{-1.6\gamma}{M(\hat{\gamma})-1}\right] \quad ,$$

where $M(\hat{\gamma}) \equiv M_i$.

F.3.1 SISO

In the context of the results in Appendix F.2, the authors in [Ekm02] derive the BER expression as a function of the predicted SNR. With (F.5) in (3.6), one obtains the instantaneous BER as a function of $\hat{\gamma}$ derived for the SISO case:

$$\begin{aligned} BER(\hat{\gamma}) =& \int_0^{\infty} BER(\gamma,\hat{\gamma})f(\gamma|\hat{\gamma})d\gamma \\ =& U(\hat{\gamma}-\bar{\gamma}\upsilon_{\mathbf{h}\epsilon_{\mathbf{h}}})\frac{a(\hat{\gamma})}{b(i)}\exp\left[\frac{c(\hat{\gamma})^2}{4b(\hat{\gamma})}\right] \quad , \end{aligned} \tag{F.18}$$

where

$$\begin{aligned} a(\hat{\gamma}) =& \frac{0.2}{\bar{\gamma}\upsilon_{\mathbf{h}\epsilon_{\mathbf{h}}}} \exp\left[-\frac{\hat{\gamma}-\bar{\gamma}\upsilon_{\mathbf{h}\epsilon_{\mathbf{h}}}}{\bar{\gamma}\upsilon_{\mathbf{h}\epsilon_{\mathbf{h}}}}\right] \ , \\ b(i) =& \frac{1}{\bar{\gamma}\upsilon_{\mathbf{h}\epsilon_{\mathbf{h}}}} + \frac{1.6}{M_i - 1} \ , \\ c(\hat{\gamma}) =& \frac{2}{\bar{\gamma}\upsilon_{\mathbf{h}\epsilon_{\mathbf{h}}}} \sqrt{\hat{\gamma}-\bar{\gamma}\upsilon_{\mathbf{h}\epsilon_{\mathbf{h}}}} \ . \end{aligned}$$

In the derivation of (F.18), two known results are employed:

$$\exp(x) = \sum_{k=0}^{\infty} \frac{x^k}{k!} \ , \tag{F.19a}$$

$$\int_0^{\infty} x^k \exp(-\alpha x) = \frac{k!}{\alpha^{k+1}} \ . \tag{F.19b}$$

It is also possible to write the instantaneous BER in (F.18) in the following form:

$$BER(\hat{\gamma}) = U(\hat{\gamma}-\bar{\gamma}\upsilon_{\mathbf{h}\epsilon_{\mathbf{h}}}) \frac{0.2}{\bar{\gamma}\upsilon_{\mathbf{h}\epsilon_{\mathbf{h}}} b(i)} \exp\left[\frac{\hat{\gamma}-\bar{\gamma}\upsilon_{\mathbf{h}\epsilon_{\mathbf{h}}}}{\bar{\gamma}\upsilon_{\mathbf{h}\epsilon_{\mathbf{h}}}} \left(\frac{1}{\bar{\gamma}\upsilon_{\mathbf{h}\epsilon_{\mathbf{h}}} b(i)} - 1\right)\right] \ , \tag{F.20}$$

where $b(i) = \frac{1}{\bar{\gamma}\upsilon_{\mathbf{h}\epsilon_{\mathbf{h}}}} + \frac{1.6}{M_i - 1}$. Expressed in this closed-form, the BER expression (F.20) can be used to obtain the predicted SNR required to achieve a defined BER. Thus, for a system with instantaneous BER constraint, i.e., $BER \leq BER_t$, the SNR thresholds are given by

$$\gamma_i = \bar{\gamma}\upsilon_{\mathbf{h}\epsilon_{\mathbf{h}}} + \frac{\bar{\gamma}\upsilon_{\mathbf{h}\epsilon_{\mathbf{h}}}}{\left(\frac{1}{\bar{\gamma}\upsilon_{\mathbf{h}\epsilon_{\mathbf{h}}} b(i)} - 1\right)} \ln\left[\frac{BER_t}{0.2} \bar{\gamma}\upsilon_{\mathbf{h}\epsilon_{\mathbf{h}}} b(i)\right] \ . \tag{F.21}$$

The authors in [FSES04] also propose an expression for the SNR thresholds in the situation of instantaneous BER constraint and constant power at transmitter for SISO. After some manipulation it is possible to show that the expression in (F.21) is equivalent to the result found in [FSES04, Equation (41)].

F.3.2 Spatial Multiplexing

Based on the results of the predicted SNR statistics for the SM configuration in Appendix F.2.2, we derive the instantaneous BER as a function of the predicted SNR. Hence,

inserting (F.9) into (3.6), one obtains the instantaneous BER as a function of $\hat{\gamma}$ derived for SM with equal number of transmit and receive antennas as follows:

$$\begin{aligned} BER(\hat{\gamma}) &= \int_0^{\infty} BER(\gamma,\hat{\gamma}) f(\gamma|\hat{\gamma}) d\gamma \\ &= U(\hat{\gamma} - \bar{\gamma}\upsilon_{\mathbf{h}\epsilon_{\mathbf{h}}}) \frac{0.2N_a}{\bar{\gamma}\upsilon_{\mathbf{h}\epsilon_{\mathbf{h}}} b(i)} \exp\left[\frac{\hat{\gamma} - \bar{\gamma}\upsilon_{\mathbf{h}\epsilon_{\mathbf{h}}} \left(\frac{N_a}{\bar{\gamma}\upsilon_{\mathbf{h}\epsilon_{\mathbf{h}}} b(i)} - 1 \right)}{\frac{\bar{\gamma}}{N_a}\upsilon_{\mathbf{h}\epsilon_{\mathbf{h}}}} \right] , \end{aligned} \tag{F.22}$$

where $b(i) = \frac{N_a}{\bar{\gamma}\upsilon_{\mathbf{h}\epsilon_{\mathbf{h}}}} + \frac{1.6}{M_i - 1}$.

Moreover, for a system with instantaneous BER constraint $BER \leq BER_t$, and constant transmit power, the SNR thresholds are given by

$$\gamma_i = \bar{\gamma}\upsilon_{\mathbf{h}\epsilon_{\mathbf{h}}} + \frac{\bar{\gamma}\upsilon_{\mathbf{h}\epsilon_{\mathbf{h}}}}{N_a \left(\frac{N_a}{\bar{\gamma}\upsilon_{\mathbf{h}\epsilon_{\mathbf{h}}} b(i)} - 1 \right)} \ln\left[\frac{BER_t}{0.2} \frac{\bar{\gamma}\upsilon_{\mathbf{h}\epsilon_{\mathbf{h}}} b(i)}{N_a} \right] . \tag{F.23}$$

F.3.3 MIMO Diversity

This section describes the derivation of a closed-form of the BER as a function of the predicted SNR in the MIMO diversity case. Inserting (F.16) into (3.6), and using the properties (F.19), we calculate the instantaneous BER as a function of $\hat{\gamma}$ derived for the MIMO diversity:

$$\begin{aligned} BER(\hat{\gamma}) &= \int_0^{\infty} BER(\gamma,\hat{\gamma}) f(\gamma|\hat{\gamma}) d\gamma \\ &= U(\hat{\gamma} - N_r\bar{\gamma}\upsilon_{\mathbf{h}\epsilon_{\mathbf{h}}}) 0.2 \left(\frac{N_t}{\bar{\gamma}\upsilon_{\mathbf{h}\epsilon_{\mathbf{h}}} b(i)} \right)^{N_t N_r} \exp\left[\frac{\hat{\gamma} - N_r\bar{\gamma}\upsilon_{\mathbf{h}\epsilon_{\mathbf{h}}} \left(\frac{N_t}{\bar{\gamma}\upsilon_{\mathbf{h}\epsilon_{\mathbf{h}}} b(i)} - 1 \right)}{\frac{\bar{\gamma}}{N_t}\upsilon_{\mathbf{h}\epsilon_{\mathbf{h}}}} \right] , \end{aligned} \tag{F.24}$$

where $b(i) = \frac{N_t}{\bar{\gamma}\upsilon_{\mathbf{h}\epsilon_{\mathbf{h}}}} + \frac{1.6}{M_i - 1}$.

For a system with instantaneous BER constraint, $BER \leq BER_t$, and constant transmit power, the SNR thresholds are given by

$$\gamma_i = N_r\bar{\gamma}\upsilon_{\mathbf{h}\epsilon_{\mathbf{h}}} + \frac{\bar{\gamma}\upsilon_{\mathbf{h}\epsilon_{\mathbf{h}}}}{N_t \left(\frac{N_t}{\bar{\gamma}\upsilon_{\mathbf{h}\epsilon_{\mathbf{h}}} b(i)} - 1 \right)} \ln\left[\frac{BER_t}{0.2} \left(\frac{\bar{\gamma}\upsilon_{\mathbf{h}\epsilon_{\mathbf{h}}} b(i)}{N_t} \right)^{N_t N_r} \right] . \tag{F.25}$$

F.3.4 Antenna Selection

For a two branch AS system, we use the result shown in Appendix F.2.4. Thus, after substituting (F.17) in (3.6), the expression of the instantaneous BER as a function of the predicted SNR is written as

$$\begin{aligned} BER(\hat{\gamma}) \approx & U(\hat{\gamma}-\bar{\gamma}\upsilon_{\mathbf{h}\epsilon_{\mathbf{h}}})\frac{0.2}{\bar{\gamma}}\left(1-\exp\left[-\frac{\hat{\gamma}-\bar{\gamma}\upsilon_{\mathbf{h}\epsilon_{\mathbf{h}}}}{\bar{\gamma}(1-\upsilon_{\mathbf{h}\epsilon_{\mathbf{h}}})}\right]\right)^{-1} \\ & \times\sum_{k=0}^{\infty}(1-\upsilon_{\mathbf{h}\epsilon_{\mathbf{h}}})^{k}\frac{\Gamma_{\text{lower}}\left(\frac{\hat{\gamma}-\bar{\gamma}\upsilon_{\mathbf{h}\epsilon_{\mathbf{h}}}}{\bar{\gamma}\upsilon_{\mathbf{h}\epsilon_{\mathbf{h}}}(1-\upsilon_{\mathbf{h}\epsilon_{\mathbf{h}}})},k+1\right)}{\Gamma(k+1)} \\ & \times\left(\frac{1}{\beta+\frac{1}{\sigma^{2}_{\epsilon_{\mathbf{h}}}}}\exp\left[-\frac{\hat{\gamma}-\bar{\gamma}\upsilon_{\mathbf{h}\epsilon_{\mathbf{h}}}}{\bar{\gamma}\upsilon_{\mathbf{h}\epsilon_{\mathbf{h}}}+\frac{1}{\beta}}\right]-\frac{1}{\beta+\frac{2}{\sigma^{2}_{\epsilon_{\mathbf{h}}}}}\exp\left[-\frac{\hat{\gamma}-\bar{\gamma}\upsilon_{\mathbf{h}\epsilon_{\mathbf{h}}}}{\bar{\gamma}\upsilon_{\mathbf{h}\epsilon_{\mathbf{h}}}}\right]\right. \\ & \left.\times\sum_{n_1=0}^{k}\left(\frac{1}{\beta\sigma^{2}_{\epsilon_{\mathbf{h}}}+2}\right)^{n_1}\frac{\Gamma_{\text{upper}}\left(\frac{\hat{\gamma}-\bar{\gamma}\upsilon_{\mathbf{h}\epsilon_{\mathbf{h}}}}{\bar{\gamma}\upsilon_{\mathbf{h}\epsilon_{\mathbf{h}}}(1-\upsilon_{\mathbf{h}\epsilon_{\mathbf{h}}})},k+1\right)}{\Gamma(n_1+1)}\right)\ , \end{aligned} \tag{F.26}$$

where $\beta=\frac{1.6}{M_i-1}$, $\Gamma(n)$ is the complete gamma function, $\Gamma_{\text{lower}}(x,n)$ is the lower tail of the incomplete gamma function, and $\Gamma_{\text{upper}}(x,n)$ is the upper tail of the incomplete gamma function.

Since (F.26) is not in a closed-form, and no other closed-form solutions are known for the BER performance of AS in function of the predicted SNR, it is not possible to analytically obtain the SNR thresholds. Nevertheless, the tractable equation obtained for the BER performance allows for a numerical evaluation of the performance.

Appendix G

Link Simulator EUTRA

The link-level simulator used in Sections 2.3 and 5.2 was initially developed by the Ph.D. students at Aalborg University: Akhilesh Pokhariyal, Basuki Priyanto, Christian Rom, and Na Wei, as well as Claudio Rosa and Frank Frederiksen from Nokia Siemens Networks. A more detailed description of the simulator can be found in [WPR+06], as well as in the Ph.D. dissertations [Pok07, Wei07].

The block diagram of the link-level chain of the simulator is shown in Figure G.1. This is a single-user downlink simulation where the data generation assumes that there is always data to transmit. The stream of bits to transmit is Cyclic Redundancy Check (CRC) encoded, divided into several blocks, and passed to the channel encoder. The UTRA Release 6 Turbo coding and rate matching algorithm are then applied. After interleaving, the bits are modulated with QAM followed by a bit remapping to place the systematic bits at more reliable constellation points [WPR+06]. The modulated symbols are then passed to the MIMO space-frequency encoder. The SFC depends on the MIMO scheme selected, and it is at this block that one of the contributions of this thesis was introduced by implementing several MIMO encoding schemes, including UTOD and ABBA [TBH00] schemes, and extending the encoding from two to four transmit antennas.

An Inverse Fast Fourier Transform (IFFT) is applied on each transmit antenna branch, and CP is added before the convolution with the multipath MIMO channel. The

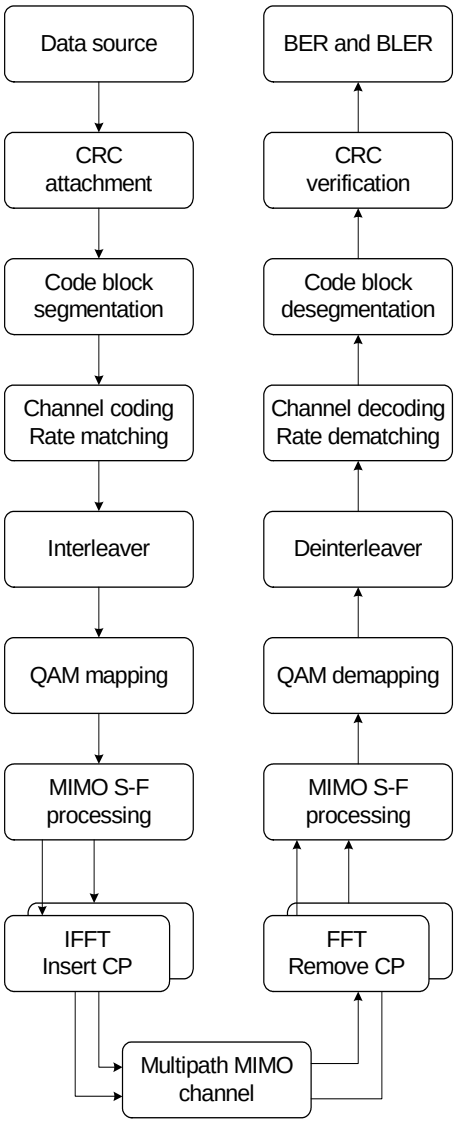

Figure G.1: Block diagram of link-level simulator

MIMO channel model is based on the contribution of [SKF+01] for the I-METRA project which has been used and validated in [Ber05]. The MIMO channel matrix with uncorrelated spatial links is pre-generated for the number of transmitters and receivers configuration to save simulation time.

The noise and interference in Section 2.3 are modeled with AWGN. However, in Section 5.2, the other cell interference is not modeled as AWGN, and the contribution of this thesis is the extension of the downlink simulator to consider simultaneous transmissions from other BSs according to the pathloss model and ISD.

The continuous time-varying impulse response channel model is too complex for a simple analysis. Therefore, a discrete time tapped delay limitation is employed to model the wideband multipath model. The resolution of the sampling depends on the bandwidth of the transmitted signal. In 3GPP, the delay of the l path is quantized in time to the nearest 1/16th chip interval $T_c = \frac{1}{3.84}\mu$s.

The receiver estimates the channel for each spatial link, and the channel estimation is assumed to be perfect. After removing the CP and passing the time domain signal through the FFT, the signal is passed to the MIMO decoder. The MIMO decoder block equalizes the transmitted symbols. Then, the inverse process to obtain the data bits is done to measure the BER and BLER.

Based on the channel estimation, the system applies link adaptation at the transmitter. The link adaptation mechanism selects the MCS based on the averaged received SNR. Particularly, the scheme adapts among QPSK, 16-QAM, and 64-QAM, as well as different coding rates ranging from 1/6 and up to 4/5. The Exponential Effective SNR Mapping (EESM) model is applied to obtain an effective SNR value for prediction of the BLER on the basis of a set of link-level AWGN performance curves. The link adaptation targets a maximum BLER of 20%.

The above described procedure is applied to the data generated for a frame of seven OFDM symbols. The simulations are then run for a total of 3000 frames, and we validate the BER curves with the number of errors before and after the coding process. The number

of uncoded bit transmitted amounts to approximately 40 million (7 OFDM symbols in a frame; 1024 data subcarriers; and QPSK modulation). As an example, in Figure 2.8, the fixed modulation SFC at 20 dB results in 4495 uncoded errors with 16-QAM, whereas LDC results in more than half million errors with QPSK. After channel coding, the number of coded bit errors drops to levels below tens of errors for very high SNR, which does not allow for a plotting of coded BER curves. The spectral efficiency curves are directly dependent on the coded BER and BLER, but are little affected by errors in their exact values, since the performance is mainly driven by the maximum achievable throughput at high SNR.

Appendix H

Dissemination of Results

During the Ph.D. studies, the following publications in technical peer-reviewed conferences and journals have been generated:

- Muhammad I. Rahman, Ragnar V. Reynisson, Daniel V.P. Figueiredo, and Ramjee Prasad, "Coordinated Sub-Carrier and Band Hopping in OFDMA based Systems," to appear in Special Issue of Wireless Personal Communications (WPC) Journal, Springer, 2008.

- Daniel V.P. Figueiredo, Zihuai Lin, and Troels B. Sørensen, "Performance of Linear Dispersion Codes with Linear Receivers," in Proc. International Symposium on Wireless Personal Multimedia Communications (WPMC), Jaipur, India, December 2007.

- Daniel V.P. Figueiredo, Zihuai Lin, and Troels B. Sørensen, "Average Error Probability of MIMO Diversity Systems in the Presence of Multiple Interferers," in Proc. IEEE International Symposium on Wireless Communication Systems (ISWCS), Trondheim, Norway, October 2007.

- Muhammad I. Rahman, Ragnar V. Reynisson, Daniel V.P. Figueiredo, and Ramjee Prasad, "Coordinated Sub-Carrier and Band Hopping in OFDMA based Systems," in Proc. IEEE International Symposium on Wireless Communication Sys-

tems (ISWCS), Trondheim, Norway, October 2007.

- Daniel V.P. Figueiredo, and Elisabeth de Carvalho, "Switching Thresholds for Rate Adaptation with MRC under Feedback Delay," in Proc. International Symposium on Wireless Personal Multimedia Communications (WPMC), San Diego, USA, September 2006.

- Daniel V.P. Figueiredo, Elisabeth de Carvalho, and Luc Deneire, "Impact of Feedback Delay on Rate Adaptation for Multiple Antenna Systems," in Proc. IEEE International Symposium on Personal, Indoor and Mobile Radio Communications (PIMRC), Helsinki, Finland, September 2006.

- Daniel V.P. Figueiredo, Muhammad I. Rahman, Nicola Marchetti, Frank H.P. Fitzek, Marcos D. Katz, Youngkwon Cho, and Ramjee Prasad, "Transmit Diversity vs Beamforming for Multi-user OFDM Systems," in Proc. International Symposium on Wireless Personal Multimedia Communications (WPMC), Abano Terme, Italy, June 2004.

Moreover, the collaboration with industry in the projects JADE and IST-SURFACE led to the certification of one patent, and the co-authoring of several project deliverables.

Patents

- Daniel V.P. Figueiredo, Elisabeth de Carvalho, Luc Deneire, Sung-Ryul Yun, David Mazzarese, and Sung-Kwon Hong, "Transmission Strategies for Downlink Multi-User OFDMA," Samsung, Korean Patent KR2006-0021584, March 8, 2006.

Project Deliverables

- Troels B. Sørensen, Daniel V.P. Figueiredo, Yuanye Wang, Wsewolod Warzanskyj, et al., "Description of the Network Optimal Transmit and Receive," IST-SURFACE Deliverable D5, December 2007.

- Antonio Fasano, Sergio Barbarossa, Loreto Pescosolido, Gesualdo Scutari, Luis G. Ordóñes, Eduardo Calvo, Javier R. Fonollosa, Alba Pagès-Zamora, Troels B. Sørensen, Daniel V.P. Figueiredo, Istvan Z. Kovàcs, et al., "Preliminary Design of the Multi-user Optimal Transmit and Receive Strategy," IST-SURFACE Deliverable D4, December 2006.

- Daniel V.P. Figueiredo, Elisabeth de Carvalho, and Luc Deneire, "Transmission Strategies in MIMO Scenarios with Channel Prediction," JADE project deliverable PD-WP1-1-Jun06-MIMOSwicthing, Aalborg University, Denmark, June 2006.

- Daniel V.P. Figueiredo, Elisabeth de Carvalho, and Luc Deneire, "Transmission Strategies in MIMO Scenarios with Channel Prediction," JADE project deliverable PD-WPB-WA2-Dec05-swicthing, Aalborg University, Denmark, December 2005.

- Muhammad I. Rahman, Ragnar V. Reynisson, and Daniel V.P. Figueiredo, "Sub-carrier and Band Hopped Orthogonal Frequency Division Multiple Access (SCBH-OFDMA)," JADE project deliverable TN-WPB-WA4-Oct05, Aalborg University, Denmark, October 2005.

- Daniel V.P. Figueiredo, Elisabeth de Carvalho, and Luc Deneire, "Transmission Strategies in Multi-user Scenarios," JADE project deliverable TN-WPB-WA2-Oct05, Aalborg University, Denmark, October 2005.

- Muhammad I. Rahman, Huan C. Nguyen, Daniel V.P. Figueiredo, Ragnar V. Reynisson, and Elisabeth de Carvalho, "Initial Recommendations for Access Techniques and Duplexing for Cellular Systems," JADE project deliverable B-2005-06-2, Aalborg University, Denmark, June 2005.

- Megumi Kaneko, Nicola Marchetti, and Daniel V.P. Figueiredo, "Multi-user Diversity in Scheduling," JADE project deliverable D3.2[2], Aalborg University, Denmark, January 2005.

- Muhammad I. Rahman, Nicola Marchetti, Daniel V.P. Figueiredo, Huan C. Nguyen,

Ragnar V. Reynisson, and Seshaiah Ponnekanti, "Multi-antenna Techniques in Multi-user OFDM Systems," JADE project deliverable D3.2[1],Aalborg University, Denmark, September 2004.

- Muhammad I. Rahman, Søren S. Christian, Suvra S. Das, Basak Can, Ragnar V. Reynisson, Anders B. Olsen, Jesper M. Kristensen, Nicola Marchetti, Daniel V.P. Figueiredo, and Petar Popovski, "Comparison of Various Modulation and Access Schemes under Ideal Channel Conditions," JADE project deliverable D3.1[1], Aalborg University, Denmark, July 2004.

Bibliography

[3GP06a] 3GPP, "Physical layer aspects for evolved Universal Terrestrial Radio Access (UTRA)," Technical Specification TR 25.814 (V7.1.0), September 2006.

[3GP06b] ——, "Requirements for Evolved UTRA (E-UTRA) and Evolved UTRAN (E-UTRAN)," Technical Specification TR 25.913 (V7.3.0), March 2006.

[3GP07] ——, "Spatial Channel Model for Multiple Input Multiple Output (MIMO) simulations," Technical Specification TR 25.996 (V7.0.0), June 2007.

[AG00] M. S. Alouini and A. J. Goldsmith, "Adaptive modulation over nakagami fading channels," *Kluwer Journal on Wireless Personal Communications*, vol. 13, no. 1, pp. 119–143, 2000.

[Ala98] S. M. Alamouti, "A simple transmit diversity technique for wireless communications," *IEEE Journal on Selected Areas in Communications*, vol. 16, no. 8, pp. 1451–1458, 1998.

[And05] J. G. Andrews, "Interference cancellation for cellular systems: a contemporary overview," *IEEE Wireless Communications Magazine*, vol. 12, no. 2, pp. 19–29, 2005.

[App76] S. Applebaum, "Adaptive arrays," *IEEE Transactions on Antennas and Propagation*, vol. 24, no. 5, pp. 585–598, 1976.

[AR01] Y. Akyildiz and B. D. Rao, "Statistical performance analysis of optimum combining with co-channel interferers and flat Rayleigh fading," in *Proc.*

IEEE Global Communications Conference (GLOBECOM), vol. 6, San Antonio, TX, USA, November 2001, pp. 3663–3667.

[BÖ6] H. Bölcskei, *Space-Time Wireless Systems: From Array Processing to MIMO Communications*, D. Gesbert, C. Papadias, and A.-J. van der Veen, Eds. New York, NY, USA: Cambridge University Press, 2006.

[Bar04] S. Barbarossa, "Trace-orthogonal design of MIMO systems with simple scalar detectors, full diversity and (almost) full rate," in *Proc. IEEE Workshop on Signal Processing Advances in Wireless Communications (SPAWC)*, Lisbon, Portugal, July 2004, pp. 308–312.

[Ber05] L. Berger, "Performance of Multi-Antenna Enhanced HSDPA," Ph.D. dissertation, Aalborg University, Denmark, 2005.

[BH01] G. Bauch and J. Hagenauer, "Analytical evaluation of space-time transmit diversity with FEC-coding," in *Proc. IEEE Global Communications Conference (GLOBECOM)*, vol. 1, San Antonio, TX, USA, November 2001, pp. 435–439.

[BKRM+03] L. T. Berger, T. E. Kolding, J. Ramiro-Moreno, P. Ameigeiras, L. Schumacher, and P. E. Mogensen, "Interaction of transmit diversity and proportional fair scheduling," in *Proc. IEEE Vehicular Technology Conference (VTC)*, vol. 4, Jeju, Korea, April 2003.

[BZR05] J. P. Burke, J. R. Zeidler, and B. D. Rao, "CINR difference analysis of optimal combining versus maximal ratio combining," *IEEE Transactions on Wireless Communications*, vol. 4, no. 1, pp. 1–5, 2005.

[CA03] C. Chayawan and V. A. Aalo, "Average error probability of digital cellular radio systems using MRC diversity in the presence of multiple interferers," *IEEE Transactions on Wireless Communications*, vol. 2, no. 5, pp. 860–864, 2003.

[Car86] A. B. Carlson, *Communication Systems*. New York, NY, USA: McGraw-Hill, 1986.

[CEGHJ02] S. Catreux, V. Erceg, D. Gesbert, and R. W. Heath Jr, "Adaptive modulation and MIMO coding for broadband wireless data networks," *IEEE Communications Magazine*, vol. 40, no. 6, pp. 108–115, 2002.

[CFD+06] E. D. Carvalho, D. V. P. Figueiredo, L. Deneire, S.-R. Yun, D. Mazzarese, and S.-K. Hong, "Transmission Strategies for Downlink Multi-User OFDMA," Korean Patent KR2006-0 021 584, March 8, 2006.

[CFS97] J. Cui, D. D. Falconer, and A. U. H. Sheikh, "Performance evaluation of optimum combining and maximal ratio combining in the presence of co-channel interference and channel correlation for wireless communication systems," *Mobile Networks and Applications*, vol. 2, no. 4, pp. 315–324, 1997.

[CG01] S. T. Chung and A. J. Goldsmith, "Degrees of freedom in adaptive modulation: a unified view," *IEEE Transactions on Communications*, vol. 49, no. 9, pp. 1561–1571, 2001.

[CJS07] G. Caire, N. Jindal, and S. Shamai, "On the required accuracy of transmitter channel state information in multiple antenna broadcast channels," in *Proc. Asilomar Conference on Signals, Systems and Computers*, Pacific Grove, CA, USA, November 2007, pp. 287–291.

[CLH01] S. T. Chung, A. Lozano, and H. C. Huang, "Low complexity algorithm for rate and power quantization in extended V-BLAST," in *Proc. IEEE Vehicular Technology Conference (VTC)*, vol. 2, Atlantic City, NJ, USA, October 2001.

[Col07] S. R. Colás, "Channel Modelling and SINR Evaluation in MBMS for LTE," Master's thesis, Aalborg University, 2007.

[CS99] J. Cui and A. U. H. Sheikh, "Outage probability of cellular radio systems using maximal ratio combining in the presence of multiple interferers," *IEEE Transactions on Communications*, vol. 47, no. 8, pp. 1121–1124, 1999.

[DB05] M. Ding and S. Blostein, "Low-feedback adaptive-rate MIMO spatial multiplexing with zero forcing detection," in *Canadian Workshop on Information Theory*, Edmonton, Canada, 2005.

[DTB02] M. O. Damen, A. Tewfik, and J. C. Belflore, "A construction of a space-time code based on number theory," *IEEE Transactions on Information Theory*, vol. 48, no. 3, pp. 753–760, 2002.

[Ekm02] T. Ekman, "Prediction of Mobile Radio Channels: Modeling and Design," Ph.D. dissertation, Uppsala University, Sweden, 2002.

[ESA02] T. Ekman, M. Sternad, and A. Ahlen, "Unbiased power prediction of Rayleigh fading channels," in *Proc. IEEE Vehicular Technology Conference (VTC)*, vol. 1, Vancouver, Canada, September 2002, pp. 280–284.

[FB06] A. Fasano and S. Barbarossa, "Iterative MMSE decoder for trace-orthogonal space-time coding," in *Proc. IEEE International Conference on Acoustics, Speech, and Signal Processing (ICASSP)*, vol. 4, Toulouse, France, May 2006.

[FC06] D. V. P. Figueiredo and E. D. Carvalho, "Switching thresholds for rate adaptation with MRC under feedback delay," in *Proc. International Symposium on Wireless Personal Multimedia Communications (WPMC)*, San Diego, CA, USA, September 2006.

[FCD06] D. V. P. Figueiredo, E. D. Carvalho, and L. Deneire, "Impact of feedback delay on rate adaptation for multiple antenna systems," in *Proc. IEEE International Symposium on Personal, Indoor and Mobile Radio Communications (PIMRC)*, Helsinki, Finland, September 2006.

[Fla03] "OFDM for Mobile Data Communications," Online Tutorial, Whitepaper, Flarion Technologies, March 2003.

[FLS07a] D. V. P. Figueiredo, Z. Lin, and T. B. Sørensen, "Average error probability of MIMO diversity systems in the presence of multiple interferers," in *Proc. IEEE International Symposium on Wireless Communication Systems (ISWCS)*, Trondheim, Norway, October 2007.

[FLS07b] ——, "Performance of linear dispersion codes with linear receivers," in *Proc. International Symposium on Wireless Personal Multimedia Communications (WPMC)*, Jaipur, India, December 2007.

[Fos96] G. J. Foschini, "Layered space-time architecture for wireless communication in a fading environment when using multiple antennas," *Bell Labs Technical Journal*, vol. 1, no. 2, pp. 41–59, 1996.

[FPKHJ05] A. Forenza, A. Pandharipande, H. K., and R. W. Heath Jr, "Adaptive MIMO transmission scheme: exploiting the spatial selectivity of wireless channels," in *Proc. IEEE Vehicular Technology Conference (VTC)*, vol. 5, Stockholm, Sweden, May 2005, pp. 3188–3192.

[FRM+04] D. V. P. Figueiredo, M. I. Rahman, N. Marchetti, F. H. P. Fitzek, M. D. Katz, Y. Cho, and R. Prasad, "Transmit diversity vs beamforming for multiuser OFDM systems," in *Proc. International Symposium on Wireless Personal Multimedia Communications (WPMC)*, Abano Terme, Italy, September 2004.

[FSES04] S. Falahati, A. Svensson, T. Ekman, and M. Sternad, "Adaptive modulation systems for predicted wireless channels," *IEEE Transactions on Communications*, vol. 52, no. 2, pp. 307–316, 2004.

[God04] L. Godara, *Smart Antennas*. Boca Raton, FL, USA: CRC Press, Inc., 2004.

[Goe99] D. L. Goeckel, "Adaptive coding for time-varying channels using outdated fading estimates," *IEEE Transactions on Communications*, vol. 47, no. 6, pp. 844–855, 1999.

[Gol05] A. J. Goldsmith, *Wireless Communications*. New York, NY, USA: Cambridge University Press, 2005.

[GSS+03] D. Gesbert, M. Shafi, D. Shiu, P. Smith, and A. Naguib, "From theory to practice: an overview of MIMO space-time coded wireless systems," *IEEE Journal on Selected Areas in Communications*, vol. 21, no. 3, pp. 281–302, 2003.

[HG03] L. He and H. Ge, "A new full-rate full-diversity orthogonal space-time block coding scheme," *IEEE Communications Letters*, vol. 7, no. 12, pp. 590–592, 2003.

[HH02] B. Hassibi and B. M. Hochwald, "High-rate codes that are linear in space and time," *IEEE Transactions on Information Theory*, vol. 48, no. 7, pp. 1804–1824, 2002.

[HJL05] R. W. Heath Jr and D. J. Love, "Multimode antenna selection for spatial multiplexing systems with linear receivers," *IEEE Transactions on Signal Processing*, vol. 53, no. 8, pp. 3042–3056, 2005.

[HJP02] R. W. Heath Jr and A. J. Paulraj, "Linear dispersion codes for MIMO systems based on frame theory," *IEEE Transactions on Signal Processing*, vol. 50, no. 10, pp. 2429–2441, 2002.

[HJP05] ——, "Switching between diversity and multiplexing in MIMO systems," *IEEE Transactions on Communications*, vol. 53, no. 6, pp. 962–968, 2005.

[HMT04] B. M. Hochwald, T. L. Marzetta, and V. Tarokh, "Multiple-antenna channel hardening and its implications for rate feedback and scheduling," *IEEE Transactions on Information Theory*, vol. 50, no. 9, pp. 1893–1909, 2004.

[Hol02] H. Holm, "Adaptive Coded Modulation Performance and Channel Estimation Tools for Flat Fading Channels," Ph.D. dissertation, Norwegian University of Science and Technology, Trondheim, Norway, 2002.

[HP03] S. Hara and R. Prasad, *Multicarrier Techniques for 4G Mobile Communications*. Norwood, MA, USA: Artech House, Inc., 2003.

[HT01] J. Heiskala and J. Terry, *OFDM Wireless Lans: A Theoretical and Practical Guide*. Indianapolis, IN, USA: Sams Publishing, 2001.

[HT04] H. Holma and A. Toskala, *WCDMA for UMTS: Radio Access for Third Generation Mobile Communications*. New York, NY, USA: John Wiley & Sons, Inc., 2004.

[HT06] ——, *HSDPA/HSUPA for UMTS: High Speed Radio Access for Mobile Communications*. New York, NY, USA: John Wiley & Sons, Inc., 2006.

[IEE04] *IEEE Standard for Local and Metropolitan Area Networks Part 16: Air Interface for Fixed Broadband Wireless Access Systems*, IEEE Std. 802.16-2004, October 2004.

[IEE06] *IEEE Standard for Local and Metropolitan Area Networks Part 16: Air Interface for Fixed Broadband Wireless Access Systems*, IEEE Std. 802.16e-2005, February 2006.

[ITU97] "Guidelines for evaluation of radio transmission technologies for IMT-2000," ITU-R, Recommendations M.1225, 1997.

[JC94] W. C. Jakes and D. C. Cox, *Microwave Mobile Communications*. Wiley-IEEE Press, 1994.

[JSC+07] M. Jordan, M. Senst, Y. Cui, G. Ascheid, and H. Meyr, "Downlink based intercell time synchronization using maximum likelihood estimation," in *Proc. IST Mobile and Wireless Communications Summit*, Budapest, Hungary, July 2007, pp. 1–5.

[KH95] R. Knopp and P. A. Humblet, "Information capacity and power control in single-cell multiuser communications," in *Proc. IEEE International Conference on Communications (ICC)*, vol. 1, Seatlle, WA, USA, June 1995.

[Kim02] B. Kim, "Smart Base Station Antenna Performance for Several Scenarios - an Experimental and Modeling Investigation," Ph.D. dissertation, Virginia Polytechnic Institute and State University, Blacksburg, VA, USA, 2002.

[KMAH02] K. Kopsa, G. Matz, H. Artes, and F. Hlawatsch, "Space-time synchronization algorithms for UMTS/TDD systems with strong co-channel interference," in *Proc. IEEE Global Communications Conference (GLOBECOM)*, vol. 1, Taipei, Taiwan, November 2002, pp. 254–258.

[KT03] Y. Ko and C. Tepedelenlioglu, "Space-time block coded rate-adaptive modulation with uncertain SNR feedback," in *Proc. Asilomar Conference on Signals, Systems and Computers*, vol. 1, Pacific Grove, CA, USA, November 2003, pp. 1032–1036.

[KVC02] P. Kyritsi, R. A. Valenzuela, and D. C. Cox, "Channel and capacity estimation errors," *IEEE Communications Letters*, vol. 6, no. 12, pp. 517–519, 2002.

[LLC02] V. K. N. Lau, Y. Liu, and T. A. Chen, "Optimal multi-user space time scheduling for wireless communications," in *Proc. IEEE Vehicular Technology Conference (VTC)*, vol. 4, Vancouver, Canada, September 2002.

[LR99] J. C. Liberti and T. S. Rappaport, *Smart Antennas for Wireless Communications: IS-95 and Third Generation CDMA Applications.* Upper Saddle River, NJ, USA: Prentice Hall PTR, 1999.

[LS99] Y. Li and N. R. Sollenberger, "Adaptive antenna arrays for OFDM systems with cochannel interference," *IEEE Transactions on Communications*, vol. 47, no. 2, pp. 217–229, 1999.

[LW00] K. F. Lee and D. B. Williams, "A space-frequency transmitter diversity technique for OFDM systems," in *Proc. IEEE Global Communications Conference (GLOBECOM)*, vol. 3, San Francisco, CA, USA, November 2000, pp. 1473–1477.

[LZW06] J. Liu, J. K. Zhang, and K. M. Wong, "On the Design of Minimum BER Linear Space-Time Block Codes for MIMO Systems Equipped with MMSE Receivers," *IEEE Transactions on Signal Processing*, vol. 54, no. 8, pp. 3147–3158, 2006.

[MAT] Matlab - the language of technical computing. [Online]. Available: http://www.mathworks.com/products/matlab/

[MG03] X. Ma and G. B. Giannakis, "Full-diversity full-rate complex-field space-time coding," *IEEE Transactions on Signal Processing*, vol. 51, no. 11, pp. 2917–2930, 2003.

[MKL06] J. Moon, J. Y. Ko, and Y. H. Lee, "A framework design for the next-generation radio access system," *IEEE Journal on Selected Areas in Communications*, vol. 24, no. 3, pp. 554–564, 2006.

[MS98] J. Medbo and P. Schramm, "Channel models for HIPERLAN/2 in different indoor scenarios," COST 259 TD(98)70, ETSI BRAN, Bradford, UK, April 1998.

[NAP04] H. T. Nguyen, J. B. Andersen, and G. F. Pedersen, "Capacity and performance of MIMO systems under the impact of feedback delay," in *Proc. IEEE International Symposium on Personal, Indoor and Mobile Radio Communications (PIMRC)*, vol. 1, Barcelona, Spain, September 2004.

[NH04] S. Nagaraj and Y.-F. Huang, "Multiple antenna transmission with channel state information: a low-rate feedback approach," *IEEE Signal Processing Letters*, vol. 11, no. 6, pp. 573–576, June 2004.

[NP00] R. V. Nee and R. Prasad, *OFDM for Wireless Multimedia Communications*. Norwood, MA, USA: Artech House, Inc., 2000.

[OHH04] G. E. Oien, H. Holm, and K. J. Hole, "Impact of channel prediction on adaptive coded modulation performance in Rayleigh fading," *IEEE Transactions on Vehicular Technology*, vol. 53, no. 3, pp. 758–769, 2004.

[Par00] J. D. Parsons, *The Mobile Radio Propagation Channel*. New York, NY, USA: John Wiley & Sons, Inc., 2000.

[Pat03] M. Patzold, *Mobile Fading Channels*. New York, NY, USA: John Wiley & Sons, Inc., 2003.

[PNG03] A. J. Paulraj, R. Nabar, and D. Gore, *Introduction to Space-Time Wireless Communications*. New York, NY, USA: Cambridge University Press, 2003.

[Pok07] A. Pokhariyal, "Downlink Frequency-Domain Adaptation and Scheduling - A Case Study Based on the UTRA Long Term Evolution," Ph.D. dissertation, Aalborg University, Denmark, 2007.

[PP97] A. J. Paulraj and C. B. Papadias, "Space-time processing for wireless communications," *IEEE Signal Processing Magazine*, vol. 14, no. 6, pp. 49–83, 1997.

[Pro01] J. G. Proakis, *Digital Communication*. New York, NY, USA: McGraw-Hill, 2001.

[Rah07] M. I. Rahman, "Channelization, Link Adaptation and Multi-antenna Techniques for OFDM(A) Based Wireless Systems," Ph.D. dissertation, Aalborg University, Denmark, 2007.

[Rap96] T. S. Rappaport, *Wireless Communications: Principles and Practice*. Piscataway, NJ, USA: IEEE Press, 1996.

[RDF04] M. I. Rahman, S. S. Das, and F. H. P. Fitzek, "OFDM Based WLAN Systems," Aalborg University, Denmark, Tech. Rep. R-04-1002, January 2004.

[RG97] H. Rohling and R. Gruneid, "Performance comparison of different multiple access schemes for the downlink of an OFDM communication system," in *Proc. IEEE Vehicular Technology Conference (VTC)*, vol. 3, Phoenix, AZ, USA, May 1997, pp. 1365–1369.

[SAT82] O. E. Smith, S. I. Adelfang, and J. D. Tubbs, "A Bivariate Gamma Probability Distribution with Application to Gust Modeling," *NASA Technical Memorandum*, vol. 82483, 1982.

[SBM+04] G. L. Stüber, J. R. Barry, S. W. McLaughlin, Y. E. G. Li, M. A. Ingram, and T. G. Pratt, "Broadband MIMO-OFDM wireless communications," *Proceedings of the IEEE*, vol. 92, no. 2, pp. 271–294, February 2004.

[SH98] A. Shah and A. M. Haimovich, "Performance analysis of optimum combining in wireless communications with Rayleigh fading and cochannel interference," *IEEE Transactions on Communications*, vol. 46, no. 4, pp. 473–479, 1998.

[SH03] H. Schoeneich and P. A. Hoeher, "Single antenna interference cancellation: iterative semi-blind algorithm and performance bound for joint maximum-likelihood interference cancellation," in *Proc. IEEE Global Communications Conference (GLOBECOM)*, vol. 3, San Francisco, CA, USA, December 2003.

[SKF+01] L. Schumacher, J. P. Kermoal, F. Frederiksen, K. I. Pedersen, A. Algans, and P. E. Mogensen, "MIMO channel characterization," IST-METRA Project Deliverable 2, February 2001.

[SLWR01] A. Seeger, A. Lobinger, R. Wiedmann, and B. Raaf, "Downlink eigenbeamformer with combining of eigenbeams," in *Proc. IEEE Global Communica-*

tions Conference (GLOBECOM), vol. 5, San Antonio, TX, USA, November 2001, pp. 1269–1273.

[SP04] N. Sharma and C. B. Papadias, "Full-rate full-diversity linear quasi-orthogonal space-time codes for any number of transmit antennas," *EURASIP Journal on Applied Signal Processing*, vol. 2004, no. 9, pp. 1246–1256, 2004.

[TAG99] X. Tang, M. S. Alouini, and A. J. Goldsmith, "Effect of channel estimation error on M-QAM BER performance in Rayleigh fading," *IEEE Transactions on Communications*, vol. 47, no. 12, pp. 1856–1864, 1999.

[TBH00] O. Tirkkonen, A. Boariu, and A. Hottinen, "Minimal non-orthogonality rate 1 space-time block code for 3+ Tx antennas," in *Proc. IEEE International Symposium on Spread Spectrum Techniques and Applications (ISSSTA)*, vol. 2, Parsippany, NJ, USA, September 2000.

[Tel95] E. Telatar, "Capacity of multi-antenna gaussian channels," AT&T-Bell Labs Internal Tech. Memo., June 1995.

[THJ05] T. Tang and R. W. Heath Jr, "Space-time interference cancellation in MIMO-OFDM systems," *IEEE Transactions on Vehicular Technology*, vol. 54, no. 5, pp. 1802–1816, 2005.

[TJC99] V. Tarokh, H. Jafarkhani, and A. R. Calderbank, "Space-time block coding for wireless communications: performance results," *IEEE Journal on Selected Areas in Communications*, vol. 17, no. 3, pp. 451–460, 1999.

[Ven03] R. Venkatasubramanian, "Beamforming for MC-CDMA," Master's thesis, Virginia Polytechnic Institute and State University, Blacksburg, VA, USA, 2003.

[VTL02] P. Viswanath, D. N. C. Tse, and R. Laroia, "Opportunistic beamforming

using dumb antennas," *IEEE Transactions on Information Theory*, vol. 48, no. 6, pp. 1277–1294, 2002.

[Wei07] N. Wei, "MIMO Techniques in UTRA Long Term Evolution," Ph.D. dissertation, Aalborg University, Denmark, 2007.

[WPR+06] N. Wei, A. Pokhariyal, C. Rom, B. E. Priyanto, F. Frederiksen, C. Rosa, T. B. Sorensen, T. E. Kolding, and P. E. Mogensen, "Baseline E-UTRA downlink spectral efficiency evaluation," in *Proc. IEEE Vehicular Technology Conference (VTC)*, Montreal, Canada, September 2006, pp. 1–5.

[WSKM06] N. Wei, T. B. Sørensen, T. E. Kolding, and P. E. Mogensen, "Analysis and evaluation of link adaptation including MIMO adaptation," in *Proc. IEEE Vehicular Technology Conference (VTC)*, Montreal, Canada, September 2006, pp. 1–5.

[ZL03] Y. J. Zhang and K. B. Letaief, "Optimizing power and resource management for multiuser MIMO/OFDM systems," in *Proc. IEEE Global Communications Conference (GLOBECOM)*, vol. 1, San Francisco, CA, USA, December 2003.

Vita

Daniel V.P. Figueiredo was born in 1980 in Lisbon, Portugal. He started university in 1998 and obtained the *Licenciatura* (5-year degree) in October 2003 in Electronics and Computers Engineering at Instituto Superior Técnico (IST), Technical University of Lisbon, Portugal. In spring 2002, he spent one semester at Politecnico di Milano, Italy, as an exchange student with an ERASMUS scholarship. In February 2004, he joined the Wireless Networking Group (WING) at the Institute of Electronic Systems, Aalborg University, and he has been enrolled as a Ph.D. student from June 2004. Since August 2006, he is with the Radio Access Technology (RATE) section of the Institute of Electronic Systems at Aalborg University.

The main topics of research include spatial diversity and multiplexing, link adaptation, and multicarrier systems. He has been actively engaged in IEEE volunteer activities, co-organizing a number of events including the first and second occurrences of the international conference *Annual IEEE Student Paper Conference* (AISPC'07 and AISPC'08).

Contact email: dvpfig@gmail.com